An analysis of taenidial fold formation via the study of *Blimp-1* and *pri*

Arzu Ozturk Colak

Department de Genética
Facultat de Biología
Universidad de Barcelona

AN ANALYSIS OF TAENIDIAL FOLD FORMATION VIA THE STUDY OF *BLIMP-1* AND *PRI*

Memoria presentada por

ARZU ÖZÜRK ÇOLAK

para optar al grado de Doctor
por la Universidad de Barcelona

Esta investigación ha sido realizada en
Institute for Research in Biomedicine (IRB Barcelona)
y en el Instituto de Biología Molecular de Barcelona (IBMB-CSIC)

El Tutor	Los Directores	La Autora
Dr. Emili Saló Boix	Dr. Sofia J. Araújo, Dr. Jordi Casanova Roca	Arzu Özürk Çolak

ACKNOWLEDGEMENTS

First of all, I would like to thank my supervisors Sofia Araújo and Jordi Casanova for their continuous help in my project. During our SJA meetings that took place in Jordi's office and we usually end up eating whatever Jordi has in his secret stash, I have learnt a lot about science and many other things. Sofia and Jordi, I am really grateful for your great supervision which helped me mature scientifically and personally during my life in Barcelona.

I would like to thank to Marta, Xavi, Sara, Marc, Andreu, Kyra, Anni, Gaelle, Nareg, Mahi, Beatrice, Pilar, Ivette, Neus, Guillem, Guille, Elisenda, Delia, Pablo, Oscar, Gaylord, Marco, Ale, Friedemann and Cristina for all the lab meetings and the discussions. I would like to also thank to Yolanda, Nico and Esther for all the technical help.

My friends, all of you made my life richer, funnier and more fun. Ivette, Lorena, Guillem, Guille, mama Pilar, Oskito, Neus, Hector, Vero, Yolanda, Gaylord and Mahi thank you all for the get-togethers in which we shared so many meals, played so many games and have so much fun! Cookie, Oskito, Yolanda and Gaylord thanks for your warm welcome and accepting me to the dark side ☺. Mariajo, thanks for your always smiling face and helping me with the boring wedding documents! Oskito, you've been my close friend, my tourist and (of course!) gourmet guide in Barcelona and many places in Spain, and the witness in our wedding ceremony. I don’t know whether I can thank you enough but thank you sooooo much for being in my life for four (and hopefully more) years! Cookie, you taught me so many things about the experiments and also life. Thanks for being with me anytime I need and being our mama! Lorena and Ivette, thanks for all the laughs we shared during lunches, meriendas and dinners in Rosa Negra with mojitos and margarittas! You’ve made my life more colorfull! One day we were crossing the street with Oskito on our way to metro we heard a voice saying “Que Passsaaaaa”. From that time on, you’ve been in my life, Lorena. Thanks for being the most frequently seen person in the photos in my mobile (according to a relative in Turkey) and all the great things we shared together: the dinners we shared (always very close to your current apartments), the meals we had in your home in Areyns de Munt, our (most of the time meaningless) visits to Ikea and our quest in finding my wedding dress! Guillem, known as the Illuminati and the whistling (previously) annoying guy, thanks for all the fun conversations we had about the TV series, games, books and movies!

I would like to also thank to my friends from the institute: Silvia, Pep, Benji, Pablo and Constanze. Thanks for all the fun times and outside of Barcelona trips we shared together! The Organizer, Silvia, I am sooo lucky to get the chance to know you and be friends with you. Thanks to your always smiling face and your sincere friendship, my life in Barcelona got much more fulfilling.

I would like to also thank to my mother, father and brother for their limitless love and continuous support.

Last but not least I would like to thank to Ilker, my love, my husband and my best friend. As many other things in my life, without you this work wouldn’t be

possible. Thanks for being there for me in both joyful and bad times, always believing in me and supporting me.

TABLE OF CONTENTS

INTRODUCTION **1**
1. Tubular structures **1**
2. *Drosophila melanogaster* as a model organism **1**
3. Development of *Drosophila* embryonic trachea **2**
3.1. Early stages of tracheal development: stage 11 and 12 3
3.2. Generating a continuous tube via fusion cells 3
3.3. Organization of the embryonic tracheal cells 4
3.4. Apical secretion and tube expansion 5
3.5. Late stages of tracheal development: stage 16 and 17 7
4. *Drosophila* cuticle **8**
4.1. Intraluminal chitin filament 9
4.2. Taenidial folds 9
4.2.1. Genes involved in formation of taenidial folds 12
4.2.1.a. B-lymphocyte-inducing maturation protein-1 (Blimp-1) 15
4.2.1.b. Polished rice (pri) 19
4.2.2. Lessons from larval taenidial folds 21

OBJECTIVES **23**

MATERIALS AND METHODS **25**
1. Materials **25**
Biological Materials 25
1.2. Chemicals, Buffers, Enzymes and Supplies 26
1.3. Solutions 27
1.4. Antibodies, Stains and Probes 27
2. Methods **28**
2.1. Molecular Biological Techniques 28
2.1.1. Isolation of Genomic DNA 28
2.1.2. Synthesis of RNA probes for in-situ hybridization 29
2.2. Histological Techniques 30
2.2.1. Cuticle preparation of embryos 30
2.2.2. Fixation of embryos 30
2.2.3. Antibody staining of embryos 31
2.2.4. Antibody staining of larval tissues 31
2.2.5. 2A12 staining 31
2.2.6. Phalloidin staining 32
2.2.7. Fluorescent in-situ hybridization 32
2.3. Generation of FLP-out clones 33
2.4. Image Acquisition and Processing 33
2.5. *In vivo* experiments 34
2.5.1.Time-lapse experiments 34
2.5.2. Air-filling experiments 34
2.6. Tube size quantifications and statistics 34

RESULTS **35**
1. Dynamics of taenidial folds and F-actin bundles **35**
2. Genes involved in formation of taenidial folds **39**
2.1 Blimp-1 and pri 39
2.1.1 Expression pattern of *Blimp-1* and *pri* 39
2.1.2 Loss of function phenotypes of *Blimp-1* and *pri* 42
2.1.2.a Taenidial folds and actin rings phenotype 43
2.1.2.b Denticle belts and cuticle phenotype 48
2.1.2.c Tube expansion phenotype 50

2.1.2.d Apical cell shape phenotype 51
2.1.2.e Air-filling phenotype 52
2.1.3 Do *Blimp-1* and *pri* function together? 54
2.1.3.a Blimp-1 and pri expression in mutants for pri and Blimp-1 54
2.1.3.b Pri expression in Blimp-1 over/ectopic expression 56
2.1.3.c. Blimp-1, pri double mutant 56
2.1.4 Downstream candidates of *Blimp-1* and *pri* 58
2.1.5 Upstream candidates of *Blimp-1* and *pri* 61
2.1.6 Overexpression and ectopic expression phenotypes of *Blimp-1* 63
2.1.6.a Taenidial folds phenotype 63
2.1.6.b Tube expansion phenotype 65
2.1.6.c Apical cell shape phenotype 66
3. Chitin is required for proper F-actin bundling 67
4. The effect of "actin genes" on taenidial fold formation 69
5. The effect of cell shape on taenidial fold orientation 70
6. Single cells contribution to form a supra-cellular structure 71
6.1. Rescue of *Blimp-1* and *pri* mutant phenotypes 71
6.2. *Blimp-1* over/ectopic expression clones 74
6.3. Effect of cellular junctions in taenidial fold formation 75
CONCLUSIONS 79
DISCUSSION 81
REFERENCES 89
RESUMEN EN CASTELLANO 99
APPENDICIES 101
Appendix A. List of Abbreviations 101
Appendix B. Movie Legends 103

LIST OF FIGURES

Figure 1: Life cycle of *Drosophila melanogaster* 1
Figure 2: Development of embryonic tracheal system. 2
Figure 3: *Drosophila* tracheal tree 4
Figure 4: Organization and intercellular junctions of tracheal cells 5
Figure 5: Apical secretion, tube expansion and clearance 6
Figure 6: Diametric and axial tube expansion in the absence of chitin modifications and chitin synthesis 7
Figure 7: Biosynthesis of chitin in *Drosophila* tracheal system 8
Figure 8: Taenidial folds structure 10
Figure 9: Dynamics of chitin structures via TEM analysis 12
Figure 10: The taenidial folds in the absence of *Blimp-1* and *pri* 14
Figure 11: The rescue of the taenidial folds phenotype in the *Sec24CD* mutant background 15
Figure 12: Gene structure of Prdm1/Blimp-1 and its interactions with epigenetic modifiers 16
Figure 13: Tracheal phenotypes associated with *Blimp-1* 18
Figure 14: Gene structure and mutant phenotypes of of *pri/tal* 19
Figure 15: Dynamics of chitin structures via fluorescent labeling 36
Figure 16: F-actin bundles and taenidial folds in embryonic and larval tracheas 37
Figure 17: Dynamics of taenidial folds and F-actin bundles 38
Figure 18: *Blimp-1* is expressed in the tracheal system 40
Figure 19: Expression pattern of *Blimp-1* and *pri* 42
Figure 20: A P-element insertion in the *Blimp-1* gene region results in a protein null mutant 42
Figure 21: Intraluminal chitin filament in the *Blimp-1* and *pri* mutant embryos 43
Figure 22: Taenidial folds in the *Blimp-1* and *pri* mutant embryos 44
Figure 23: Taenidial folds and F-actin bundles in the *pri* mutant embryos 45
Figure 24: F-actin bundles in the *pri* mutant embryo 46
Figure 25: Taenidial folds and F-actin bundles in the *Blimp-1* mutant embryos 47
Figure 26 *In vivo* F-actin bundles formation in the *Blimp-1* mutant embryo 48
Figure 27: Denticle belts and F-actin at the epidermis in the *Blimp-1* and *pri* mutant embryos 49
Figure 28: Chitin levels in *Blimp-1* mutant embryos 50
Figure 29: Tube expansion in the *Blimp-1* and *pri* mutant embryps 51
Figure 30: Apical cell shape in the *Blimp-1* and *pri* mutant embryos 52
Figure 31: Air-filling of the tracheal tubes in the *Blimp-1* and *pri* mutant embryos 53
Figure 32: Expression pattern of *Blimp-1* in the absence of *pri* 54
Figure 33: Expression of *pri* alters prematurely in the *Blimp-1* mutant embryo 55
Figure 34: The *pri* expressing cells in the loss of function of *Blimp-1* correspond to the fusion cells 55
Figure 35: Expression pattern of *pri* in the loss of function of *Blimp-1* 56
Figure 36: Taenidial folds and F-actin bundles in the *Blimp-1*, *pri* double mutant embryo 57
Figure 37: Tube expansion in *Blimp-1*, *pri* double mutant embryos 58
Figure 38: Expression pattern of Knk in *Blimp-1* mutant embryos 59
Figure 39: Expression pattern of Verm in *Blimp-1* and *pri* mutant embryos 60
Figure 40: Expression pattern of Pio in *Blimp-1* and *pri* mutant embryos 60

Figure 41: Expression pattern of *Blimp-1* and *pri* in *trh* and *vvl* mutant embryos..... 62
Figure 42: Expression pattern of *Blimp-1* and *pri* in the absence of ecdysone synthesis..... 63
Figure 43: The expression domain of *AbdB-GAL4* driver at different stages of embryogenesis..... 64
Figure 44: Taenidial folds in *Blimp-1* over/ectopic expression condition..... 65
Figure 45: Tube expansion phenotype of *Blimp-1* over/ectopic expression condition..... 66
Figure 46: Apical cell shape and taenidial folds in *Blimp-1* over/ectopic expression condition..... 67
Figure 47: Taenidial folds and F-actin bundles in *kkv* and *knk* mutant embryos..... 68
Figure 48: Taenidial folds and F-actin bundles in *DAAM* and *Tec29* mutant embryos..... 69
Figure 49: Taenidial folds in the *Src42A* mutant embryo..... 71
Figure 50: Taenidial folds orientation phenotype is rescued in the *Blimp-1* and *pri* mutant embryos..... 72
Figure 51: The orientation of taenidial folds is not regulated cell-autonomously..... 73
Figure 52: Taenidial folds in the *Blimp-1* over/ectopic expression clones..... 74
Figure 53: Apical cell shape in the *Blimp-1* over/ectopic expression clones..... 75
Figure 54: Taenidial folds and F-actin bundles in the absence of cellular junctions..... 76
Figure 55: The taenidial folds in the absence of cellular junctions become discontinuous at the apical cell boundaries..... 77
Figure 56: Formation of taenidial folds..... 88

INTRODUCTION

1. Tubular structures

All living organisms need to exchange gas, liquid or solid materials with their outside world. While unicellular organisms can facilitate this exchange easily through their cell membranes, multicellular organisms require tubular organ systems like lungs, vascular system and kidneys in mammals, and salivary gland, excretory system and tracheal system in flies. How these tubular networks are formed and how they function have been the focus of many scientists for several years. Strikingly their findings revealed that many major key components involved in tube formation and branching morphogenesis are conserved from invertebrates to mammals (reviewed in Andrew and Ewald, 2010). In this study we use *Drosophila melanogaster* as a model organism and its tracheal system as a model system to study tubular organ development.

2. *Drosophila melanogaster* as a model organism

As a model organism, *Drosophila melanogaster* has many advantages: (1) It is a comparatively easy organism to handle; (2) Its whole genome has been sequenced; (3) Thanks to many genetic tools available, its gene structure can be easily modified permanently or temporarily; (4) It has a short life cycle (around 10 days, **Figure 1**). (5) Last but not least it is comparatively cheap.

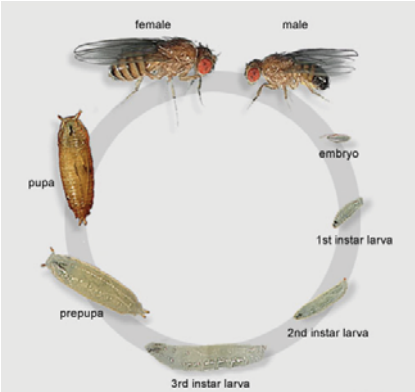

Figure 1: Life cycle of *Drosophila melanogaster*. At 25°C under standard conditions, the *Drosophila* life cycle takes around 10 days and it consists of embryonic period around 1 day, 1st instar larval

period around 1 day, 2nd instar larval period for 1 day, 3rd instar larval period for 2-3 days and pupal period for 4-5 days (from FlyMove).

The short life cycle of *Drosophila melanogaster* starts with the female flies laying their embryos preferably on a piece of fermenting fruit (hence *D. melanogasters* are also referred as fruit flies). At the end of almost one day, the embryos hatch and form 1st instar larvae, which then become 2nd instar larvae in a day. After another day, the grown 2nd instar larvae hatch and give rise to wandering 3rd instar larvae. In the first 48 hours, the 3rd instar larvae feed on the food source and grow in weight while during the last stages of 3rd instar they enter into a quiescent state and stop feeding. Then they become pupae and undergo metamorphosis that lasts about for four to five days. At the end the of metamorphosis, the adult flies emerge from their pupal cases and the cycle starts from the beginning. In this study we are specifically interested in embryonic period, which is divided into 17 stages and lasts around 22h at 25C.

3. Development of *Drosophila* embryonic trachea

An overview of the embryonic tracheal system development in *Drosophila* is depicted in **Figure 2**.

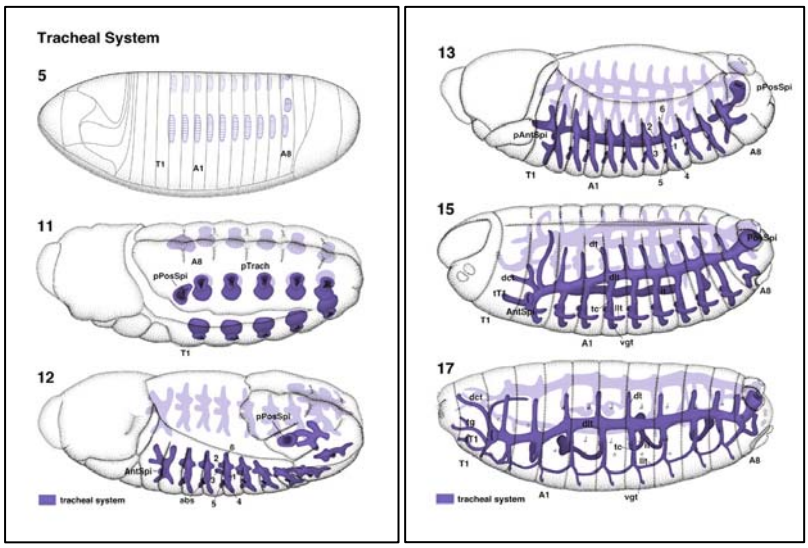

Figure 2: Development of embryonic tracheal system. The tracheal cells that give rise to larval tracheal tree at the end of embryogenesis are projected to the cluster of cells shown at stage 5. There are 10 placodes on each side of the embryo that starts invagination at stage 11. After invagination, the tracheal cells begin to respond to the Bnl signaling and migrate in order to form a continuous tracheal tree at the end of embryogenesis (from Atlas of *Drosophila* Development by Volker Hartenstein).

3.1. Early stages of tracheal development: stage 11 and 12

The *Drosophila* embryonic trachea development starts by stage 11 when locally restricted expression of two transcription factors *trachealess* (*trh*) and *ventral veinless* (*vvl*) leads to differentiation of ectodermal cells into tracheal cells (Anderson et al., 1995a; de Celis et al., 1995a; Isaac and Andrew, 1996; Wilk et al., 1996). At that stage, the cells are grouped as 20 clusters, named placodes, which then give rise to 10 tracheal metameres on each side of embryo. After getting specified as tracheal cells, placodes invaginate from the epidermis. Then the cells start to sense local Fibroblast Growth Factor/*branchless* (FGF, (*bnl*)) signaling through their FGF Receptor/*breathless* (*btl)* and migrate towards the chemoattractant (Klambt et al., 1992; Sutherland et al., 1996). Formation of the functional tracheal tree solely depends on cell migration and cell shape changes since no cell division occurs throughout the *Drosophila* embryonic tracheal development(Samakovlis et al., 1996a).

3.2. Generating a continuous tube via fusion cells

From stage 13 to 16, migrating tracheal cells encounter others from their neighboring placodes and the tracheal metameres fuse with each other in order to form the continuous network of tubes that consists of the Dorsal Trunk (DT), Dorsal Branches (DB), Visceral Branches (VB), Spiracular Branches (SB), Lateral Trunk (LT) and Ganglionic Branches (GB) (**Figure 3**). The cells that mediate fusion between branches are called fusion cells. There are five fusion cells in each tracheal metamere. Two of them are located at the thickest tube, DT, one of them is located at DB and the remaining two at the LT (**Figure 3**). Different than the other tracheal cells, fusion cells express two transcription factors *escargot* (*esg*-also expressed in the tip cells) and *dysfusion* (*dys*) (Jiang and Crews, 2003; Samakovlis et al., 1996b). After meeting with their counterparts, the fusion cells undergo through highly orchestrated cell shape changes leading to ring shaped cells with high accumulation of *Drosophila* E-cadherin (*D*E-cad) and F-actin (Tanaka-Matakatsu et al., 1996).

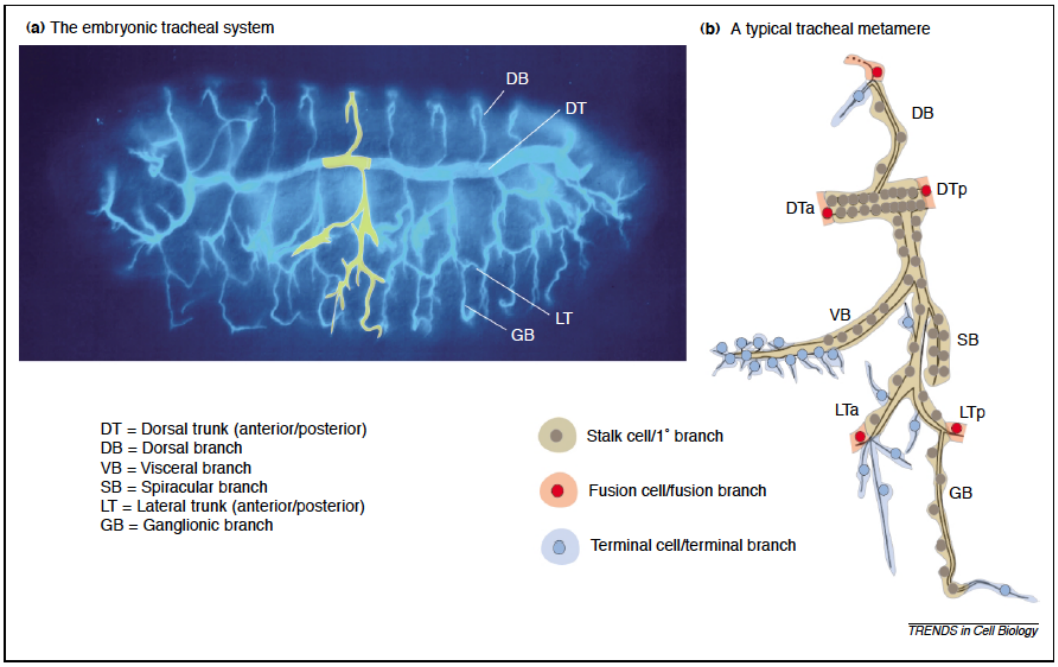

Figure 3: *Drosophila* tracheal tree: (a) Antibody staining against luminal antigens showing different types of branches in the *Drosophila* tracheal system at the end of embryogenesis. (b) Schematic representation of a typical tracheal metamere showing the location of fusion cells in red, terminal cells in blue and remaining cells, stalk cells and primary branch cells, in brown from (Uv et al., 2003).

3.3. Organization of the embryonic tracheal cells

The *Drosophila* embryonic trachea is composed of sheet of epithelial cells that have polarized cell membranes containing apical and basolateral domains (**Figure 4**). The apical domain of the tracheal cells facing the lumen is in contact with apical extra cellular matrix (ECM) whereas the basolateral domain is in contact with the neighboring tracheal cells and basal substratum (**Figure 4**).

The apical domain of plasma membrane of the tracheal cells contains a distinct region that is called subapical region (SAR, **Figure 4**). The complexes that form SAR function in many distinct cellular processes as well as functioning in the generation and/or maintenance of the apical-basal polarity (reviewed in Knust and Bossinger, 2002).

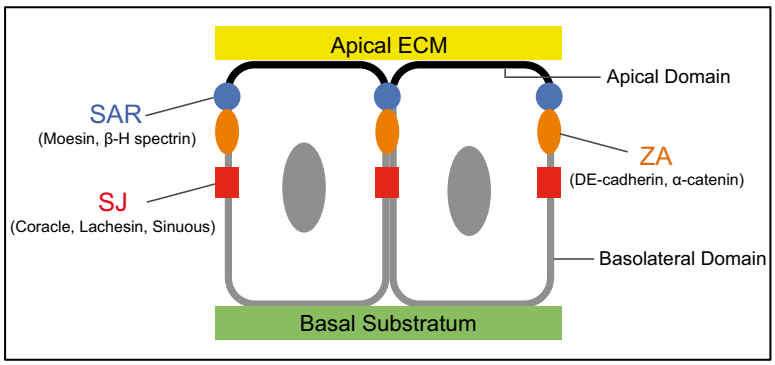

Figure 4: Organization and intercellular junctions of tracheal cells. *Drosophila* tracheal cells are epithelial cells with highly polarized plasma membranes containing two domains: apical and basolateral. The former faces apical extracellular matrix while the latter faces basal substratum. Intercellular junctions of the tracheal cells can be grouped into three groups: subapical region (SAR, in blue), zonula adherens (ZA, in orange) and septate junction (SJ, in red).

Just beneath the apical domain, zonula adherens (ZA) is located (**Figure 4**). This region is composed of many adherens junction molecules like DE-cadherin and α- catenin. The function of ZA components is to provide a close adhesion between the cells (Knust and Bossinger, 2002). Related to this function, the cellular level of DE-cadherin was published to play a crucial role in the process of intercalation which is exchanging places of the cells in a spatially oriented manner during tube elongation (Shaye et al., 2008). The second group of cell-cell junctions, located under ZA, is the septate junctions (SJs) that contribute to the barrier function of the tracheal cells (**Figure 4**). Interestingly, SJs have also been reported to function in the apical secretion of chitin modifiers Vermiform and Serpentine (Wang et al., 2006). Some of the SJ components are Coracle, Lachesin and Sinuous (Knust and Bossinger, 2002; Strigini et al., 2006; Wu et al., 2004).

3.4. Apical secretion and tube expansion

The apical plasma membranes of the cells facing the tracheal tube are in contact with the luminal extracellular matrix that is formed by a secretory burst depositing molecules like chitin, chitin deacetylases Vermiform and Serpentine and chitin binding proteins Gasp and Obstructor-A into the lumen (Jayaram et al., 2008; Luschnig et al., 2006; Norum et al., 2010; Tiklová et al., 2013; Tonning et al., 2005). This secretory burst immediately precedes tube expansion and is believed to directly contribute to it (**Figure 5**).

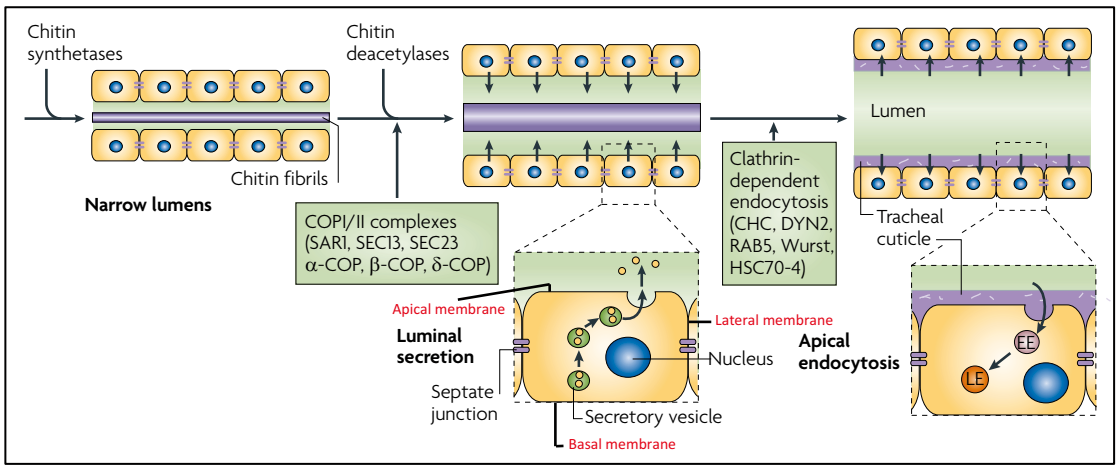

Figure 5: Apical secretion, tube expansion and clearance. During embryonic trachea development, three major events take place sequentially. First, an apical secretory burst that depends on COPI and COPII complexes occurs. Consequently, the lumens that are initially formed as narrow tubes expand. Chitin that is located inside the tracheal lumens modified by chitin deacetylases also plays a role in this expansion. At last, as the embryos come closer to hatching, the tracheal lumens gets cleared by clatherin dependent endocytosis leading to the degradation of luminal material passing through first early endosomes (EE) and then late endosomes (LE) from (Bryant and Mostov, 2008).

During embryonic development, the tracheal tubes grow in diameter (circumferential expansion) and length (axial expansion) until they achieve their characteristic branch sizes ranging from 0.2µm to 50µm (Manning and Krasnow, 1993). For each branch, this size differs. The widest tube, DT, expands two folds axially and three folds circumferentially from stage 14 to 16 in order to achieve its proper dimensions at the end of the embryogenesis (Beitel and Krasnow, 2000).

Mutations in many genes revealed several factors that are involved in axial and circumferential tube expansion. The axial tube expansion has been linked to septate-junction-dependent-deposition of chitin modifiers Vermiform and Serpentine into the lumen (Luschnig et al., 2006; Swanson et al., 2009; Wang et al., 2006). Alternative tube elongation mechanisms have emerged upon analysis of mutations in *convoluted* and *serrano* genes (Chung et al., 2009; Swanson et al., 2009). Additionally, disruption of Rho-Diaphanous-Myosin V transport, which is responsible for luminal deposition of chitin binding protein Gasp and ZP (Zona Pelicula) protein Piopio, also resulted in excessive tube length (Massarwa et al., 2009). More recently, mutant embryos for the gene encoding the tyrosine kinase Src42A showed that tube elongation is also controlled by axial cell surface expansion through Src42A-dependent recycling of E-Cadherin at adherens junctions (Förster and Luschnig, 2012).

Although tube elongation relies on many mechanisms that are chitin-independent, diametric tube expansion mainly relies on chitin that is located inside the tracheal lumen (intraluminal chitin filament). The tracheal tubes fail to expand uniformly in the absence of chitin synthesis, either due to either the lack of chitin synthase *kkv* or lack of an enzyme required for chitin biosynthesis (namely UDP-N-acetylglucosamine) coded by *mummy* (**Figure 6**) (Araújo et al., 2005; Beitel and Krasnow, 2000; Devine et al., 2005; Tonning et al., 2005). Non-uniform tube diameter was also observed upon overexpression of the genes encoding chitin binding proteins Gasp and Obstructor-A, and also in the absence of Knickopf and Retroactive proteins which are required for chitin filament assembly (Moussian et al., 2006b; Tiklová et al., 2013).

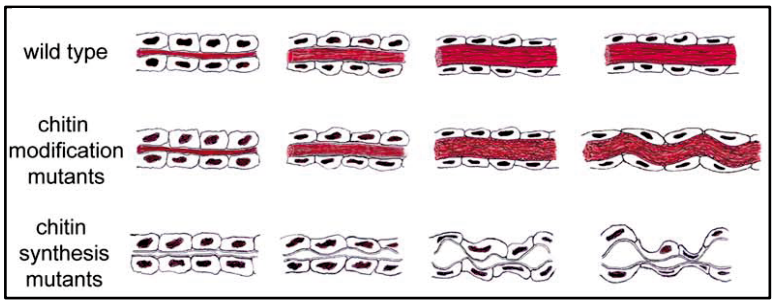

Figure 6: Diametric and axial tube expansion in the absence of chitin modifications and chitin synthesis. Schematic representation of the tube expansion process in four steps in wild type, chitin mutants and chitin synthesis mutants. The absence of chitin modifications and chitin synthesis affect tube expansion in a different manner. In chitin modification mutants the tracheal tube expands excessively axially while in chitin synthesis mutants, the tracheal tubes expand non-uniformly diametrically. Intraluminal chitin filament in red from (Luschnig et al., 2006).

3.5. Late stages of tracheal development: stage 16 and 17

During the last stages of embryogenesis three main tracheal events occur. The first one is the formation of taenidial folds, which starts around stage 15 a little bit earlier than the other two events (see next section for a detailed description of taenidial folds and their formation). The second main event is clearance of tracheal lumen from any solid and liquid material through clathrin dependent endocytosis (Tsarouhas et al., 2007). During tracheal development many luminal proteins along with chitin are deposited into the tracheal lumen. At the end of embryogenesis, tracheal tubes are cleared from these molecules and that allows filling of the lumen with gas, the third main event. As described by Tsarouhas *and collaborators*, upon

random appearance of the first gas bubble, the tracheal lumen fills with air in 10 minutes (Tsarouhas et al., 2007).

4. *Drosophila* cuticle

Apical extracellular matrices (aECM) play crucial roles in organ physiology and morphogenesis along with protecting the animal against physical and chemical damage, infection and dehydration. The *Drosophila* cuticle is an aECM produced by the epidermis, the tracheal, hind- and foregut epithelia. Composed of chitin, proteins and lipids, the insect cuticle has a layered structure compromising envelope, the protein rich epicuticle and the chitin rich procuticle (Moussian et al., 2005). Formation of this layered structure requires coordinated synthesis, distribution and modification of its components.

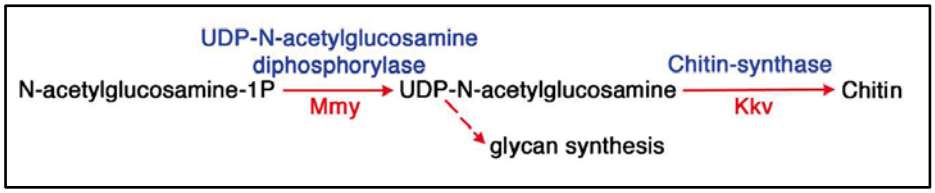

Figure 7: Biosynthesis of chitin in *Drosophila* tracheal system. Schematic representation of the reaction catalyzed by Mmy and Kkv from (Araújo et al., 2005).

One of the main components of *Drosophila* cuticle is the polymer of beta 1,4-N-Acetlyglucosamine (GlcNAc), also known as chitin. It is produced by a transmembrane chitin synthase as a result of the conversion of cytoplasmic uridine diphosphate-N-aceytlglucosamine (UDP-GlcNAc) into long polysaccharide chains (**Figure 7**) (Araújo et al., 2005; Merzendorfer and Zimoch, 2003). In the genome of *Drosophila* there are two chitin synthase genes: *Chitin Synthase-1*/*Krotzkopf verkehrt* (*CS-1*/*Kkv*) and *Chitin Synthase-2* (*CS-2*). While the former is required for the synthesis of chitin at the epidermis and tracheal system, the latter functions in hindgut epithelia (Moussian et al., 2005). It has been reported that the expression pattern of *kkv* transcript coincides with the first appearance of chitin in the tracheal system at stage 13 (Moussian et al., 2005). In the absence of *kkv* the tracheal tubes fail to accomplish uniform tube expansion (**Figure** 6) specifically at the fusion points that are formed by the fusion cells. Moreover, the apical surface of the non-fusion cells shows an expanded apical profile as well as irregular apical accumulation of β-H

spectrin indicating that lack of chitin synthesis causes subapical cytoskeletal organization defects (Tonning et al., 2005).

Interestingly, the lack of embryonic cuticle production is also observed in the absence of Halloween gene family members such as *shadow* (*sad*), *shade* (*shd*) and *disembodied* (*dib*) (reviewed in Gilbert and Warren, 2005). Failure to produce embryonic cuticle in the mutants of Halloween gene family members indicate that chitin synthesis is regulated by the insect steroid hormone ecdysone (Petryk et al., 2003).

4.1. Intraluminal chitin filament

In the tracheal system of developing *Drosophila* embryos, there are two chitin structures: intraluminal chitin filament and taenidial folds.

The intraluminal chitin filament is composed of parallel chitin polymers that form a chitin cylinder spanning the entire length of the tracheal tubes. Upon deposition of polysaccharide chitin into intracellular space, chitin deacetylases Vermiform and Serpentine modify its structure (Luschnig et al., 2006). Along with other luminal components, Vermiform and Serpentine contribute to the assembly of chitin filament (Jaźwińska et al., 2003; Luschnig et al., 2006; Moussian et al., 2006b; Tiklová et al., 2013). The intraluminal chitin filament has been reported to regulate the diametric tube expansion (Araújo et al., 2005; Devine et al., 2005; Tonning et al., 2005).

During embryonic development the chitin filament grows diametrically as the tracheal tubes expand circumferentially. Near the end of embryogenesis however, the chitin filament gets thinner and thinner until it is completely cleared from the lumen (**Figure 5**) (Moussian et al., 2006a; Tsarouhas et al., 2007).

4.2. Taenidial folds

Taenidial folds are cuticle ridges that form annular rings and run a helical course around lumen (**Figure 8**). These folds prevent the collapse of the tracheal tubes while allowing them to expand and contract. Because of this, the taenidial folds

have been resembled to the corrugated hose of a vacuum cleaner (Manning and Krasnow, 1993).

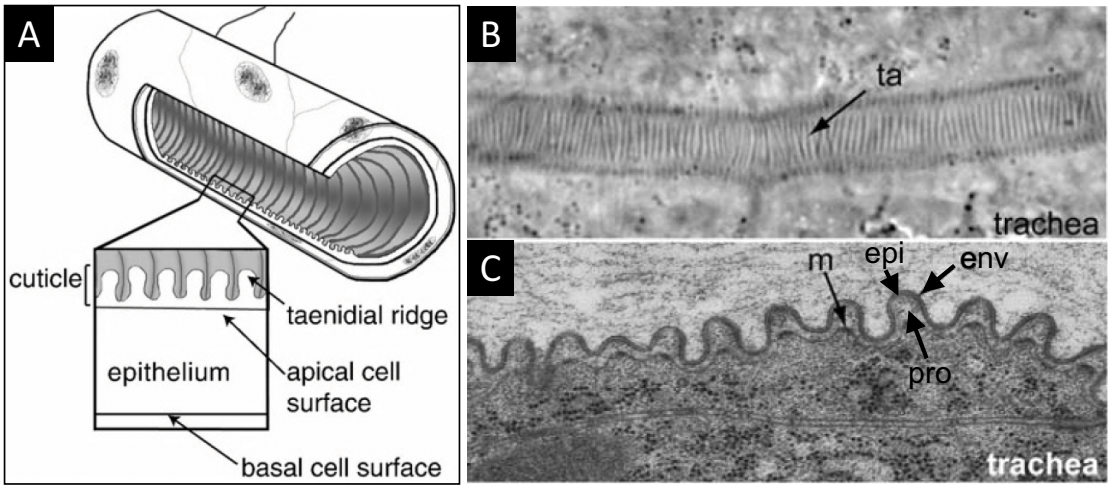

Figure 8: Taenidial folds structure. (A) Schematic representation of a mature tracheal tube with taenidial folds, shown magnified in the cross section. (B) Taenidial folds during late stages of embryogenesis visualized under the light microscope. (C) TEM analysis of a longitudinal of a tracheal tube showing the cell membrane (m) and layers of taenidial folds structure envelope (e), epicuticle (epi) and procuticle. Note the electron dense areas at the tips of each membrane folds (taken and/or adapted from Araújo et al., 2005; Glasheen et al., 2010; Kondo et al., 2007; Uv and Moussian, 2010).

The size of each fold varies depending on the size of the tube where they are located. In wide tracheal tubes formed by multiple cells, the fold depth can reach up to several micrometers which in narrow unicellular tubes it is around 50nm (Manning and Krasnow, 1993).

Using Transmission Electron Microscope (TEM) imaging, Moussian *and collaborators* visualized the chitin structures in the developing embryonic tracheal system and noticed that as one, the intraluminal chitin filament, is degraded, the taenidial folds are formed (**Figure 9**) (Moussian et al., 2006a). Formation of taenidial folds starts with the deposition of envelope fragments at late stage 15. Those fragments come together to produce a continuous envelope that covers the entire apical surface of the tracheal cells. At the same time, small periodic taenidial bulges with an outer lining of the envelope followed by the apical membrane of the cells emerge from the flat luminal surface. As the embryo develops, each taenidium grows in depth while the apical surface of the cells becomes flat under the taenidial folds (**Figure 9**).

Taenidial folds extend beyond the limits of single cells, spanning through multiple cells creating a supra-cellular structure. The origin of this supra-cellular structure has been a curiosity for scientists almost over a century (reviewed in Uv and Moussian, 2010). In 1929, Thomson suggested that the geometrical basis for the taenidial folds "results from some simple physical laws and is produced by forces, which are unaffected by the existence of cell boundaries in the tracheal epithelium and act simply in the chitinous lining at the moment when it is being secreted". Another theory from Locke (1958) stated that during cuticle expansion, which occurs axially and circumferentially, an axial restraint causes the cuticle buckle and form the taenidial folds. Recently, the observations of Uv and Moussian together with the observations of Matusek and collaborators unveil the involvement of the apical plasma membrane and cortical cytoskeleton in taenidial fold formation. First, the periodic electron dense points in the apical plasma membrane, which are believed to be the chitin synthesis complex, indicate a non-uniform chitin deposition resulting in repetitive organization of taenidial folds (**Figure 8C**) (Uv and Moussian, 2010). Second, just prior to chitin deposition, formation of repetitive apical F-actin cables that define the future position of taenidial folds are reported (**Figure 9G**) (Matusek et al., 2006). Although these theories and observations give us some hints about how the taenidial folds are originated, it is still unclear according to what the position of how the apical F-actin cables are formed at precise points, how the orientation of the taenidial folds are regulated, how do they communicate with each other to maintain the continuity of this supra-cellular structure, how do the individual cells contribute to the formation of this supra-cellular structure and what is the connection between actin cytoskeleton and cuticle deposition. The answers of these questions will be fundamental to our understanding of epithelial tube morphogenesis.

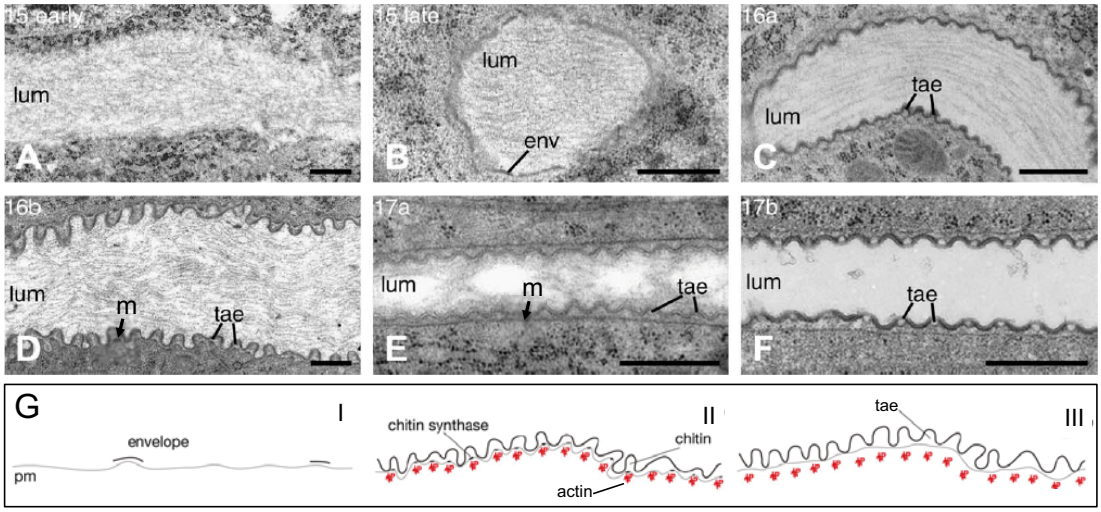

Figure 9: Dynamics of chitin structures via TEM analysis. Posterior cells of the dorsal trunk visualized at different stages of embryonic development. (A) Intraluminal chitin filament is visible inside the lumen (lum). (B) The envelope (env) is deposited as fragments. (C) The taenidial bulges (tae) become visible as the envelope becomes continuous. (D) The apical membrane of the cells (m), which follows the taenidial bulges at the beginning, becomes flatter. (E) Intraluminal chitin filament is getting cleared from the lumen as the apical membrane of the cells becomes flat under the taenidial folds. (F) Almost all intraluminal chitin filament is cleared from the lumen. (G) Schematic representation of a summary of taenidial fold formation that is shown A-F. Additionally, the actin bundles (red spots), that are located just below the plasma membrane (pm), are shown as underlaining bulges of taenidial folds (taken and/or adapted from Moussian, 2010; Moussian et al., 2006a).

4.2.1. Genes involved in formation of taenidial folds

In the literature there are a number of genes (listed in **Table 1**) that when mutated impair embryonic taenidial folds. According to the molecular function of their encoded proteins, these genes fall into 6 groups. The taenidial folds are formed by secretion of chitin into the aECM, thus it is not surprising that the most crowded group contains the genes involved in chitin metabolism: chitin synthesis genes *kkv* and *mummy*/cyst, chitin binding protein encoding genes *gasp* and *obst-A*, and chitin modifying enzyme encoding gene *verm*. Like many other developmental processes, the formation of taenidial folds are controlled by the activity of the genes through specific transcription factors, and hence the second most crowded group includes transcription factors encoding genes *Blimp-1*, *grh*, *peb*, and *ttk*. The involvement of septate junction proteins encoding genes *Lac* and *sinu*, as well as Arf1-COPI secretory pathway component encoding gene *garz*, and COPII complex component encoding gene *Sec24 CD* in taenidial fold formation can be explained by the reported activity of septate junctions and COPI/COPII complexes on secretion of Verm (Jayaram et al., 2008; Norum et al., 2010; Wang et al., 2006). The two extracellular

matrix (ECM) proteins encoding genes *conv* and *dp* might be involved in taenidial fold formation directly or indirectly by stabilizing the ECM.

Table 1: The genes involved in embryonic taenidial fold formation.
NA = not assigned

Gene	Encodes for	Reference
Gasp	chitin binding protein	(Tiklová et al., 2013)
kkv	chitin syntase	(Moussian, 2010; Moussian et al., 2005)
mummy	enzyme required for chitin synthesis	(Araújo et al., 2005)
obst-A	chitin binding protein	(Tiklová et al., 2013)
verm	chitin deacetylase	(Wang et al., 2006)
Blimp-1	transcription factor	(Ng et al., 2006)
grh	transcription factor	(Hemphälä et al., 2003)
peb	transcription factor	(Wilk et al., 2000)
ttk	transcription factor	(Araújo et al., 2007)
Lac	component of septate junction	(Strigini et al., 2006)
sinu	component of septate junction	(Wu et al., 2004)
conv	matrix organizing/cell adhesion protein	(Swanson et al., 2009)
dp	extracellular matrix protein	(Wilkin et al., 2000)
garz	component of Arf1-COPI secretory pathway	(Wang et al., 2012)
Sec24CD	cargo-binding subunit of COPII complex	(Förster et al., 2010; Norum et al., 2010)
pri/tal	NA	(Kondo et al., 2007)

The absence of the genes listed in **Table 1** effects taenidial folds in different ways. In *kkv* mutant embryos taenidial folds are described as occasionally flattened (Moussian, 2010; Moussian et al., 2005). In *mummy* mutant embryos taenidial folds are reported to be absent (Araújo et al., 2005). In the absence of *verm* and upon overexpression of *obst-A* and *gasp* taenidial folds are described as irregular with disorganized chitin-rich procuticle layer (Tiklová et al., 2013; Wang et al., 2006). In the loss of function of *pri/tal*, *Blimp-1*, *peb*, and *dp* taenidial folds are also reported to be absent (Kondo et al., 2007; Ng et al., 2006; Wilk et al., 2000; Wilkin et al., 2000). In mutants of *ttk* and *grh* taenidial folds are described as irregular in shape, size and pattern, and in places disrupted, respectively (Araújo et al., 2007; Hemphälä et al., 2003). In *conv* mutant embryos taenidial folds are described as abnormal, frequently misshapen and flattened (Swanson et al., 2009). In both *sinu* and *Lac* mutants taenidial folds are reported to have a highly irregular folding pattern (Strigini et al.,

2006; Wu et al., 2004). Finally, in the absence of *garz* taenidial folds are described as deformed and hollow (Wang et al., 2012).

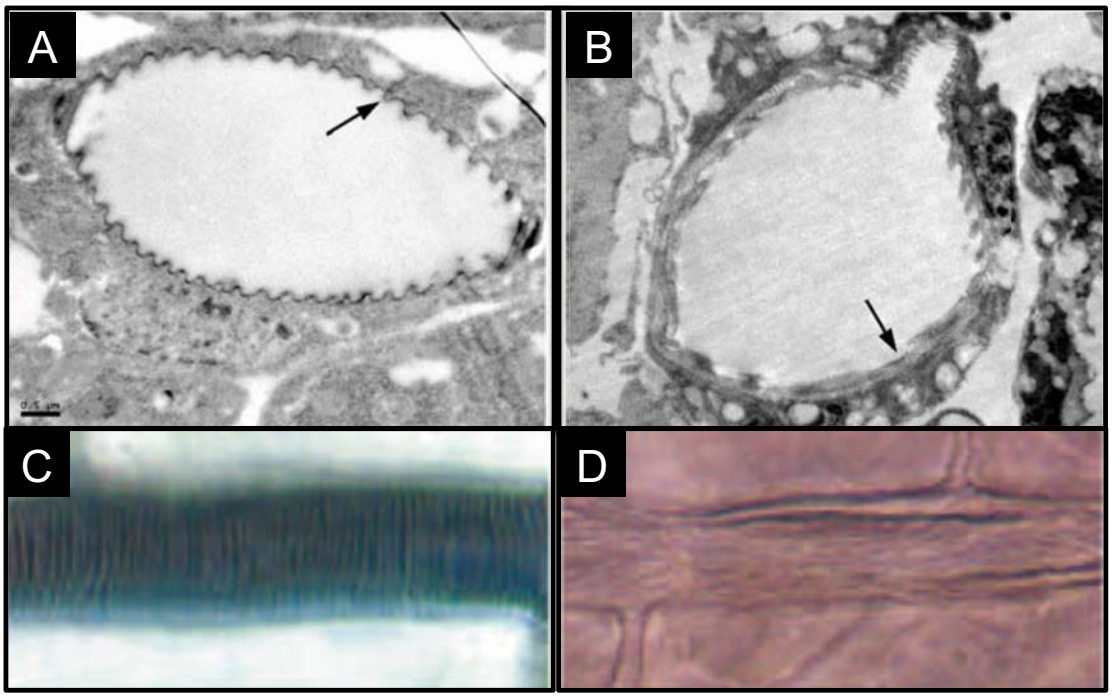

Figure 10: The taenidial folds in the absence of *Blimp-1* and *pri*. TEM images of the dorsal trunk of (A) a wild-type embryo and (B) a homozygous *Df(3L)Exel6106* (that spans *Blimp-1* gene region) mutant embryo. (A) Wild-type taenidial folds and (B) dramatically reduced and irregular taenidial folds in the absence of *Blimp-1* are indicated with arrows. Differential interference contrast images of the dorsal trunk in (C) wild-type and (D) pri^{1}/pri^{2} embryos (from Kondo et al., 2007; Ng et al., 2006).

The taenidial folds phenotype of *SecCD* mutant embryos reported in 2010 by Förster and collaborators. In the absence of the Halloween gene, *SecCD* (also known as *sten*), encoding for the cargo binding subunit of COPII complex, the taenidial folds fail to form (**Figure 11**). Strikingly, when the mutant phenotype is rescued with the GFP-Sten expression in random single cells, the authors observed that the taenidial folds are extended around the entire lumen covering the surface of the rescued cell and up to one cell diameter away from the surface of the rescued cell (**Figure 11**) (Förster et al., 2010).

Figure 11: The rescue of the taenidial folds phenotype in the *Sec24CD* mutant background. (A) Tracheal metameres 8-10 of a *Sec24CD* mutant embryo stained for chitin. GFP-Sten expression driven by *Abd-B-GALl4* rescues the taenidial folds phenotype at the posterior end of the embryo. (B) Mosaic analysis in which GFP-Sten expression is induced in random individual cells. Dorsal trunk of an embryo stained with chitin showing a rescued cell (the apical membrane outlined in orange) and two neighboring cells (the apical membranes outlined in blue). Note that the taenidial folds are also partially rescued in the neighboring cells (from Förster et al., 2010).

Among these genes, we have choosen to work with *Blimp-1* and *pri/tal* because as a result of their loss of function taenidial folds are reported to be absent. And also because of their previously published functions in other systems/organisms (see below).

4.2.1.a. B-lymphocyte-inducing maturation protein-1 (Blimp-1)

Drosophila Blimp-1 (*B-Lymphocyte Inducing Maturation Protein-1)* is the homolog of human *Prdm1* (*Positive regulatory domain containing 1*) that belongs to the Prdm family whose members contain a conserved N-terminal domain, known as positive regulatory domain (PR domain) (Buyse et al., 1995; Tunyaplin et al., 2000). This domain has been related to the SET methyltransferase domain that is important for the regulation of chromatin-mediated gene expression (Huang et al., 1998). As the other members of the family, Blimp-1 contains the PR domain however the experimental evidence implies that Blimp-1 requires other proteins to execute its methyltransferase activity (**Figure 12**) (reviewed in Bikoff et al., 2009). In mammalian B cells, for example, Blimp-1 associates with the methyltransferase, G9a, and in mouse germ cells it interacts with arginine methyltransferase Prmt5 to regulate gene expression patterns (Ancelin et al., 2006; Győry et al., 2004).

In all Prdm family members except one, Prdm11, the PR domain is followed by a variable number of zinc finger repeats (Fumasoni et al., 2007; Kinameri et al., 2008; Sun et al., 2008). Blimp-1 contains five zinc finger motives that mediate nuclear import, DNA binding and recruitment of histone modifier enzymes

(Tunyaplin et al., 2000). In addition to its PR and zinc finger domains, Blimp-1 also contains a proline-rich domain through which it interacts with repressor proteins such as Groucho, LSD1 and HDAC2 (**Figure 12**) (Ren et al., 1999; Su et al., 2009; Tunyaplin et al., 2000; Yu et al., 2000).

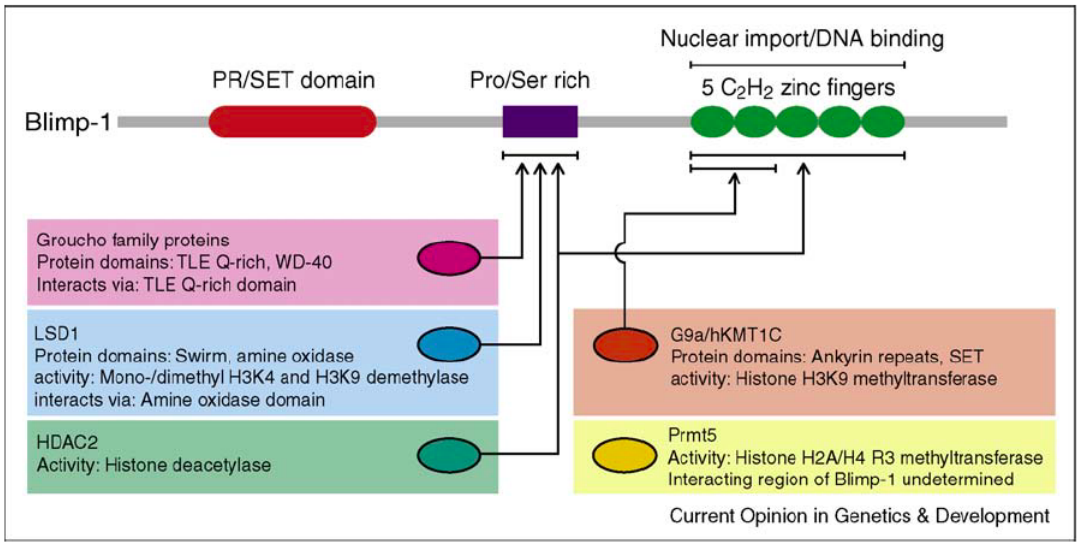

Figure 12: Gene structure of Prdm1/Blimp-1 and its interactions with epigenetic modifiers. Schematic representation of Prdm1/Blimp-1 gene region that contain a PR/SET domain, a Proline/Serine rich domain and five zinc finger motives. Via its Pro/Ser rich and zinc finger domains Prdm1/Blimp-1 interacts with epigenetic modifiers to regulate differentiation from (Bikoff et al., 2009).

Prdm1 was originally identified in humans as a transcription repressor that binds to the positive regulatory domain of the interferon β promoter, silencing the β interferon gene (Keller and Maniatis, 1991). Three years later, Blimp-1 was independently identified in the mouse immune system as the primary regulator of B cell differentiation (Turner et al., 1994). The sequence similarities between these two genes led Shi Huang to analyze and report that Blimp-1 is the murine homolog of human Prdm1 (Huang, 1994).

Blimp-1 controls cell fate decisions in the embryo of many organisms (reviewed in Bikoff et al., 2009; Hohenauer and Moore, 2012). In mouse embryos, for example, Blimp-1 functions in the generation of pluripotent primordial germ cells (Ohinata et al., 2005). During mouse and zebrafish photoreceptor development, *Blimp-1* plays a role in stabilization or maintenance of the photoreceptor identity (Brzezinski et al., 2010; Katoh et al., 2010). Another conserved role of Blimp-1 in

vertebrates is controlling the limb outgrowth in mouse and zebrafish embryos (Mercader et al., 2006; Robertson et al., 2007).

Up to date, there are only a few reports focusing on Blimp-1 in the developing *Drosophila* embryo. The first one published in 2006 by Ng and collaborators reveals the function of *Blimp-1* in the terminal differentiation of the tracheal system (see below) (Ng et al., 2006). In the second report, *Blimp-1* has been identified as an ecdysone inducible gene, which product binds and regulates the *ftz-f1* gene (Agawa et al., 2007). By acting as a transcriptional repressor *Blimp-1* prevents premature expression of *ftz-f1*. *Ftz-f1* (*Ftz transcription factor 1*) is another ecdysone-inducible gene that encodes a transcription factor functioning in the activation of a homeobox segmentation gene *fushi tarazu* (Agawa et al., 2007; Ueda and Hirose, 1990). In the third report, the authors present more evidence on the ecdysone regulating the expression of *Blimp-1* during embryonic development (Chavoshi et al., 2010).

In their report, Ng and collaborators describe the expression pattern of *Blimp-1* and show that it is expressed in different cell linages from early stages of the embryonic development. They stated that in the epidermal and tracheal cells the expression starts at stage 12 and stage 14, respectively. The authors also report that in the absence of *Blimp-1*, the shape of the tracheal tubes is disrupted and look like string of sausages (**Figure 13B**). At the same time, the tracheal cells appear to be larger and rounder compared to the wild-type and lack taenidial folds (**Figures 10B, 13H**). All these results together with the junctional disorganization revealed with immunostaining of septate junction component Coracle (**Figure 13F**) and the altered localization of apical surface protein Fat-like (**Figure 13D**) lead the authors to suggest that organization of apical luminal surface of the tracheal cells is compromised in the absence of *Blimp-1* function. Moreover, the authors also reported that upon overexpression of *Blimp-1,* DT of the embryo shows luminal constrictions and interruptions (**Figure 13I**) (Ng et al., 2006).

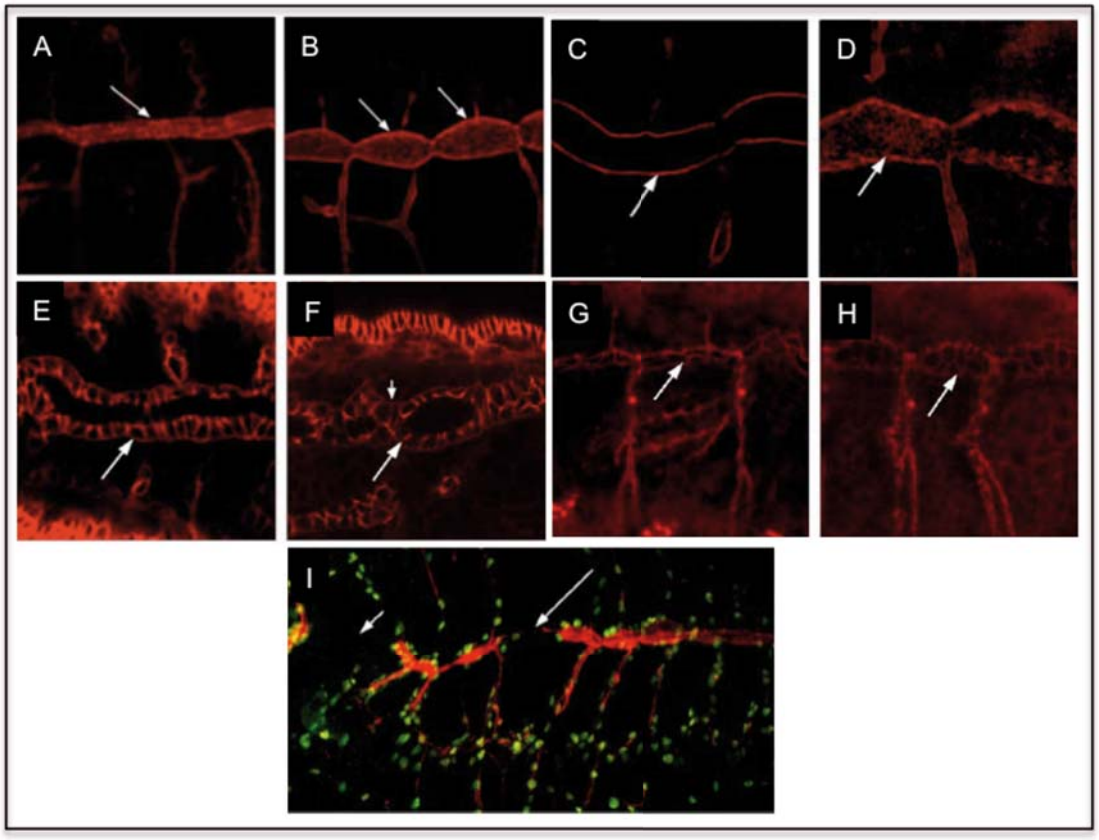

Figure 13: Tracheal phenotypes associated with *Blimp-1*. Stage 16 (A) wild-type and (B) homozygous *Df(3L)Exel6106* (that spans *Blimp-1* gene region) mutant embryos stained with luminal marker 2A12. Tracheal lumen with (A) a uniform diameter and (B) a sausage shape. Stage 16 (C) wild-type and (D) homozygous *Df(3L)Exel6106* mutant embryos showing apical localization of Ftl. (C) The normal staining of Ftl in wild-type (D) is altered into a diffused staining in the mutant embryoStage 16 (E) wild-type and (F) homozygous *Df(3L)Exel6106* mutant embryos showing normal localization of Cor in SJs. Note the junctional disorganization in the mutant embryo (short arrow in panel F).. Stage 16 (G) wild-type and (H) homozygous *Df(3L)Exel6106* mutant embryos stained with anti-DE-cad to label the apical cell surface. Note the larger and rounder shape of apical cell surface in homozygous *Df(3L)Exel6106* mutant embryos (H). (I) Stage 16 *btl-gal4*; *UAS-blimp-1* embryo stained with luminal marker 2A12 and antiGFP, showing luminal constriction (long arrow) and interruption (short arrow) in the dorsal trunk (from Ng et al., 2006).

In addition to its function in the embryonic development, *Drosophila Blimp-1* is also reported to function during prepupal periods. As in the case of embryonic stages, ecdysone regulates the expression of *Blimp-1* and Blimp-1 acts as a transcriptional repressor that prevents premature expression of *ftz-f1* during prepupal stages (Agawa et al., 2007). Interestingly, it has been also shown that ectopic expression of *Blimp-1* causes a delay in pupation indicating that *Blimp-1* plays an important role in the developmental timing of the organism (Agawa et al., 2007).

4.2.1.b. Polished rice (pri)

Polished rice (*pri*, also known as tarsalless (*tal)*) is a gene initially thought to encode for non-protein coding RNAs but that has been later found to encode four similar peptides whose length is changing from 11 to 32 amino acids (Kondo et al., 2007). The gene structure of *pri* is shown in **Figure 14**. The *pri* gene contains 10 sORFs; among them, only five are transcribed (as a polycistronic mRNA) and from them, only four are translated (Kondo et al., 2007).

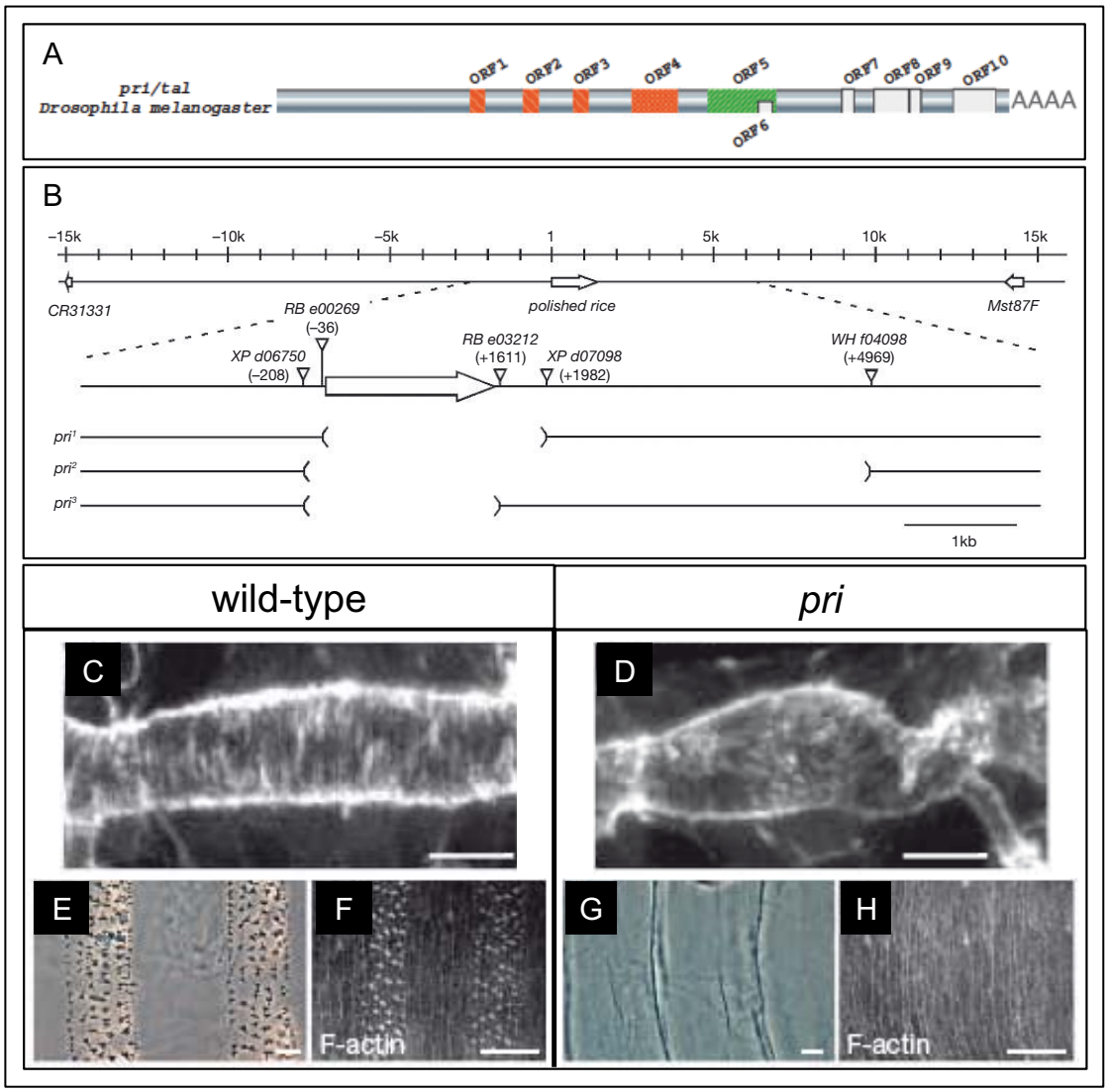

Figure 14: Gene structure and mutant phenotypes of of *pri/tal*. (A) Schematic representation of *Drosophila pri/tal* gene region containing 10 open reading frames from which only first 5 of them are known to be transcribed and only first 4 of them are known to be translated (from Hashimoto et al., 2008). (B) Schematic representation of deficiency chromosomes that uncovered the *pri gene*. GFP fluorescence of *btl-GAL4-UAS-GFP-Moe* in (C) wild-type and (D) pri^1/pri^3 embryos showing (C) parallel F-actin bundles in the wild-type embryo and (D) disorganized F-actin in the *pri* mutant embryo. Cuticle preparations (E, G) and phalloidin stainings of (E, G) wild-type (D, E) and pri^1/pri^2 (F, H) embryos. (F, G) Note that both the denticle belts and the F-actin are absent in mutant embryos (from Kondo et al., 2007).

During *Drosophila* embryonic development, *pri* mRNA is expressed in the epithelial cells forming the tracheal system and the epidermis. *Pri* was shown to function in two actin-based morphogenesis events: formation of denticle belts at the epidermis and taenidial folds in the tracheal system (Kondo et al., 2007).

Denticle belts are chitin structures that require filamentous F-actin assembly for their generation (Delon et al., 2003; Price et al., 2006; Walters et al., 2006). During the formation of denticle belts, *pri* acts as a post-translational modifier that converts the transcription factor Shavenbaby (Svb) from a repressor to an activator (Kondo et al., 2010). *Svb* is essential for the apical F-actin extensions at the site of denticle belts (Delon et al., 2003). In the absence of *pri* both the denticle belts and the F-actin assembly are disturbed, which can be attributed to the lack of Svb as an activator (**Figure 14**) (Kondo et al., 2010).

As in the case of denticle belts, F-actin assembly located under the taenidial folds plays an essential role in their formation (Matusek et al., 2006). In the absence of *pri* both the taenidial folds and the F-actin bundles failed to form (**Figure 10, Figure 14**) (Kondo et al., 2007). Unlike denticle belts, though, *svb* does not play a role in taenidial fold formation and it does not function downstream of *pri* during this process (Kondo et al., 2010).

In addition to its function in trachea and epidermis morphogenesis, *pri* also functions in leg, wing and external sensory organ development (Matusek et al., 2006; Pi et al., 2011; Pueyo and Couso, 2011; Pueyo and Couso, 2008). During leg development, two functions of *pri* have been reported. One of them occurs during mid third-instar leg development while the other one takes place at pupa. In the former *pri* triggers a signal that patterns the activity of tarsal boundary and regulates the expression of several genes (Pueyo and Couso, 2008). In the latter function, Pri peptides control Notch signaling, which plays a role in segmentation of the *Drosophila* leg (Pueyo and Couso, 2011). Finally, during wing and external sensory organ development, overexpression of *pri* promotes sensory organ precursors and wing specification while suppressing DV-boundary formation (Pi et al., 2011).

4.2.2. Lessons from larval taenidial folds

The taenidial fold formation is a repeated process that takes place in embryogenesis as well as each larval molting. Although some of the genes (*peb*, *obst-A* and *SecCD*) that are reported to function in the embryonic taenidial fold formation have been also reported to play a role in this process during larval development, it is not known whether the remaining genes involved in larval taenidial fold formation (*Mmp1*, *Hr78*, *DAAM*, *uif*, *Src42A* and *Tec29*/*Btk29A*) are involved in the embryonic taenidial fold formation. Yet, the information obtained via those larval genes gives us some insights about the players of this process and how exactly this process occurs.

In 2006, Matusek and collaborators reported some crucial aspects of the larval taenidial fold formation. 1) They discovered the existence of apical F-actin bundles that run perpendicular to the tube axis and the number of those rings and taenidial folds reported to be equal to each other. 2) The disturbance of apical F-actin cables through the absence of *Drosophila* formin DAAM (Dishevelled-associated activator of morphogenesis), results in formed but disorganized taenidial folds. This observation revealed the importance of F-actin cables in the formation of taenidial folds. 3) The authors reported that F-actin cables are located at the level of adherens junctions raising the possibility that neighboring cells might be communicating through their adherens junctions to determine the position of F-actin cables and thus the position of taenidial folds. 4) The authors noticed that the fusion cells secrete a different kind of cuticle that has a dotty pattern instead of parallel running apical ridges of taenidial folds. 5) Through epistasis analysis the authors showed that two non-receptor tyrosine kinases, Src42A and Tec29, work with *DAAM* in organizing the cytoskeleton and determining the pattern of taenidial folds. 6) The authors reported that actin is disorganized in DAAM and Tec29 mutant embryos (Matusek et al., 2006).

Another report published by Glasheen and collaborators revealed that the larval tracheal tubes elongate between molts by increasing their intertaenidial distance. But the distance between the newly formed taenida at molts is not affected by the taenidial folds formed at earlier steps, suggesting that taenidial spacing is driven by intracellular processes rather than the preceding taenidia at the aECM.

Additionally, the authors showed the importance of an extracellular component, Matrix metalloproteinase 1 (Mmp1), in taenidial expansion and tube elongation. Mmp1 localizes in periodically spaced puncta that are in register with the taenidial spacing and in its absence the taenidial interval remains fixed and the larvae do not elongate their trachea as their bodies grow in size (Glasheen et al., 2010).

The larval phenotypes of genes in the ecdysteroid pathway, such as the orphan receptor Hr78, indicates the importance of ecdysone also in the formation of taenidial folds (Fisk and Thummel, 1998).

OBJECTIVES

Taenidial folds are specialized derivatives of the extracellular matrix (ECM) that extend beyond the limits of single cells. They span through multiple cells creating a supra-cellular structure. The main aim of this project is to use taenidial folds as a model system for ECM patterning and to understand how cells collaborate to create a supra-cellular structure. In particular, we address this aim by means of studying *Blimp-1* and *pri*, two genes known to be required for taenidial fold formation. We aim to achieve this goal by:

1. Characterizing the formation of taenidial folds and F-actin bundles in *wild-type* embryos.
2. Analyzing the detailed expression pattern of *Blimp-1* and *pri*.
3. Analyzing mutant phenotypes of *Blimp-1* and *pri* on taenidial folds and F-actin bundles.
4. Revealing new downstream and upstream factors of *Blimp-1* and *pri*.
5. Revealing new genes involved in taenidial fold formation.
6. Analyzing how do the single cells contribute to the formation of this supra-cellular structures.

MATERIALS AND METHODS

1. Materials

Biological Materials

Unless stated otherwise, all the *Drosophila Melanogaster* strains were raised at 25°C under standard conditions and all the overexpression and the RNA interference experiments were carried out, using GAL4/UAS system, at 29°C (Brand and Perrimon, 1993). The mutant chromosomes were balanced over LacZ or GFP marked balancer chromosomes. The fly stocks used in the experiments are listed and described in **Table 2**. The embryos were staged as described in "Stages of *Drosophila* Embryogenesis" by Campos-Ortega and Hartenstein (Campos-Ortega and Hartenstein, 1997)**.**

Table 2: Fly strains used during the study. The following abbreviations are used: Chr. = Chromosome number; BDSC = Bloomington *Drosophila* Stock Center; TDSC= Tubingen *Drosophila* Stock Collection; CIS = Created in the course of the study.

Allele /Construct	Chr.	Description	Origin
y^1w^{118}	I	used as the *wild-type*	J. Casanova
Blimp-1 mutant 1	III	*Bimp-1* mutant allele created via P-element insertion in the *Blimp-1* gene region	BDSC 15195
Blimp-1 mutant 2	III	*Blimp-1* mutant allele created via P-element insertion in the *Blimp-1* gene region	BDSC 205941
pri^1	III	*pri* mutant allele created via deletion of *pri* gene region via Flp-FRT recombination	S. Hayashi
pri^2	III	*pri* mutant allele created via deletion of *pri* gene region via Flp-FRT recombination	S. Hayashi
pri^3	III	*pri* mutant allele created via deletion of *pri* gene region via Flp-FRT recombination	S. Hayashi
Blimp-1$^-$, *pri*$^-$	III	*Blimp-1* mutant allele recombined pri^3 allele	CIS
shd^2	III	*shd* mutant allele created via EMS mutagenesis	TDSC
vvl^{6A3}	III	*vvl* mutant allele created via X-ray	J. Casanova
kkv^1	III	*kkv* mutant allele created via EMS mutagenesis	B. Moussian
knk^{7A69}	III	*knk* mutant allele created via EMS mutagenesis	B. Moussian
Tec29 mutant	II	*Tec29* mutant allele created via P-element insertion in the *Tec29* gene region	BDSC 102398
$DAAM^{Ex68}$	I	Excision allele of *DAAM* created via remobilization of two P-elements	J. Mihaly
$Src42A^{E1}$	II	*Src42A* mutant allele created via EMS mutagenesis	BSC 6408
Src24A.CA	II	Constitutively active form of *Src42A*	S. Lusching
Src42A.DN	III	Dominant negative form of *Src42A*	S. Lusching
svb^{R9}	I	Imprecise excision allele of the svb^{107} insertion	F. Payre
sn^{AL2}	I	*sn* mutant allele created via P-element insertion in the *sn* gene region	BDSC 845
f^{36a}	I	*f* mutant allele created via springer transposon insertion in the *f* gene region	BDSC 43

sn^{3}, *f*^{36a}	I	*sn* mutant allele recombined with *f* mutant allele	M. Llimargas
UAS constructs			
UAS-dstal-RNAi	II	UAS fused to *pri-RNAi*	J.P. Couso
UAS-Blimp-1-RNAi	II	UAS fused to *Blimp-1-RNAi*	S. Roy
UAS-α-cat-RNAi	II	UAS fused to *alpha-catenin-RNAi*	BDSC 38987
UAS-Blimp-1 72.1	III	UAS fused to *Blimp-1* gene	S. Araújo
UAS-Blimp-1 40.2	II	UAS fused to *Blimp-1* gene	S. Araújo
UAS-tal^{e1}	III	UAS fused to *pri* gene	J.P. Couso
UAS-SrcGFP	II	UAS fused to *SrcGFP* construct that marks the plasma cell membrane	S. Luschnig
UAS-Blimp-1, UAS-SrcGFP	II	*UAS-Blimp-1* recombined with *UAS-SrcGFP* construct	CIS
UAS-cd8GFP	III	UAS fused to *cd8GFP* construct that marks the plasma cell membrane	BDSC 5137
GAL4 drivers			
btl-GAL4	II	GAL4 fused to *btl* promoter	M. Affolter
btl-MoeGFP	III	*btl* promoter fused to *MoesinGFP* construct that marks the F-actin structures inside the cell	S. Hayashi
Blimp-1^{-}*, btl-MoeGFP*	III	*Blimp-1* mutant allele recombined with *btl-MoesinGFP* construct	CIS
pri3, btl-MoeGFP	III	*pri*^{3} mutant allele recombined with *btl-MoesinGFP* construct	CIS
hsFLP^{122}*; btlRFPMoe, btl >y*$^{+}$ *>GAL4*	I, II	Heat shock *FLIP* promoter activating *btl-GAL4* to generate clones	M. Affolter
AbdB-GAL4	III	GAL4 fused to *AbdB* promoter	E. Sanchez
AbdB-GAL4, Blimp-1^{-}	III	*Blimp-1* mutant allele recombined with *AbdB-GAL4* driver	CIS
AbdB-GAL4, pri^{3}	III	*pri* mutant allele recombined with *AbdB-GAL4* driver	CIS
AbdB-GAL4, UAS-cd8GFP	III	*UAS-cd8GFP* construct recombined with *AbdB-GAL4* driver	CIS

1.2. Chemicals, Buffers, Enzymes and Supplies

All the chemicals, buffers, enzymes and supplies used in this study and their suppliers are listed in **Table 3**.

Table 3: Chemicals, buffers, enzymes and supplies used in the course of the study.

Name	**Supplier**
Genomic DNA Purification Kit	Thermo Scientific
Chemicals	
Tween 20	Sigma
Triton	Roche
BSA	Roche
Formaldehyde	Panreac AppliChem
Heptane	Panreac
MeOH	Panreac AppliChem
Triton	Roche
EDTA	Sigma-Aldrich
NaOAc	J. T. Baker
EtOH	Panreac
Buffers	
10X PCR Buffer (with MgCl)	Biotools
1X Transcription Buffer	Fermentas
Enzymes	
T3/T7	Fermentas
Taq polymerase	Biotools

Supplies	
dNTP Mix	Thermo Scientific
Cy3 Amplification Reagent	NEN Life Sciences
TSA Amplification Diluent	NEN Life Sciences
DIG RNA labeling mix	Roche
RNasin	Roche
DNasin	Roche
Paint Pellet	Novagen
Fluoromount	Sothern Bitech
Oil 10-S	VWR

1.3. Solutions

The solutions used in this study and their contents are listed in **Table 4**.

Table 4: Contents of solutions utilized in the course of the study.

Solution	Content
PBT	1X PBS 0.1% Tween 20
PBT+BSA Solution	1X PBS % 0.5 BSA % 0.1 Tween20

1.4. Antibodies, Stains and Probes

During this study one stain, two probes and several antibodies were used (all are listed in **Table 5**.). The stain Fluostain (also known as Fluorescent Brightener 28) has been reported to label the chitin structures, specifically chitin fibrils, in *Drosophila* embryos (Araújo et al., 2005). The stain was utilized as follows. After the Fluostain powder was dissolved in distilled water (1µg/1ml), the solution was used in the same step as the secondary antibodies during the antibody staining. The Chitin binding probe (CBP) has been reported to bind to chitin structures and as in the case of Fluostain, CBP was used as a secondary antibody during the antibody staining (Araújo et al., 2007). The second probe Phalloidin is a toxin that is isolated from the deadly Amanita phalloides "death cap" mushroom and it has been reported to selectively label F-actin (Wulf et al., 1979). In this study, Phalloidin conjugated to Alexa-555 was used to detect F-actin structures in the *Drosophila* embryo and it was utilized as a secondary antibody during the antibody staining.

Table 5: Antibodies, stains and probes used in the course of the study.
* not produced anymore.

Name	Antigen	Species	Dilution	Supplier/Origin
Stains/Probes				
CBP	chitin	-	1:250	NEB*
Fluostain	chitin	-	1:250	Sigma
Phalloidin	F-actin	-	1:100	Sigma-Aldrich
Primary Antibodes				
Blimp-1	Blimp-1	guinea	1:500	S. Roy
trh	trh	rat	1:500	N. Martín
2A12	2A12	mouse	1:50	DSHB
DE-cad	DE-cad	rat	1:50	DSHB
dysfusion	dysfusion	rabbit	1:50	S. T. Crews (Check)
knk	knk	rabbit	1:250	A. Uv
verm	verm	rabbit	1:250	S. Lusching
pio	pio	rabbit	1:20	M. Affolter
GFP	GFP	rabbit	1:500	Molecular Probes
pSrc	Src	rabbit	1:50	Invitrogen
spectrin	spectrin	mouse	1:20	DSHB
βGAL	βGAL	chicken	1:500	Cappel
POD-conjugated anti-Dig	Dig	-	1:1000	Roche
Secondary Antibodies				
Alexa 488	rabbit	donkey	1:500	Jakson ImmunoResearch
Alexa 488	rat	donkey	1:500	Jakson ImmunoResearch
Alexa 488	mouse	donkey	1:500	Jakson ImmunoResearch
Alexa 555	rat	donkey	1:500	Jakson ImmunoResearch
Alexa 647	guinea pig	donkey	1:500	Jakson ImmunoResearch
Biotinylated IgM	mouse	goat	1:500	Jakson ImmunoResearch

2. Methods

2.1. Molecular Biological Techniques

2.1.1. Isolation of Genomic DNA

Genomic DNA of *wild-type* flies was isolated using "Thermo Scientific Genomic DNA Purification Kit". First, the adult flies were homogenized in a micro-centrifuge tube containing 180µl Digestion Solution. Then the sample was treated with 20µg Proteinase K Solution and incubated at 56°C for 30 minutes. After, 20µl of RNase A Solution was added into the tube and the tube was incubated for 10 minutes at the room temperature. Then 200µl of Lysis Solution was added into the tube and sample was vortexed for 15 seconds. The last step was repeated with the addition of

400µl of 50% ethanol. The solution in the tube was transferred to a GeneJet DNA Purification Column inserted in a collection tube. The tube was then centrifuged for 1 minute at 6000rpm and the collection tube containing the flow-through solution was discarded. The GeneJet DNA Purification Column was placed into a 2ml collection tube. 500µl of Wash Buffer I was added into the tube and it was centrifuged for 1 minute at 8000rpm. Then the flow-through was discarded and the purification column was placed back into the collection tube. The last two steps were repeated with 500µl of Wash Buffer II and 3 minutes centrifugation at maximum speed. Finally, 200µl of Elution Buffer was added to the center of the GeneJet DNA Purification Column, the sample was incubated at room temperature for 2 minutes, and then centrifuged at 8000rpm for 1 minute. The isolated genomic DNA was stored at -20°C and used as a template for PCR reactions.

2.1.2. Synthesis of RNA probes for in-situ hybridization

With the aim of performing *in-situ hybridization* on *pri*, we synthesized the RNA probes using the PCR-based technique (David and Wedlich, 2001). The interested pri gene region (524bp, covering all coding Open Reading Frames (ORFs) of the gene) was defined, and the forward (5'TAATACGACTCACTATAGGTTTTTGGTCAATACACGGCA3') and reverse (5'AATTAACCCTCACTAAAGGAGTTTGTGGATAAGGCACGG3') primers were designed accordingly so that the PCR product carries the two RNA promoters: T3 (underlined sequence on the forward primer) and T7 (underlined sequence on the reverse primer). The interested gene region, flanked by T3 and T7 sequences, was amplified from previously isolated genomic DNA via PCR under standard PCR conditions using Taq-Polymerase (35 cycles and 60°C annealing temperature). 10µl of the PCR product was used as a template DNA for *in vivo* transcription of the sense and antisense probes while Dig-labeling was incorporated into them for 2 hours at 37°C. The remaining DNA in the medium was eliminated by addition of 2µl of DNase I and incubation of the sample at 37°C for 15 minutes. The reaction was stopped by adding 2µl of 0.5M EDTA (pH8). The newly synthesized RNA was precipitated using Paint Pellet by introducing 1µl of Paint Pellet, 2.5µl of NaOAc and 50µl of EtOH (100%) to the 25µl reaction mix, and keeping the resulting solution at room temperature for two minutes. Then the sample was centrifuged at 13000rpm for

5 minutes and the pellet was washed with EtOH (75%). Finally, the RNA probe was re-suspended in 20µl of hybridization buffer and stored at -20°C.

2.2. Histological Techniques

2.2.1. Cuticle preparation of embryos

The adult flies were put into cages containing yeast paste as the food source on peach juice agar plates in order to collect the eggs laid overnight. These eggs were then dechorionated with bleach for 3 minutes and rinsed with Trition 0,1%. With the help of a brush, they were gathered and put into a tube containing 2ml of PBS for the cuticle preparations with viteline membrane. For the cuticle preparations without viteline membrane the embryos were instead put into a tube containing 2ml of heptane and 2ml of methanol, the tube was placed on a rotator for 5 minutes, the embryos were collected from the bottom of the vial and placed in an micro-centrifuge tube, and washed once with methanol and twice with Triton 0,1%. The embryos were then recovered with a Pasteur pipette and spread on a microscope slide. Next, the embryos were dried with a tissue paper using its capillarity. Then Hoyer/Lactic that clears the soft tissue leaving behind the viteline membrane and cuticle was placed on the embryos. The slides were covered with coverslips and they were left at 56°C overnight.

2.2.2. Fixation of embryos

Upon collection of eggs laid overnight on agar plates, these were dechorionated with bleach for 3 minutes and rinsed with Trition 0,1%. With the help of a brush, they were collected and put into bottles containing the fixing solution: 4% formaldehyde for fixing the tissue (except for anti-Pio staining, for which 11% formaldehyde was used (Jaźwińska et al., 2003)), 2ml of heptane for creating holes in the viteline membrane, and 2ml of PBS for generating the medium for the function of formaldehyde. The bottles were placed on a rotator for 15-20 minutes (except for DE-cad staining, for which they were kept in the fixing solution for 10 minutes). After the removal of the bottom phase, which contains PBS and formaldehyde, 2ml of methanol was added to each tube and the tubes were vortexed for 30 seconds. The bottom phase containing devitelinated embryos and methanol were transferred into new tubes. Then they were washed with methanol twice and stored at -20°C.

2.2.3. Antibody staining of embryos

After the fixation the embryos were washed three times with PBT for 10 minutes and blocked for one hour in PBT+BSA solution. The embryos were then incubated with primary antibodies overnight at 4°C. After the removal of the primary antibodies, samples were washed three times in PBT for 10 minutes. Then the necessary secondary antibodies, stains and probes were added and samples were incubated at room temperature for 2 hours in the dark. After three washes for 10 minutes in PBT, embryos were mounted in the mounting medium Fluoromount. All primary and secondary antibodies, stains and probes, were diluted in PBT+BSA solution and their working dilutions are listed in **Table 5**.

2.2.4. Antibody staining of larval tissues

Wandering third instar larvae were dissected in PBS. The dissected mouth and trachea complexes were fixed in 4% formaldehyde (in PBS) for 20 minutes at room temperature. After three washes for 10 minutes in PBT, samples were blocked for one hour in PBT+BSA solution. Then the samples were incubated in primary antibodies overnight at 4°C. After removing the primary antibody, samples were washed in PBT for 10 minutes for three times. Then the samples were again blocked in PBT+BSA solution for 30 minutes. Upon the addition of necessary secondary antibodies, stains and probes the samples were incubated at room temperature for 2 hours in the dark. After three washes in PBT for 10 minutes, tracheas were seperated from mouth parts and mounted in Fluoromount. All primary and secondary antibodies, stains and probes were diluted in PBT+BSA solution and their working dilutions are listed in **Table 5**.

2.2.5. 2A12 staining

Previously fixed embryos were washed three times with PBT for 10 minutes and blocked with PBT+BSA solution for 30 minutes. After adding 2A12 (and other primary antibodies, if necessary) they were incubated at 4°C overnight. The next day the embryos were washed three times with PBT for 10 minutes and incubated with Biotinylated IgM (and other secondary antibodies, if necessary) for 2 hours at room temparature in the dark. Then the embryos were washed again with PBT for 10

minutes for three times and incubated with HRP streptavidin in PBT for 1 hour and 30 minutes at room temperature. To get rid of the excess and unbound HRP streptavidin, the embryos were washed with PBT for 10 minutes three times. The fluorescent signal developed after the addition of Cy3 Amplification Reagent (1:100) diluted in Amplification Diluent and incubation at room temperature in the dark for 10 minutes. The reaction was stopped by the removal of TSA-Cy3 solution and the embryos were washed with PBT for 10 minutes three times. Finally, the embryos were mounted in mounting medium Fluoromount.

2.2.6. Phalloidin staining

After the dechorionation of the overnight laid eggs, these were kept in fixation solution (4% formaldehyde, 2ml of heptane and 2ml of PBS) for 40 minutes. Instead of proceeding with the standard fixation protocol, embryos were devitelinated by hand since MeOH destroys the F-actin structures. Hand-devitelination starts with the displacement of the embryos from the top phase, which also contains heptane, into a plastic plate. After the elimination of heptane via air-drying for 3 minutes, embryos were spread evenly on the plate with a brush. Then they were collected with a double-sided sticky tape, which was then placed on a new plastic plate. The new plate was covered with PBT+BSA solution in order to prevent dehydration of embryos throughout the devitelination process. Using the tip of an injector needle, embryos were pricked and pushed out of their viteline membrane. Finally, devitelinated embryos ready for antibody and phalloidin stainings were then collected with a Pasteur pipette and placed in an micro-centrifuge tube.

2.2.7. Fluorescent in-situ hybridization

Freshly fixed embryos were washed with PBT for 5 minutes five times, then with 50% PBT+50% Hybridization Buffer (HB, with sperm) for 5 minutes, and finally with HB for 5 minutes. Then embryos were kept at 56°C for 3 hours in HB for pre-hybridization. In the last 10 minutes of pre-hybridization, probes (1:100 in HB) were prepared for hybridization by first putting them at 80°C and then putting them on ice for 5 minutes each. The probes are hybridized with the embryos at 56°C overnight. The next day the embryos were washed at 56°C with the previously warmed HB for 20 minutes twice, then with the previously warmed 50% PBT+50%

HB for 20 minutes twice and finally with the previously warmed PBT for 20 minutes twice. Then they were washed with PBT for 20 minutes three times at room temperature. After that, the embryos were incubated in POD-conjugated anti-Dig (in PBT) for 1 hour and washed with PBT for 20 minutes for three times at room temperature. The fluorescent signal developed by the addition of Cy3 Amplification Reagent (1:100) diluted in TSA Amplification Diluent and incubation at room temperature in the dark for 10 minutes. The reaction was stopped by the removal of TSA-Cy3 solution and the embryos were washed with PBT for 10 minutes three times. Finally, either the embryos were mounted in mounting medium Fluoromount or an antibody staining was done.

2.3. Generation of FLP-out clones

The FLP-out technique was used to over/ectopically express *UAS-Blimp-1, UAS-SrcGFP* recombinant construct in groups or individual embryonic tracheal cells (Nellen et al., 1996; Struhl and Basler, 1993; Zecca et al., 1996). After *UAS-Blimp-1, UAS-SrcGFP* carrying flies were crossed with *hsFLP*^{122}*; btlRFPMoe, btl >y*$^{+}$ *>GAL4* flies, the embryos generated as a result of this cross were collected on agar plates overnight. The collected embryos were heat shocked at 37°C for one hour, kept at room temperature for six hours and then fixed.

2.4. Image Acquisition and Processing

The cuticle preparation samples were analyzed under the Zeiss dark field microscope Axioskop. The images were acquired using 10x and 40x objective lenses and they were processed via image processing software Fiji (Schindelin et al., 2012).

The fluorescent histological samples were analyzed under spectral confocal microscopes Leica TCS SP2 and Leica TCS SPE. The images were acquired using 20x, 40x and 63x objective lenses and they were processed via image processing software Fiji (Schindelin et al., 2012). Unless otherwise stated, all fluorescent images shown are maximum projections of Z stack sections.

2.5. *In vivo* experiments

2.5.1.Time-lapse experiments

Dechorionated embryos were immobilized with glue on a 24mmx60mm coverslip, and then were covered with Oil 10-S that prevents dehydration of the embryos while enabling gas transfer between the embryos and their environment. To visualize *in vivo* F-actin bundling/ring formation, btl-MoeGFP construct was used in the *wild-type* and the mutant backgrounds. F-actin dynamics were imaged with a spectral confocal microscope Leica TCS SP5. The images were acquired every 5 minutes over Z stacks from stage14-17 embryos for 2-3 hours.

2.5.2. Air-filling experiments

Dechorionated embryos were placed in PBS, recovered with a Pasteur pipette, spread on a microscope slide and covered with a coverslip. The samples were then visualized under a Nikon light field microscope Eclipse 80i. The late-stage-17 embryos were imaged as they filled with air (in the case of *wild-type*s) or failed to fill with air (in the case of mutants).

2.6. Tube size quantifications and statistics

The images of *wild-type* and mutant embryos stained with the luminal marker 2A12 acquired with spectral confocal microscope Leica TCS SP2 using 10x and 63x objective lenses. The images taken with the 10x objective lens were used to locate the position of the tracheal metameres, whereas the images acquired with the 63x objective lens were used to analyze the size of the DTs. The diameter of the DTs were measured using the image processing software Fiji (Schindelin et al., 2012). The measurements were then analyzed in the spreadsheet program Microsoft Excel 2011. To represent the measurement sets, box plot graphs were drawn. The significant differences between the sets of measurements were checked using Student's t-Test with a significance level of 0.02.

RESULTS

1. Dynamics of taenidial folds and F-actin bundles

Taenidial folds are chitin structures surrounding the tubular lumen and they give mechanical strength to the tracheal tubes. In the literature, Electron Microscopy (EM) imaging has been the main way to visualize these structures during embryogenesis (Araújo et al., 2005; Araújo et al., 2007; Hemphälä et al., 2003; Moussian et al., 2006a; Ng et al., 2006; Norum et al., 2010; Swanson et al., 2009; Wang et al., 2012; Wang et al., 2006; Wilk et al., 2000; Wu et al., 2004). In the course of this study, we used a stain named fluostain to label taenidial folds (and other chitin structures) in *Drosophila* embryos and larvae, and we imaged them via confocal microscopy. Therefore we were able to co-label taenidial folds and other structures in the same embryos. In order to visualize taenidial folds better we imaged the widest tube in the tracheal system, Dorsal Trunk (DT).

As described in the introduction part, there are two kinds of chitin structures in the tracheal system; intraluminal chitin filament and taenidial folds. During embryogenesis while the latter is forming, the former disappears as it has been observed via TEM analysis by Moussian *and collaborators* (Moussian et al., 2006a). We used the thinning and disappearance of intraluminal chitin filament as a marker for developmental timing of taenidial folds. The first taenidial folds become visible at late stage 16 when the intraluminal chitin filament is still thick and dense (**Figure 15**). Interestingly, the taenidial folds formed at the fusion cells become visible later -at the beginning of stage 17- indicating that they have a different timing compared to the ones formed in the rest of the tube. Then by mid-stage 17, the intraluminal chitin filament becomes very thin while the taenidial folds become more visible. At the end of embryogenesis, the lumen is cleared from chitin fibers and the taenidial folds reach their most mature form.

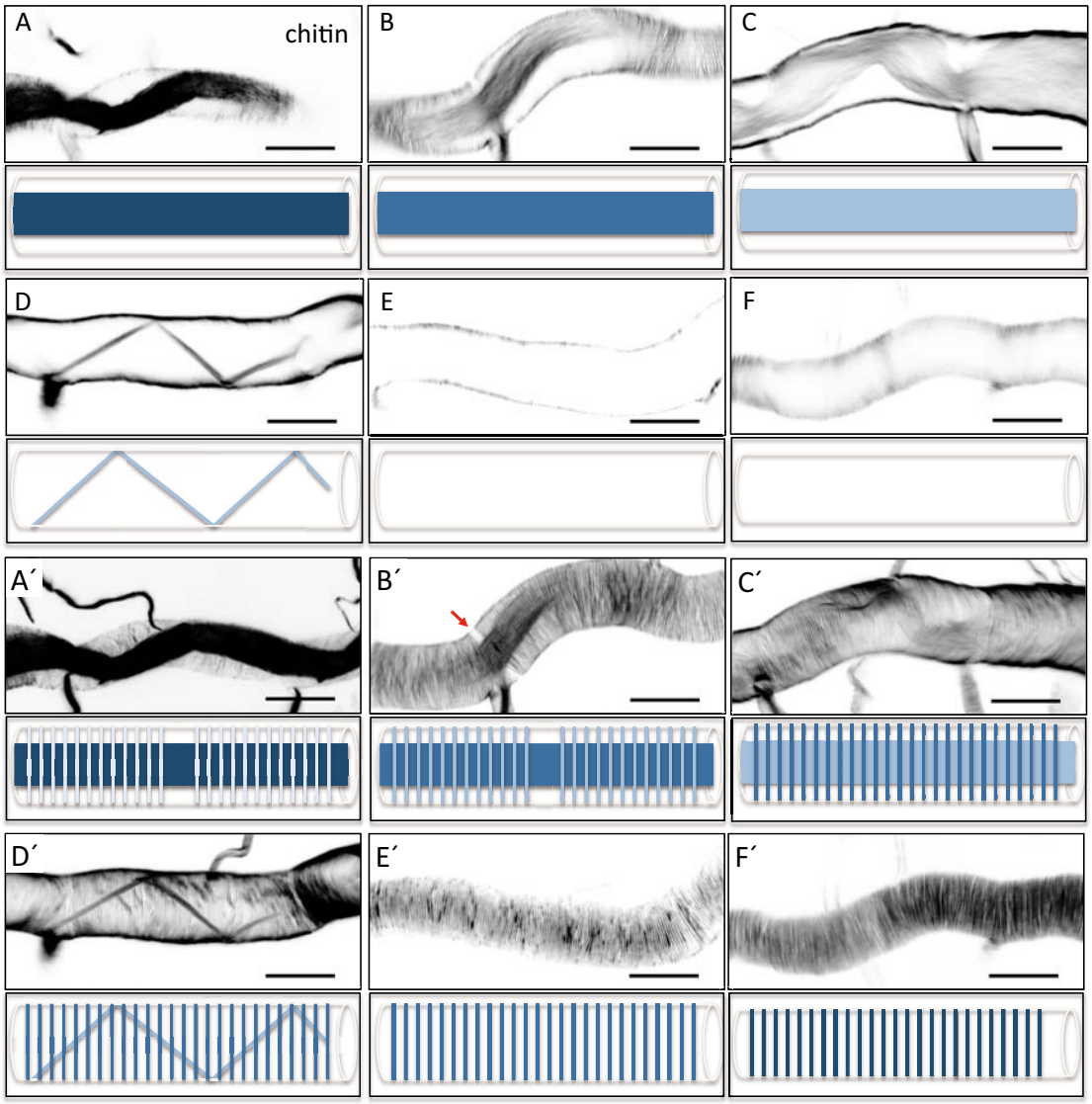

Figure 15: Dynamics of chitin structures via fluorescent labeling. *Wild-type* embryos stained with fluostain to label the chitin structures. The interested chitin structures are schematically represented under each image. Single stacks of confocal Z sections showing the dynamics of intraluminal chitin filament during late stages of embryonic development (A-F). At late stage 16 intraluminal chitin filament is thick and dense (A). As the embryo develops, it gets less and less dense (B, C) until it turns into a thin chitin fiber that runs in zigzags along the tube diameter (D). In the very last steps of embryogenesis, the intraluminal chitin filament is completely cleared from the lumen (E, F). Maximum projections of the same confocal Z sections, shown in panels A-F, used to stage embryos and visualize the dynamics of taenidial folds (A'-F'). At late stage 16 taenidial folds are newly formed and thin (A'). As the taenidial folds get thicker, it becomes obvious that the taenidial folds at fusion points are not formed yet (B', arrow). Later, the taenidial folds at fusion points are also formed which generates a continuous taenidia structure along the tube (C'). In the final steps, as the intraluminal chitin filament gets cleared from the lumen, the taenidial folds get their the most mature form (D'-F'). Scale bars =10µm.

During *Drosophila* development, actin structures contributing to chitin organization have been reported for many systems, like in denticle belts at the epidermis and in the luminal structures in the tracheal system. In 2006, Matusek *and collaborators* showed that there are parallel bundles of apical Filamentous actin (F-actin) running perpendicular to the tube axis with the same organization of taenidial folds. These results lead the authors to propose the hypothesis that by forming the actin bundles at those specific locations, the cells are labeling the position of the taenidial folds. We confirmed their results by labeling taenidial folds with fluostain and actin bundles with phalloidin in the same specimen, and checked those structures in embryonic and larval tracheas. And we observed perpendicular lines of taenidial folds over the perpendicular lines of the actin bundles (**Figure 16**).

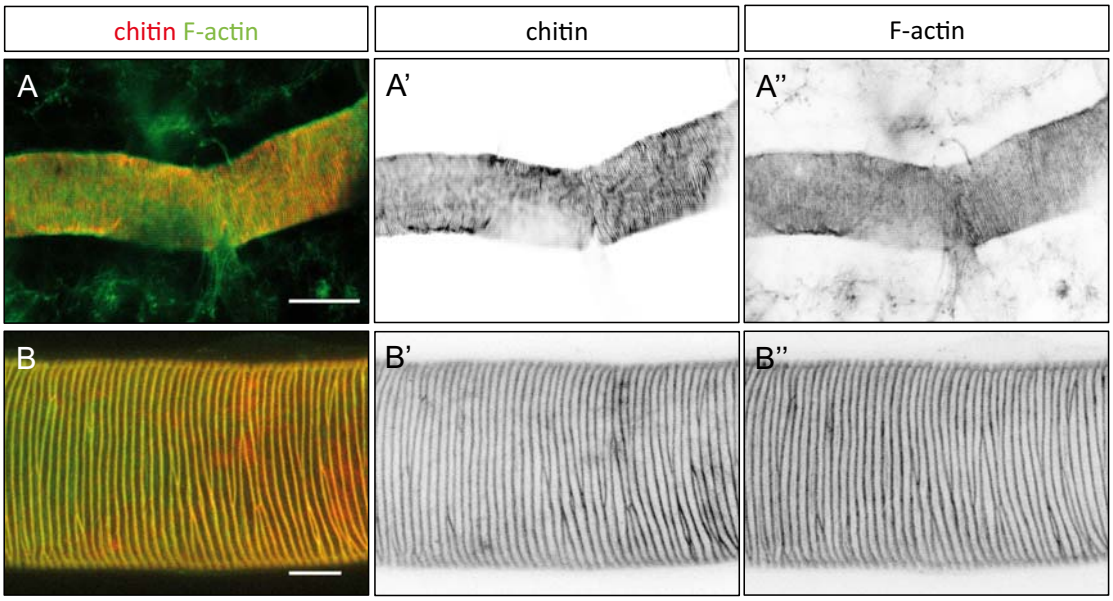

Figure 16: F-actin bundles and taenidial folds in embryonic and larval tracheas. A *wild-type* embryo stained with fluostain (red) and phalloidin (green) showing taenidial folds and F-actin bundles together (A) or separately (A', A''). A *wild-type* 3rd instar larval trachea stained with fluostain (red) and phalloidin (green) showing taenidial folds and F-actin bundles together (B) and separately (B' and B''). Scale bars =10µm.

To shed light on the relationship between apical F-actin and chitin during taenidial fold formation, we visualized taenidial folds and apical F-actin bundles at various developmental stages during embryogenesis. The first apical F-actin bundles (in the form of rings) develop at the mid-stage 16. At that time, taenidial folds are not yet filled with chitin. Then, at late stage 16, the folds start to fill with this polysaccharide and the chitin fibers co-localize with previously formed apical actin

bundles (**Figure 17**). These results suggest that there is a strong correlation between the formation of apical F-actin bundles and taenidial folds.

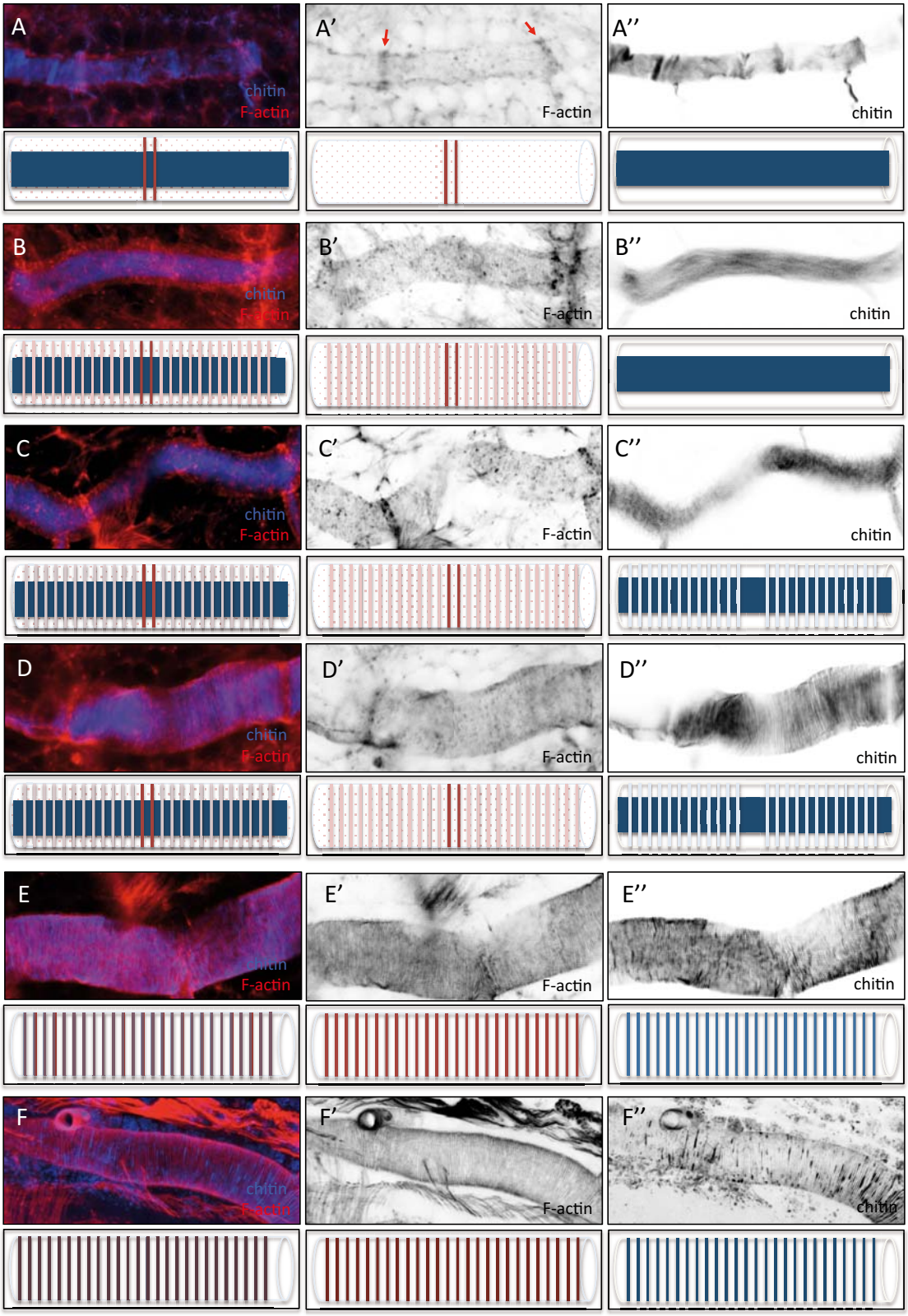

Figure 17: Dynamics of taenidial folds and F-actin bundles. *Wild-type* embryos stained with fluostain (blue) to label the chitin structures and phalloidin (red) to label F-actin bundles. The chitin

and F-actin structures are schematically represented under each image. First F-actin bundles are formed at the fusion points during the fusion process of the DT (A', arrows). Those bundles are formed as a result of highly orchestrated cell shape changes of fusion cells upon meeting with their counterparts, and they are not believed to function in taenidial fold formation. At mid-stage 16, F-actin bundles/rings become visible along the tube while the taenidial folds are not filled with chitin hence not labeled with fluostain (B). Then, very thin taenidial folds become visible (C). At first, they are not formed at fusion points (D). Later, the taenidial folds at fusion points are also formed which generates a continuous taenidia structure along the tube (E). Finally the taenidial folds and F-actin bundles get their most mature form as the trachea start to fill with air (F). Both of the stainings are shown in the merge images (A-F). The fluostain (A'-F') and phalloidin (A''-F'') stainings are shown separately. The images are single stacks of confocal Z sections (A-E).

2. Genes involved in formation of taenidial folds

2.1 Blimp-1 and pri

In the literature, there are a number of genes in the absence of which the embryonic taenidial folds are disrupted listed in **Table 1** (Araújo et al., 2005; Araújo et al., 2007; Förster et al., 2010; Hemphälä et al., 2003; Kondo et al., 2007; Moussian, 2010; Moussian et al., 2005; Ng et al., 2006; Norum et al., 2010; Strigini et al., 2006; Swanson et al., 2009; Wang et al., 2012; Wang et al., 2006; Wilk et al., 2000; Wilkin et al., 2000; Wu et al., 2004). Among these genes, we have choosen to work with *Blimp-1* and *pri/tal* because as a result of their loss of function taenidial folds are reported to be absent. And also because of their previously published functions in other systems/organisms (see below).

2.1.1 Expression pattern of *Blimp-1* and *pri*

Detailed expression analysis of both genes was performed in *wild-type* (*wt*) embryos. *Blimp-1* expression was observed using an antibody against Blimp-1 protein and *pri* expression was analyzed using *in-situ hybridization*, since there are no antibodies against Pri proteins.

The tracheal expression of both genes does not start until stage 12 and after that time point it is observed in all tracheal cells until stage 15. At the beginning of stage 15 the expression of *Blimp-1* fades away starting from DT cells and no expression is observed at the late stages of embryogenesis. *Pri* expression starts to disappear at late-stage 15 in all DT cells except fusion cells. By stage 16, *pri* expression is only restricted to the DT fusion cells. Apart from their tracheal

expression, Blimp-1 protein and *pri* mRNA are also observed in the epidermal, midgut (only for *Blimp-1*) and hindgut cells during embryogenesis (**Figure 18, 19**).

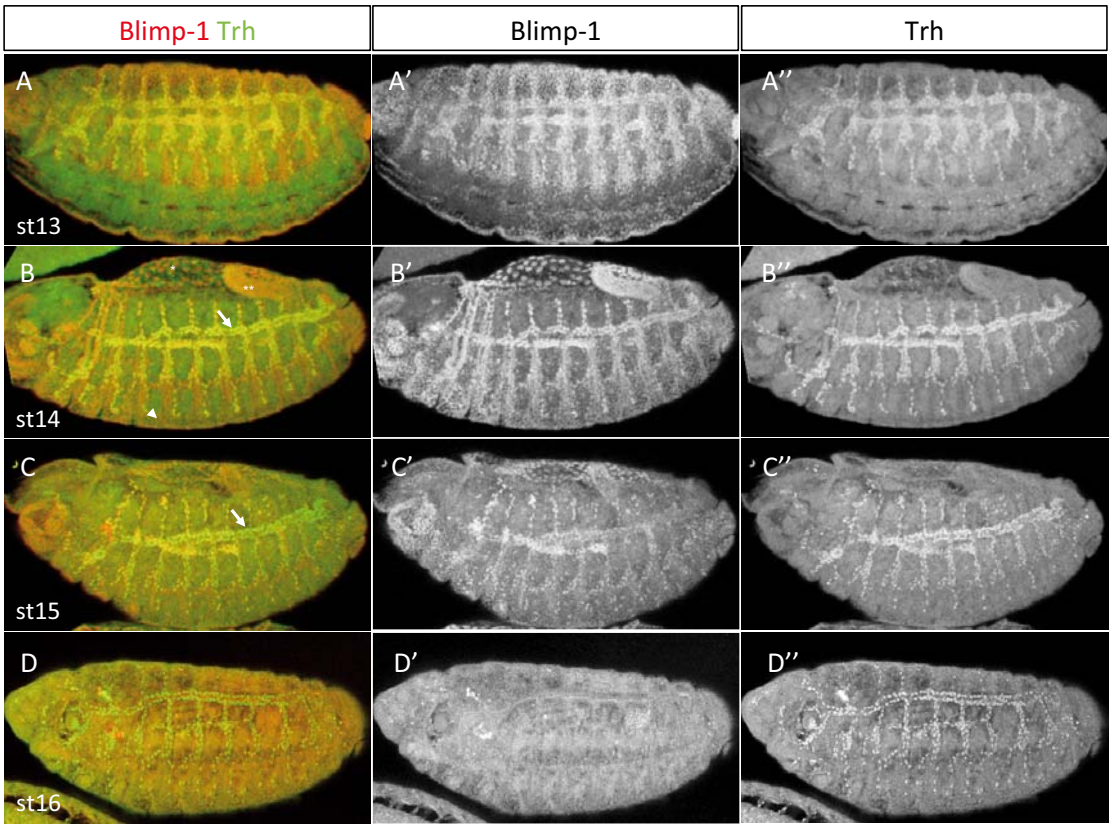

Figure 18: *Blimp-1* is expressed in the tracheal system. *Wild-type* embryos stained with anti-Trh (green) to label tracheal cells and anti-Blimp-1 (red) to label *Blimp-1* expressing cells. At stage 13/14, *Blimp-1* is expressed in tracheal (arrow) and epidermal (arrow head) cells, as well as in midgut (asterisk) and hindgut (double asterisk) (A and B). At stage 15, *Blimp-1* expression begins to gradually disappear starting from DT (C, arrow). At stage 16, there is not any *Blimp-1* expression in the tracheal system (D). Both of the stainings are shown in the merge images (A-D). The anti-Blimp-1 (A'-D') and anti-Trh (A''-D'') stainings are shown separately.

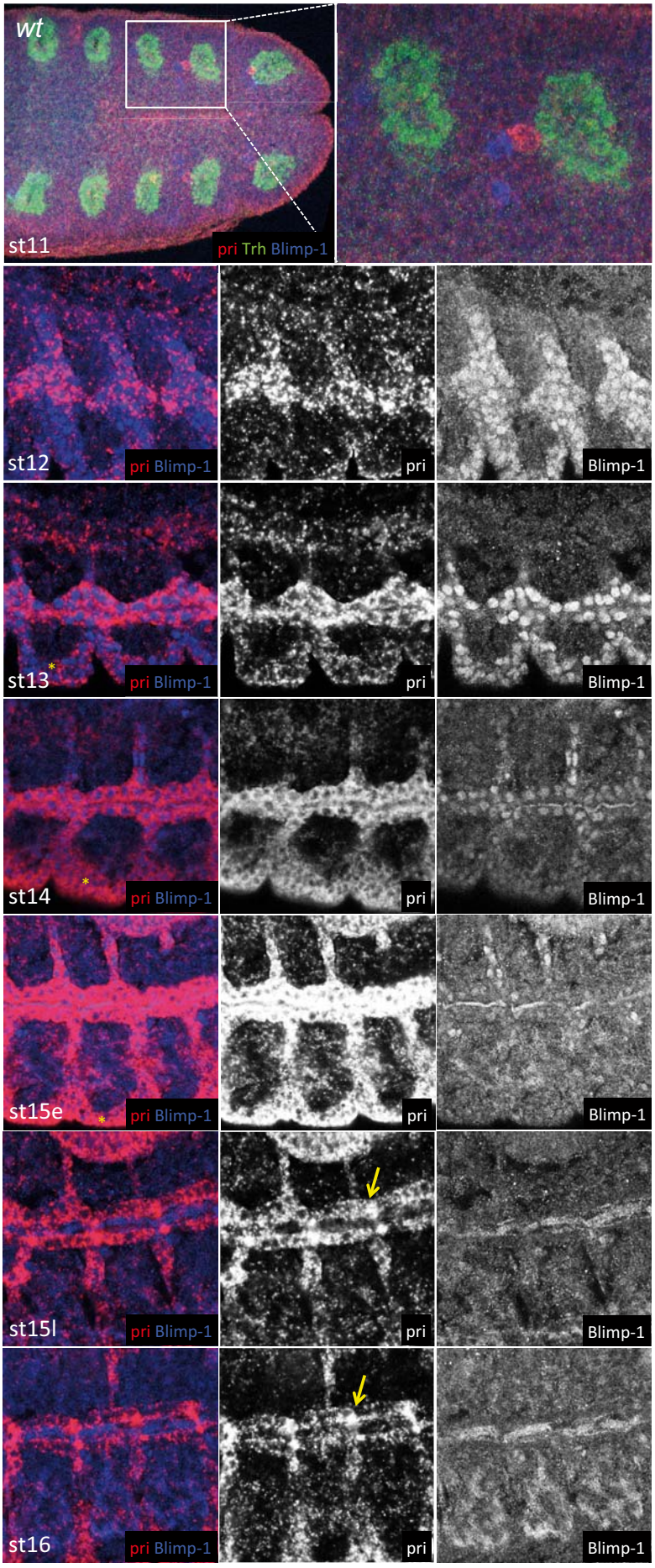
wt
st11
pri Trh Blimp-1
st12
pri Blimp-1
pri
Blimp-1
st13*
pri Blimp-1
pri
Blimp-1
st14
pri Blimp-1
pri
Blimp-1
st15e
pri Blimp-1
pri
Blimp-1
st15l
pri Blimp-1
pri
Blimp-1
st16
pri Blimp-1
pri
Blimp-1

Figure 19: Expression pattern of *Blimp-1* and *pri*. Fluorescent *in-situ hybridization* of pri (red) co-stained with anti-Blimp-1 (blue), to label *Blimp-1* expressing cells, shown either together with Blimp-1 antibody staining or by itself. At stage 11, neither *Blimp-1* nor *pri* is expressed in tracheal cells. Starting from stage 12, both *Blimp-1* and *pri* are expressed in all tracheal cells until early-stage 15 when *Blimp-1* expression begins to gradually disappear. At late-stage 15, *pri* expression also alters and becomes higher in fusion cells (arrow) while getting lower in the remaining cells. The difference of *pri* expression becomes more evident at stage 16 (arrow). All images are single stacks of confocal Z sections, except the stage 11 image, which is a maximum projection of a confocal Z section.

2.1.2 Loss of function phenotypes of *Blimp-1* and *pri*

To analyze how taenidial folds are affected in the loss of function of *Blimp*-1 and *pri*, we obtained 5 lines of *Drosophila* mutant stocks. Two of them are P-element insertions in the *Blimp-1* gene region; *Blimp-1* mutant 1 and *Blimp-1* mutant 2 (**Figure 20A**). After checking with the Blimp-1 antibody, we identified that *Blimp-1* mutant 1 (from here on it will be referred as *Blimp-1* mutant) is a protein-null mutant (**Figure 20**). The remaining 3 stocks (described in Kondo and collaborators 2007): pri^1, pri^2 and pri^3 (from here on it will be referred as *pri* mutant) were obtained as a gift from Shigeo Hayashi. Those 3 lines are generated by Flp-FRT recombination leading to a deletion of *pri* gene region and some portion of the chromosome arm –the length of which changes in each line (**Figure 13B**).

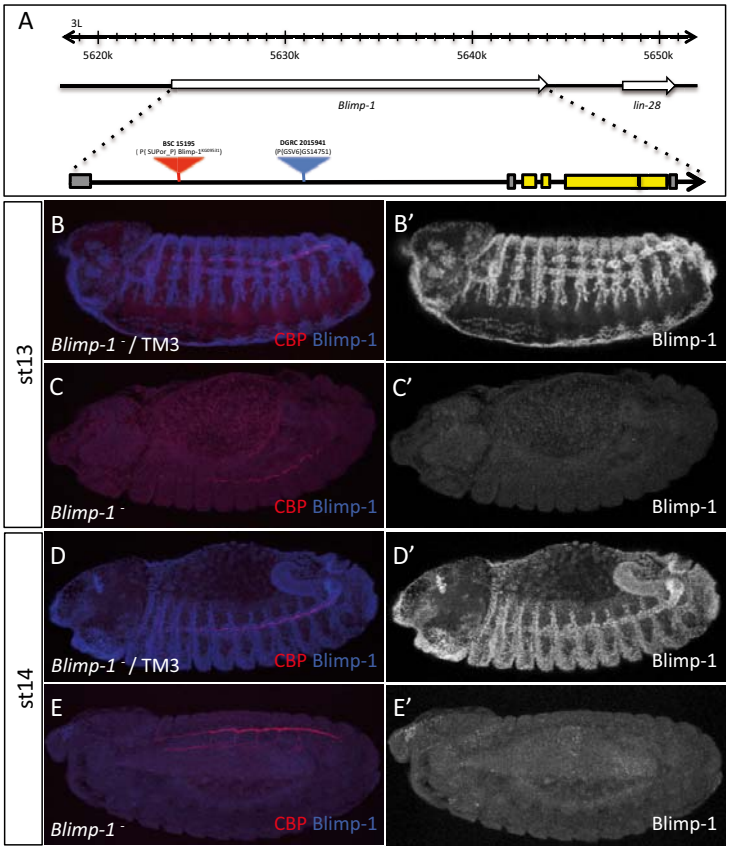

Figure 20: A P-element insertion in the *Blimp-1* gene region results in a protein null mutant. Schematic representation of *Blimp-1* gene region showing the 5' and 3' UTRs (gray), and the CDS

(yellow). The P-element insertions in the gene region resulting in the loss of function of *Blimp-1* are shown in red (*Blimp-1* mutant 1) and blue (*Blimp-1* mutant 2) (A). Embryos carrying either one (B, D) or two (C, E) copies of *Blimp-1* mutant 1 allele stained with chitin binding probe (CBP, red) to label chitin structures and anti-Blimp-1 (blue) to label *Blimp-1* expressing cells (B-E). While *Blimp-1* expression is observed in embryos carrying one copy of *Blimp-1* mutant 1 allele (B, D), there is no *Blimp-1* expression in embryos carrying two copies of *Blimp-1* mutant 1 allele (C, E). The co-stainings are shown in the merge images (B-E). The anti-Blimp-1 staining is shown separately (B'-E').

To test whether the mutant phenotypes of *Blimp-1* and *pri* that we observe are originated because of the loss of functions of *Blimp-1* and *pri* (to exclude second site mutations), we checked the tube expansion phenotypes of the *Blimp-1* mutant with a deficiency on the 3rd chromosome that covers the *Blimp-1* gene region (*Df(3L)Exel6106*) and the *pri* mutant with the transheterozygous combinations of pri^3 allele (pri^1/pri^3 and pri^2/pri^3). The three genetic combinations we checked revealed similar tube expansion phenotypes as homozygous *Blimp-1* and *pri* mutants, indicating that the mutant phenotypes of *Blimp-1* and *pri* that we observe are actually originated because of the loss of function of *Blimp-1* and *pri*.

2.1.2.a Taenidial folds and actin rings phenotype

We started our analysis by checking the chitin structures in the *Blimp-1* and *pri* mutant embryos. And we observed that while the intraluminal chitin filament is not affected by the loss of function of *Blimp-1*, the absence of *pri* results in breaks on DT and thinning of the intraluminal chitin filament (**Figure 21**).

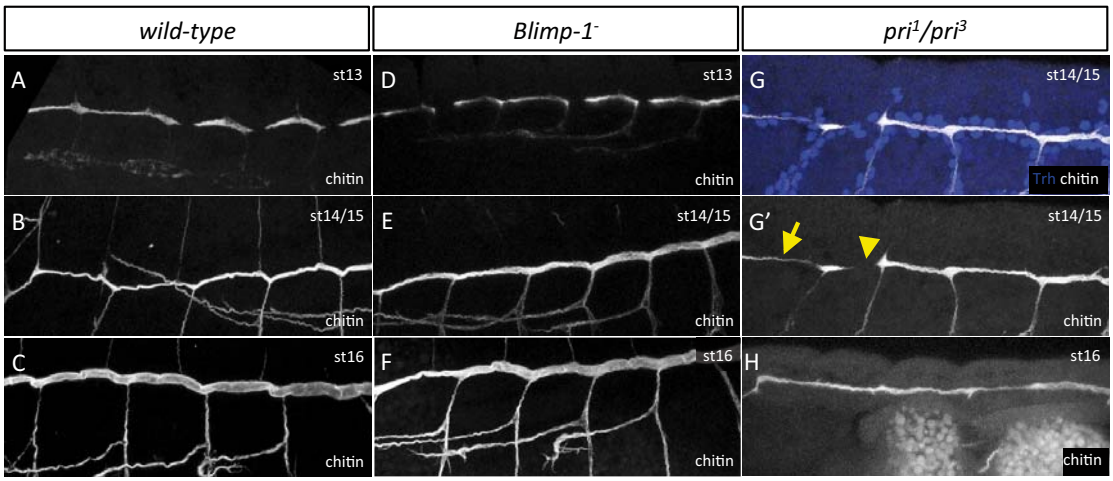

Figure 21: Intraluminal chitin filament in the *Blimp-1* and *pri* mutant embryos. *Wild-type* (A-C), *Blimp-1* (D-F) and *pri* (G, H) mutant embryos in different stages stained with fluostain to label the intraluminal chitin filament. The *pri* mutant embryo was additionally stained with anti-Trh to label the tracheal cells (G). While the intraluminal chitin filament is not affected by the loss of function of *Blimp-1* (D-F), the absence of *pri* results in a break on DT (arrow head) and thinning of the intraluminal chitin filament (arrow), which can be related to the irregular number of cells at the

breaking and thinning points (G, H). The co-staining is shown in the merge image (G). The fluostain staining is shown separately (G').

As it has been published, we observed that the taenidial folds are disrupted in both *Blimp-1* and *pri* mutants (**Figure 22**). In *Blimp-1* mutant embryos taenidial folds run parallel to the tube axis instead of being perpendicular. However, the taenidial folds formed by the fusion cells do not seem to be affected by the loss of function of *Blimp-1* (**Figure 22B**). In *pri* mutants there are variations in the taenidial folds phenotype. The majority of *pri* mutant taenidial folds run parallel to the tube axis (75%, n=12 –**Figure 22D**). In some embryos the tube appears twisted and taenidial folds seem to follow that twist in which case the taenidial folds sometimes run perpendicular to the tube axis and sometimes with a 45° angle (25%, n=12 – **Figure 22C**). These results indicate that both *Blimp-1* and *pri* contribute to the proper orientation of taenidial folds.

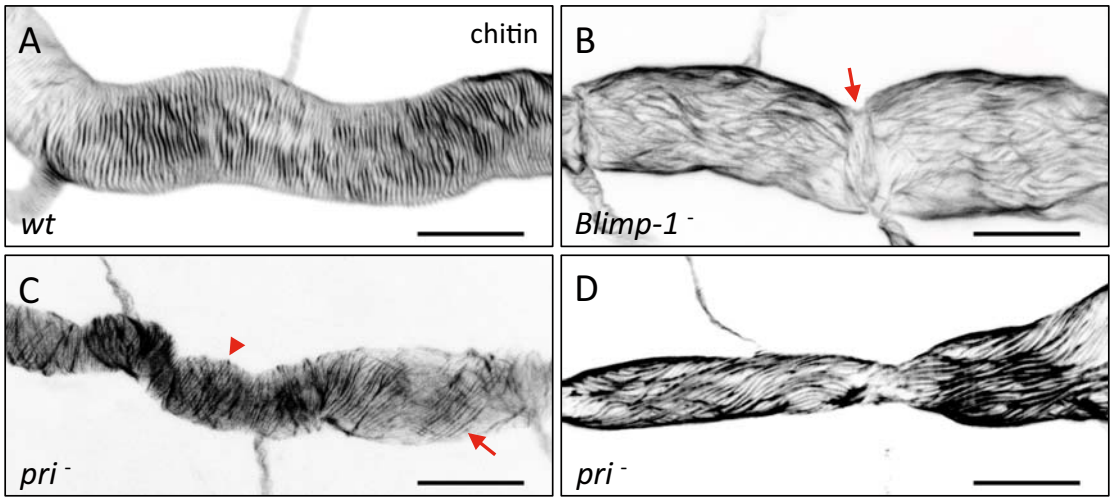

Figure 22: Taenidial folds in the *Blimp-1* and *pri* mutant embryos. *Wild-type* (A), *Blimp-1* (B) and *pri* (C, D) mutant embryos stained with fluostain to label the taenidial folds. The taenidial folds run perpendicular to the tube axis in *wild-type* embryos (A) while in the loss of function of *Blimp-1* (B) and most of the *pri* mutants they run parallel (D) with the exception of fusion points in *Blimp-1* mutants (B, arrow). In some cases, in *pri* mutants they run perpendicular to the tube axis (arrow head) or with a 45° angle (C, arrow). Scale bars =10µm.

As a next step, we checked taenidial folds and apical F-actin structures in the mutant embryos of *Blimp-1* and *pri*, to understand how the morphogenesis of chitin and actin structures is related. In mutant embryos of both genes, we observed correct apical F-actin accumulation. As in the case of taenidial folds, there are some variations of F-actin phenotypes in *pri* mutant embryos. In most of the *pri* mutant

embryos F-actin bundles run parallel to the tube axis like the taenidial folds and both of them have the same pattern of organization (92%, n=12 – **Figure 23E, F**), while in some embryos, F-actin bundles fail to form (8%, n=12 – **Figure 23D**).

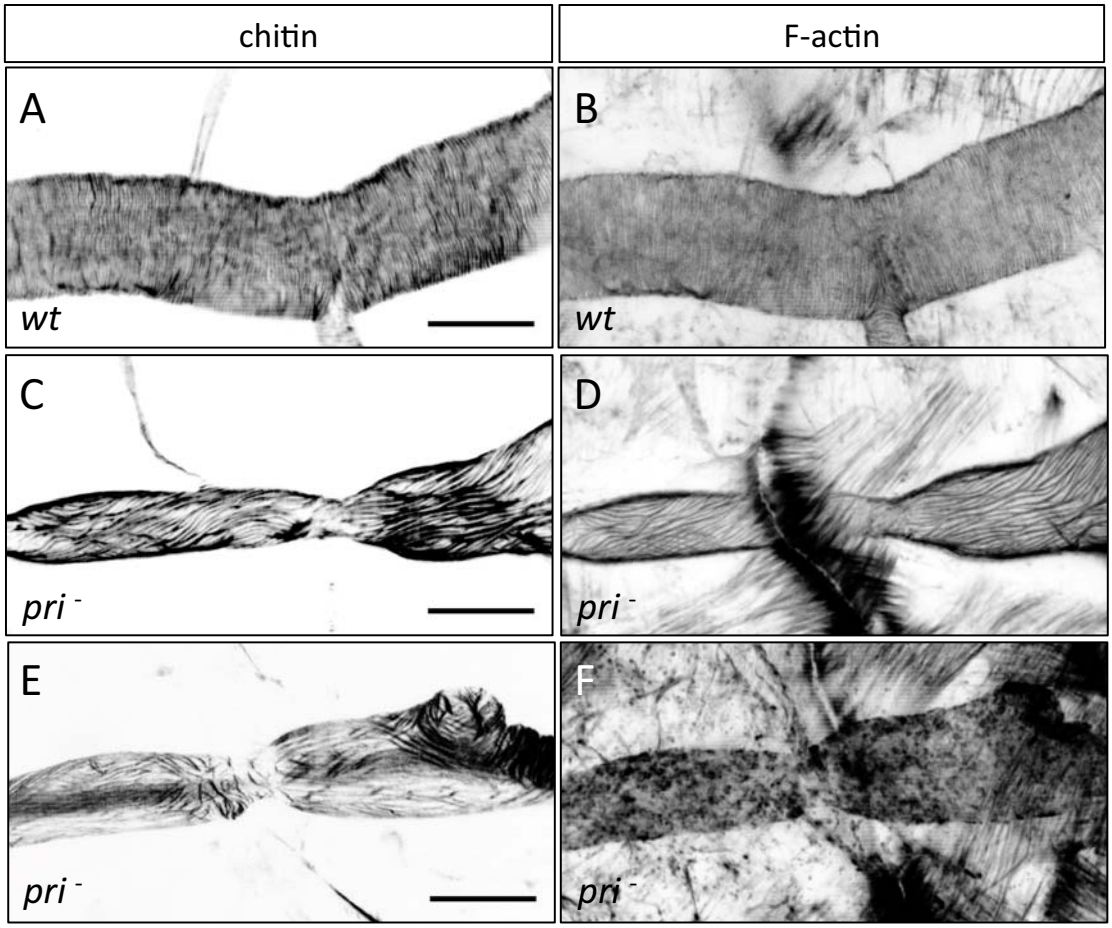

Figure 23: Taenidial folds and F-actin bundles in the *pri* mutant embryos. *Wild-type* (A, B) and *pri* (C-F) mutant embryos stained with fluostain (A, C, E) to label the taenidial folds and phalloidin (B, D, F) to label F-actin bundles. Both the taenidial folds and F-actin bundles run perpendicular to the tube axis in *wild-type* embryos (A, B) while in most of the *pri* mutants both of them are parallel to the tube axis (C, D). However in some cases, in *pri* mutants F-actin bundles fail to form (F) when taenidial folds still run parallel to the tube axis (E). Scale bars =10µm.

Reasoning that the cause of this variation might be the developmental stages of the embryos, *i.e.* the younger embryos might need more time to form the F-actin bundles while the older ones have them already, we checked F-actin bundle formation in live. To visualize *in vivo* F-actin bundles formation, *btl-MoeGFP* construct was used. Moesin (Moe) is a membrane-cytoskeleton linker that binds to F-actin through its C terminus (Dutta et al., 2002; Edwards et al., 1997). MoeGFP fused to the *btl* promoter enabled us to visualize the F-actin structures specifically in the tracheal system. This analysis revealed that *pri* mutant embryos require more time to form the

actin bundles when compared to *wild-type* embryos carrying the *btl-MoeGFP* construct. To further prove this delay, we checked F-actin structure at mid-stage 16 embryos in *pri* mutants since it is the first time F-actin bundles become visible in *wild-type* embryos. And we observed that at that stage the F-actin bundles are not formed in *pri* mutants, proving the delay in formation of F-actin bundles in *pri* mutants (**Figure 24**). This delay could be the reason why Kondo *and collaborators* reported that in *pri* mutants the F-actin is disorganized (Kondo et al., 2007).

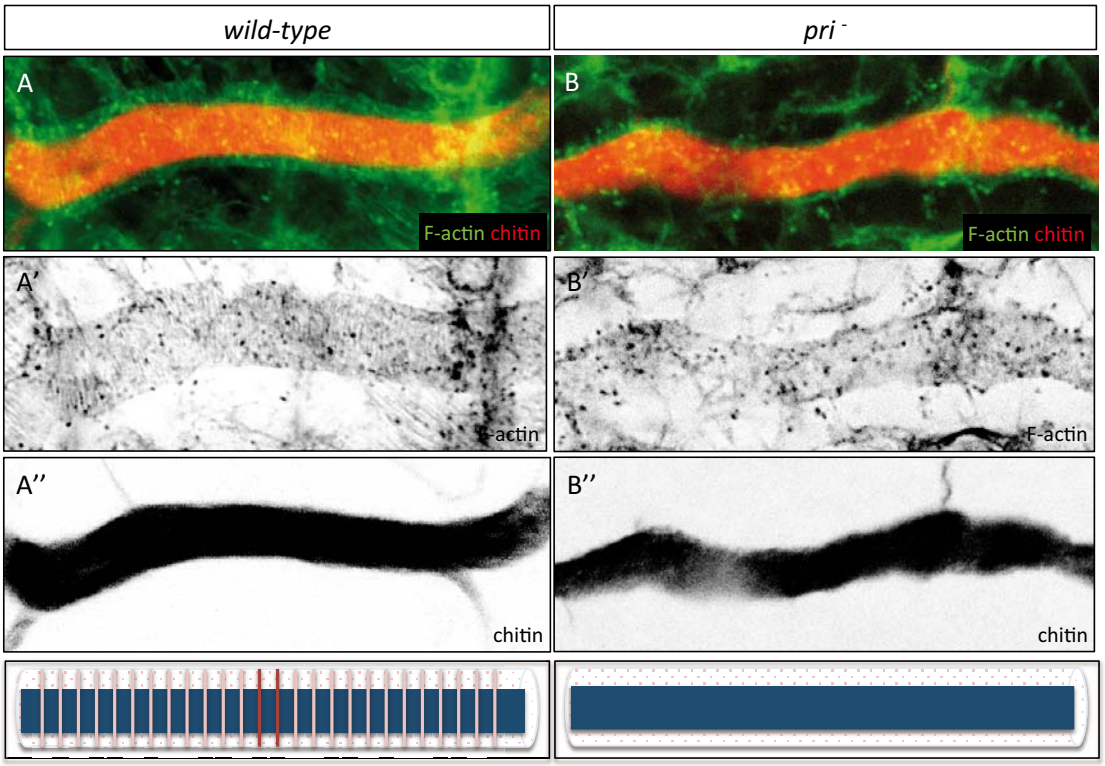

Figure 24: F-actin bundles in the *pri* mutant embryo. *Wild-type* (A) and *pri* mutant (B) embryos at mid-stage 16 stained with fluostain to label chitin structures and with phalloidin to label F-actin structures. F-actin bundles are formed in *wild-type* embryos at mid-stage 16 (A) while they are absent in *pri* mutants when in both cases taenidial folds are not visible yet (B). Both of the stainings are shown in the merge images (A and B). The phalloidin (A, B') and fluostain (A'', B'') stainings are shown seperately. The chitin and F-actin structures are schematically represented for each condition. All images are single stacks of confocal Z sections.

,

When we checked F-actin structures in *Blimp-1* mutants, we also found that there are some variations of the mutant phenotype. While in most of the *Blimp-1* mutant embryos (67%, n=18 – **Figure 25D**) F-actin does not form bundles –except at the fusion points-, in a few of them F-actin bundles are formed and they seem to have a similar orientation as the taenidial folds (33%, n=18 – **Figure 25F**).

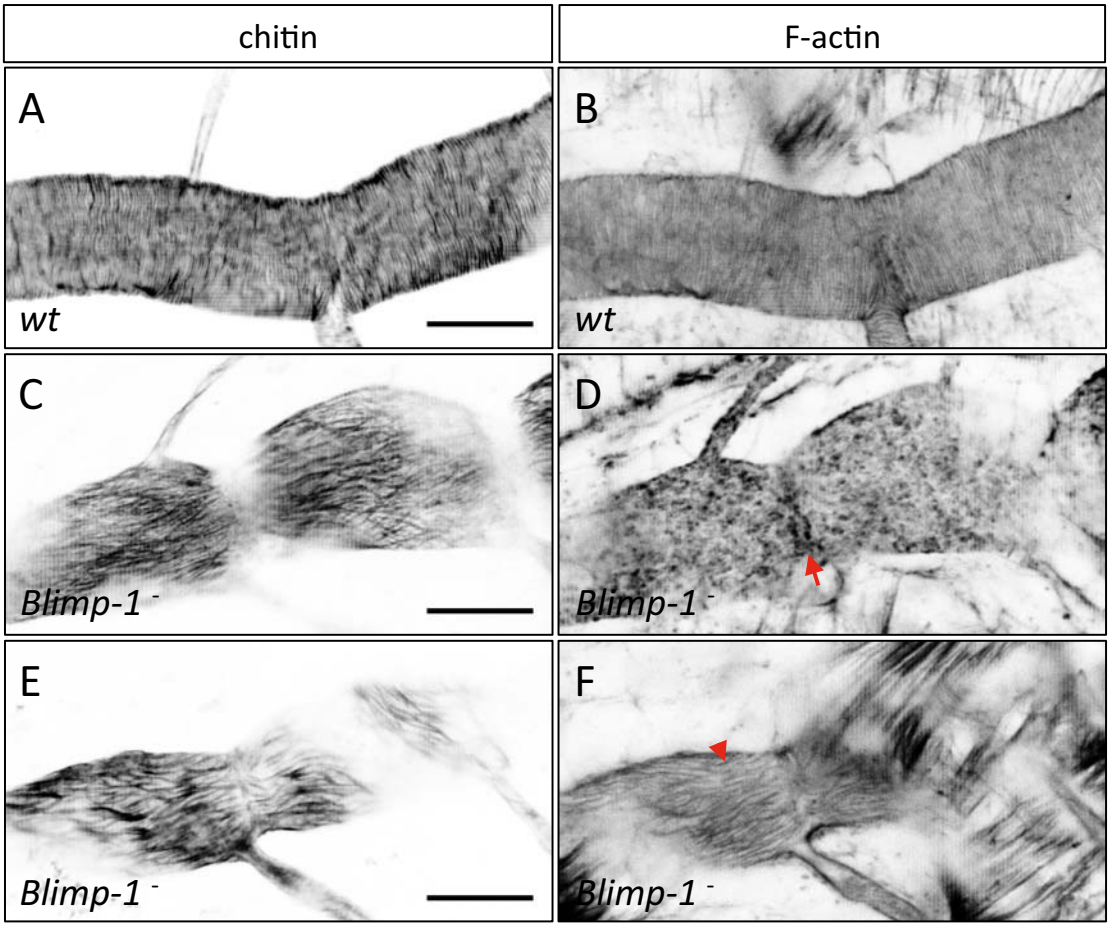

Figure 25: Taenidial folds and F-actin bundles in the *Blimp-1* mutant embryos. *Wild-type* (A, B) and *Blimp-1* mutant embryos (C-F) stained with fluostain (A, C, E) to label the taenidial folds and phalloidin (B, D, F) to label F-actin bundles. Both the taenidial folds and F-actin bundles run perpendicular to the tube axis in *wild-type* embryos (A, B) while in most of the *Blimp-1* mutants F-actin bundles fail to form except at the fusion points (D, arrow) when the taenidial folds run parallel to the tube axis except at the fusion points (C). However in some cases, in *Blimp-1* mutants faint F-actin bundles (F, arrow head) are formed when taenidial folds still run parallel to the tube axis except at the fusion points (E). The images are single stacks of confocal Z sections (C-F). Scale bars =10µm.

Again, to understand whether these variations are originating from the developmental timing of the embryos, we checked F-actin bundles formation in live using the *btl-MoeGFP* construct in *Blimp-1* mutants. During the time-lapse imaging we did not observe any F-actin bundling -except at the fusion points- (**Figure 26**), although we observed the F-actin bundles in some of the fixed tissue samples. The reason why we did not observe any F-actin bundling during time-lapse imaging might be the long duration of the image acquisition (5 minutes). But since duration time has been set according to the necessary imaging quality in the *wild-types*, we could not change the acquisition time. These results raise the possibility that the F-actin bundles in *Blimp-1* mutants are forming and deforming very fast, that might be why we were not able to observe them with a long acquisition time *in vivo* but we were able to observe them in the fixes samples if the samples are fixed just when the F-actin

bundles are formed. Even if the F-actin bundles are formed for a very short period of time, they have a similar pattern of organization as the taenidial folds (as in the case of *pri* mutant embryos) indicating a correlation between F-actin and taenidial folds not only in the *wild-type* embryos but also when their patterns are modified in a mutant background. These results reinforce the idea of a functional link between F-actin bundles and taenidial folds.

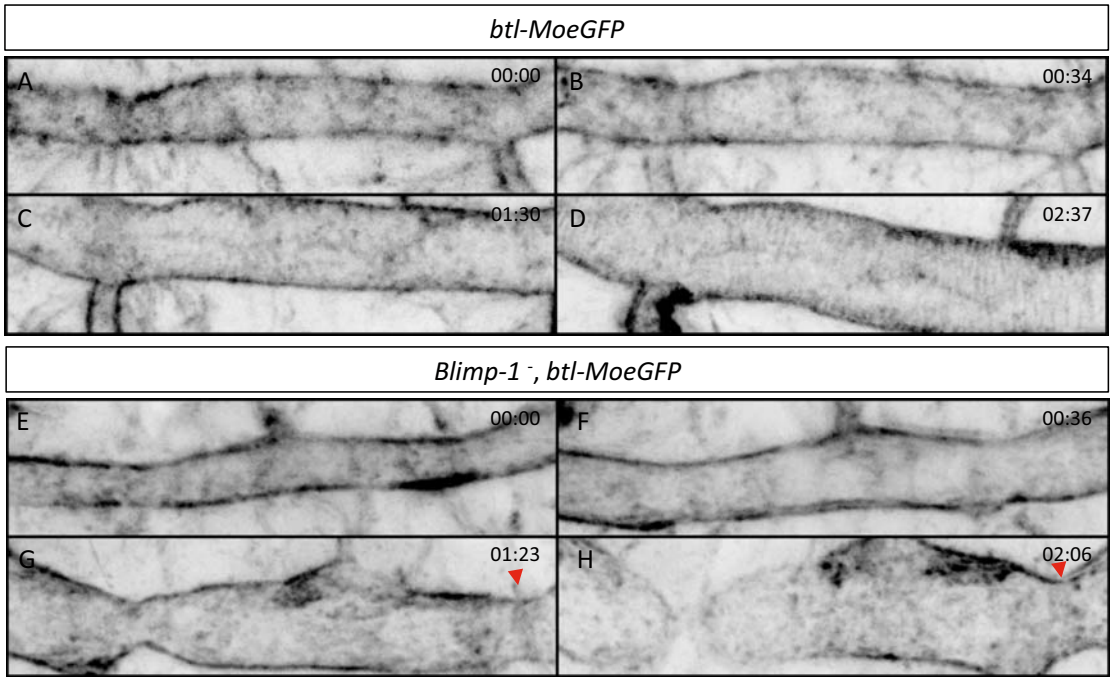

Figure 26 *In vivo* F-actin bundles formation in the *Blimp-1* mutant embryo. Time-lapse images of *wild-type* (A-D) and *Blimp-1* mutant (E-H) embryos carrying *btl-MoeGFP* constructs. In the *wild-type* embryo F-actin bundles become visible at the end of time-lapse imaging (D) while in the *Blimp-1* mutant F-actin bundles fail to form, except at fusion points (G, H, arrow).

2.1.2.b Denticle belts and cuticle phenotype

Denticle belts are chitin structures formed at the epidermis of *Drosophila* embryos. The denticle belt phenotype of *pri* mutants has been published by Kondo *and collaborators* in 2007 and they showed that in the absence of *pri*, the denticle belts fail to form (**Figure 14**) (Kondo et al., 2007). Moreover they checked the F-actin accumulation in cells forming denticle belts and they showed that they are affected in *pri* mutants. We confirmed their data by checking denticle belts and F-actin at the epidermis in *pri* mutant embryos (**Figure 27F**). In order to understand whether the effect of *Blimp-1* on chitin and actin structures affects other tissues in the embryo, we studied the denticle belts in *Blimp-1* mutant embryos. We observed that there is a

general thinning of the cuticle at the epidermis. Although the denticle belts are thinner and shorter compared to *wild-type* embryos, there are no differences regarding the F-actin accumulation in the cells (**Figure 27E**). These results suggest that the effect of *Blimp-1* on actin can be indirect (see below) while the effect of *pri* on actin organization is direct.

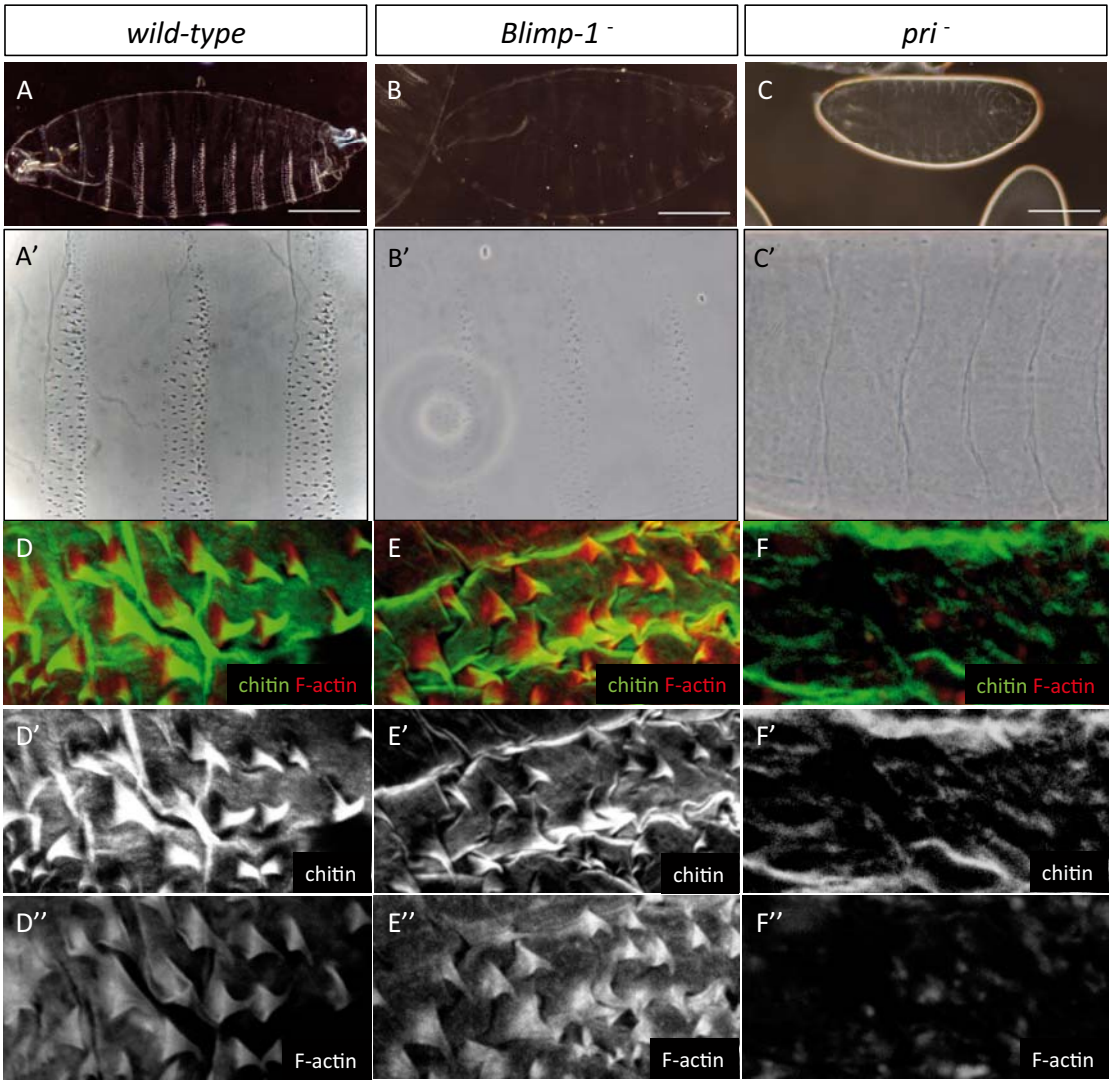

Figure 27: Denticle belts and F-actin at the epidermis in the *Blimp-1* and *pri* mutant embryos. Cuticle preparations of *wild-type* (A), *Blimp-1* (B) and *pri* (C) embryos visualized under the dark field (A-C) and bright field (A'-C'). In the *Blimp-1* mutant embryo the cuticle at the epidermis and the denticle belts, chitin structures at the epidermis, are faint (B, B') when compared to *wild-type* preparation (A, A'). While in the *pri* mutant, denticle belts are completely absent (C, C'). *Wild-type* (D), *Blimp-1* (E) and *pri* (F) embryos stained with fluostain to label chitin structures and with phalloidin to label F-actin structures. The denticle belts in the *Blimp-1* mutant seem to be shorter and thinner (E) when compared to denticle belts in the *wild-type* embryo (D). As in the case of cuticle preparations, the denticle belts are absent in the *pri* mutant embryo (F). Note the F-actin accumulations just under the denticle belts in *wild-type* (D) and *Blimp-1* (E) mutant embryos, whereas in *pri* mutants they are absent (F). Both the fluostain and phalloidin stainings are shown in the merge images (D-F). The fluostain (D'-F') and phalloidin (D''-F'') stainings are shown separately.

The general thinning of the cuticle at the epidermis led us to further analyze the effect of *Blimp-1* on chitin in the trachea and we checked the levels of chitin in *Blimp-1* mutant embryos. Our analysis revealed that the chitin signal is lower in the *Blimp-1* mutant embryos when compared to the heterozygote controls in the same preparation (**Figure 28**). The low levels of chitin in the tracheal system and the thin cuticle at the epidermis in *Blimp-1* mutants, suggests that *Blimp-1* affects chitin levels in *Drosophila* embryos.

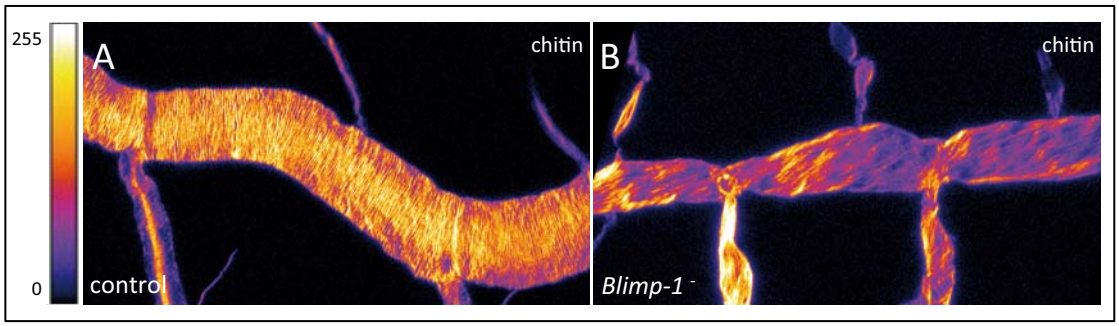

Figure 28: Chitin levels in *Blimp-1* mutant embryos. Stage 17 *Blimp-1* heterozygous (control, A) and *Blimp-1* homozygous mutant (B) embryos stained with fluostain to label chitin structures. After the acquisition, the images are converted into color-coded images in which different levels of fluorescent signals are matched with different colors. The color code is shown on the left. The lowest signal (0) is represented as black and as the signal increases the color changes from purple to white, which is the highest signal (255). While in the control DT mostly red and yellow colors are observed, in the *Blimp-1* mutant DT there are mostly purple and red colors indicating that the fluorescent signal level of fluostain is lower in the *Blimp-1* mutant DT.

2.1.2.c Tube expansion phenotype

It has been reported that in the mutant embryos of *Blimp-1* and *pri*, the DT (it will be referred as the tube, unless stated otherwise) shape is different from their *wild-type* counterparts (Kondo et al., 2007; Ng et al., 2006). When Kondo *and collaborators* checked the time course dilation of DT in *pri* mutant and control embryos, they found that the tube does not expand enough at fusion points in *pri* mutants. To verify their data and to compare it with the circumferential tube expansion in *Blimp-1* mutants, we analyzed the tube size and shape in both mutants using 2A12 as a luminal marker. We measured the tube diameter at fusion points of Tr7-Tr8 and Tr8-Tr9 and the largest tube diameter between fusion points at Tr8. We observed that *Blimp-1* mutant embryos have significantly (p value: 4.39E-07) larger tube diameter between fusion points than the *wild-type* ones, while at the fusion points the diameter is similar to *wild-type* (**Figure 29**). In correlation with Takefumi Kondo´s results, we found that in *pri* mutants the tube diameter is significantly (Tr7-

Tr8 p value: 6.34E-05 and Tr8-Tr9 p value: 0.0001) smaller at fusion points than the *wild-type* tubes. Additionally we revealed that the tube diameter between the fusion points is also significantly (p value: 0.001) smaller than *wild-type* (**Figure 29**). The different tube diameters observed in *Blimp-1* and *pri* mutant DTs suggest that the cause of the bubble phenotype is different for both mutants. *Blimp-1* seems to be required for tube expansion in non-fusion part of the tube while *pri* seems to have a general effect on tube expansion, suggesting that they might be affecting tube expansion via different mechanisms.

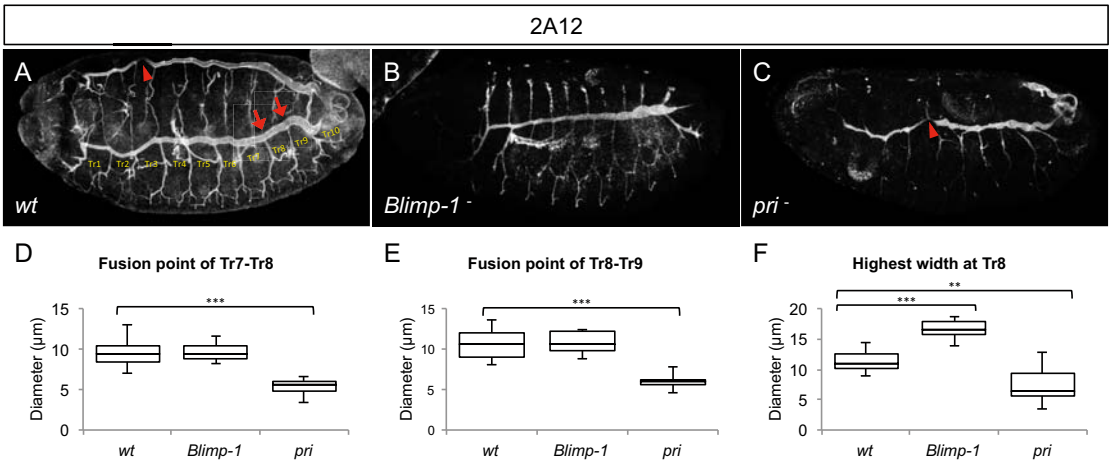

Figure 29: Tube expansion in the *Blimp-1* and *pri* mutant embryos. *Wild-type* (A), *Blimp-1* mutant (B) and *pri* mutant (C) embryos stained with luminal marker 2A12. The *wild-type* uniform tube expansion is disrupted in both mutants. Note the break in DT in *pri* mutants (arrow head) that also occurs occasionally in *wild-type* (arrow head). The tube expansion phenotypes of *Blimp-1* and *pri* mutant embryos represented in box plots (D-F). The diameter of *pri* mutant at fusion points of Tr7-Tr8 and Tr8-Tr9 (arrows), and along Tr8 is significantly lower than the *wild-types* when the diameter of *Blimp-1* mutant is only significantly different along Tr8. *Wild-type* n=15 *Blimp-1* mutant n=10 and *pri* mutant n=10. The whiskers of the box plots represent the minimum and the maximum of the data values (Spear style); ** represents the p value ≥ 0.001; *** represents p value < 0.001.

2.1.2.d Apical cell shape phenotype

Taenidial fold formation, F-actin bundling and tube expansion are three processes regulated by the apical domain of the cell membrane that forms the apical cell surface. Hence the problems in these processes observed in *Blimp-1* and *pri* mutant embryos can be related to the problems in the apical cell surface. The alterations in apical cell shape as a result of the absence of *Blimp-1* has been already reported (Ng et al., 2006). Using anti-DE-cad, we labeled the apical cell membrane, in both *Blimp-1* and *pri* mutants and revealed that the apical cell shape is different in *pri* mutants from the *wild-type* cells. Additionally, we observed that in *Blimp-1* mutants,

the longest cell axis appears to be perpendicular to the tube axis, while in the *wild-type* it is parallel to the tube axis (**Figure 30B**). Most of the *Blimp-1* mutant cells have a similar apical cell surface suggesting a uniform organization throughout the tube (except for the fusion cells, which already have a distinct apical cell shape that does not seem to be affected by the loss of function of *Blimp-1*). In *pri* mutants the apical cell shape is severely affected and we could not define any similarities between any two cells demonstrating a uniform organization throughout the tube (**Figure 30C**). In summary, the apical cell shape is disturbed differently in *Blimp-1* and *pri* mutants and this can be correlated with their different tube expansion phenotypes.

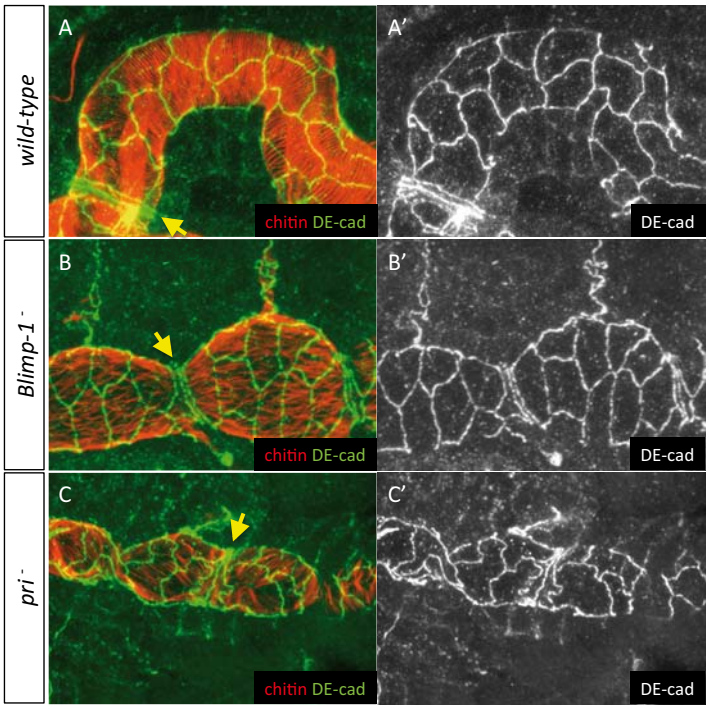

Figure 30: Apical cell shape in the *Blimp-1* and *pri* mutant embryos. *Wild-type* (A), *Blimp-1* mutant (B) and *pri* mutant (C) embryos stained with anti-DE-cad (green) to label the cell surface and fluostain (red) to label the taenidial folds. In the *Blimp-1* mutant embryo apical cell shape is elongated perpendicular to the tube axis (B) while it is mostly parallel to the tube axis in the *wild-type* embryo (A). In the *pri* mutant embryo apical cell shape is disorganized (C). The distinct apical cell shape of the fusion cells (A, arrow) does not seem to be affected by the loss of function of *Blimp-1* (B, arrow) but it is affected by the absence of *pri* (C, arrow). Both of the stainings are shown in the merge images (A-C). The anti-DE-cad staining is shown separately (A'-C').

2.1.2.e Air-filling phenotype

The processes that are affected in Blimp-1 and pri mutants are apical cell surface and tube expansion, F-actin bundle and taenidial fold formation. Since they are all tube maturation processes, we wondered whether the other tube maturation processes like tube clearance and air-filling are affected in *Blimp-1* and *pri* mutants.

In the *wild-type* embryos, at the end of embryogenesis, the tracheal tubes are first cleared from the material inside the lumen (chitin, some solid and liquid molecules) and then they are filled with air (Tsarouhas et al., 2007). When we checked late-stage 17 embryos of *Blimp-1* and *pri* mutants we observed that they do not air-fill (**Figure 31**), which can be explained by absence or incomplete tube clearance. Then we checked whether the tracheal tubes in *Blimp-1* and *pri* mutants are cleared from chitin and we observed that there is no intraluminal chitin filament in late-stage 17 embryos of *Blimp-1* and *pri* mutants, as in the *wild-type* (**Figure 31**). We concluded that the inability of tracheal tubes to fill with air in *Blimp-1* and *pri* mutants is not due to the lack of chitin clearance.

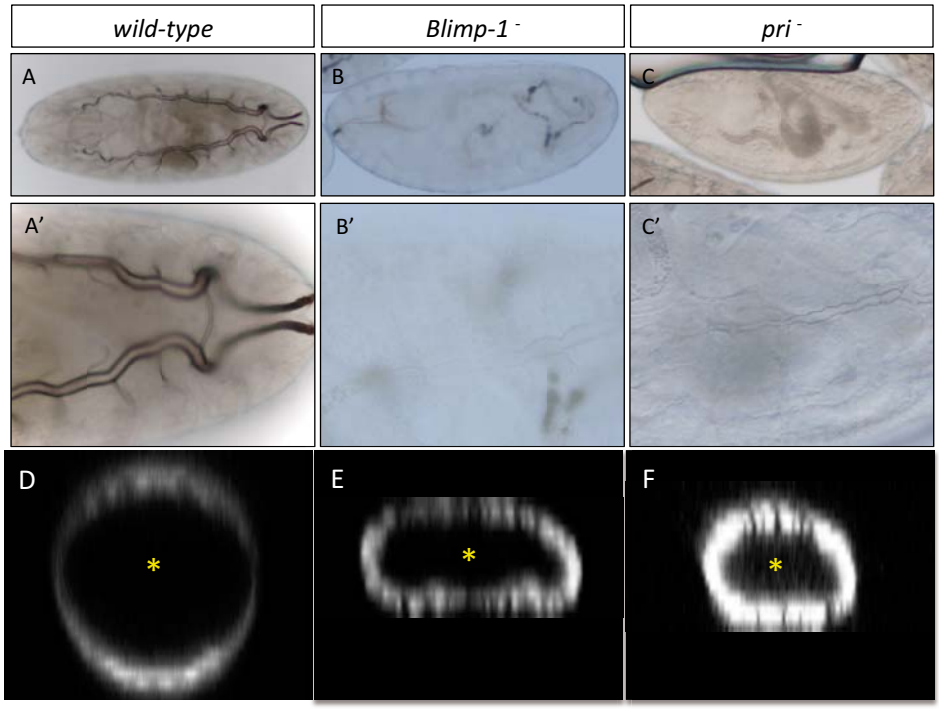

Figure 31: Air-filling of the tracheal tubes in the *Blimp-1* and *pri* mutant embryos. W*ild-type* (A), *Blimp-1* mutant (B) and *pri* mutant (C) embryos visualized *in vivo* to monitor the air-filling of the tracheal tubes. While in *wild-type* embryos the trachea fills with air at the end of the embryogenesis, the *Blimp-1* and *pri* mutants' trachea fail to fill with air. The embryos visualized under light microscope with a 10x objective lens (A-C) and a 40x objective lens (A'-C'). Late stage 17 w*ild-type* (D), *Blimp-1* mutant (E) and *pri* mutant (F) embryos stained with fluostain to label chitin structures. Orthogonal views of the embryos showing inside of the lumen (asterisk). Note the absence of intraluminal chitin filament inside tracheal lumen of w*ild-type* (D), *Blimp-1* mutant (E) and *pri* mutant (F) embryos.

2.1.3 Do *Blimp-1* and *pri* function together?

2.1.3.a Blimp-1 and pri expression in mutants for pri and Blimp-1

Similar taenidial fold phenotypes of *Blimp-1* and *pri* mutants led us wonder whether they function together. To answer this question, we analyzed the expression pattern of *Blimp-1* and *pri* in each others' mutant embryos.

The expression pattern of *Blimp-1* is not altered in the absence of *pri*, which indicates that *pri* does not regulate *Blimp-1* expression (**Figure 32**).

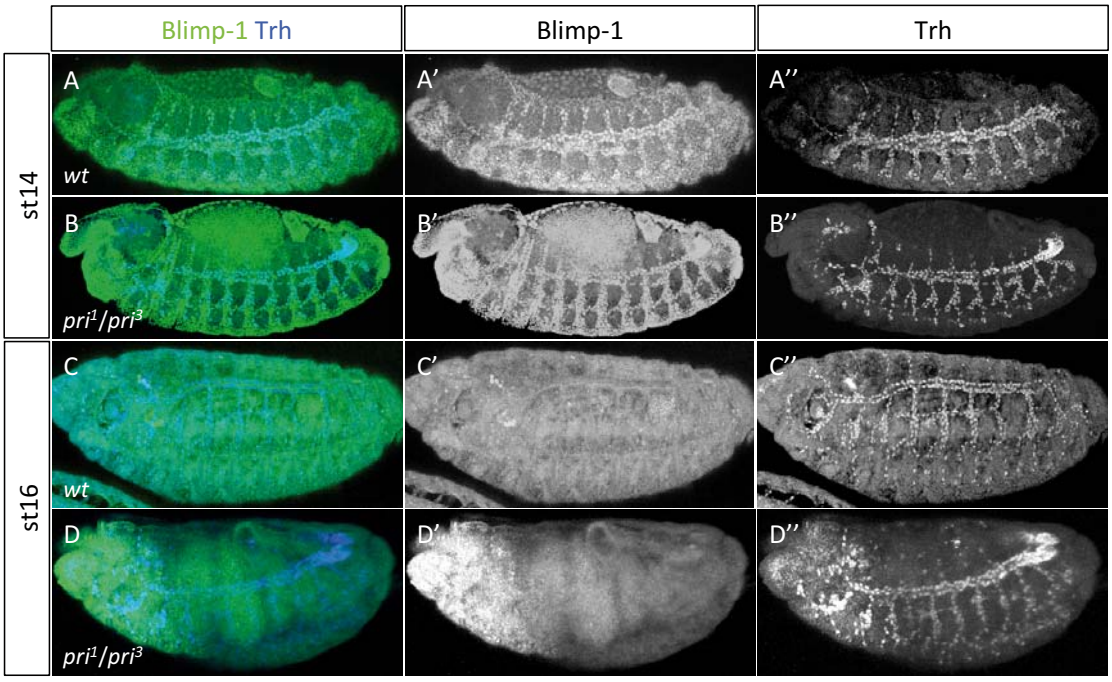

Figure 32: Expression pattern of *Blimp-1* in the absence of *pri*. Stage 14 (A, B) and stage 16 (C, D) *wild-type* (A, C) and *pri* mutant (B, D) embryos stained with anti-Trh (blue) to label tracheal cells and anti-Blimp-1 (green) to label *Blimp-1* expressing cells. In the absence of *pri* expression pattern of *Blimp-1* does not change. As in the *wild-type* embryo, it is expressed in all tracheal cells at stage 14 (A) and its expression disappears at stage 16 (C) in the *pri* mutant embryo (B and D). The co-stainings are shown in the merge images (A-D). The anti-Blimp-1 (A'-D') and anti-Trh (A''-D'') stainings are shown separately.

However, when we checked the expression of *pri* in *Blimp-1* mutants, we observed that expression of *pri* at stage 14 in *Blimp-1* mutants resembles the expression of *pri* at *stage-16-wild-type* embryos (**Figure 33**). In both cases, *pri* expression is lower in non-fusion cells than their stage-14-*wild-type* counterparts.

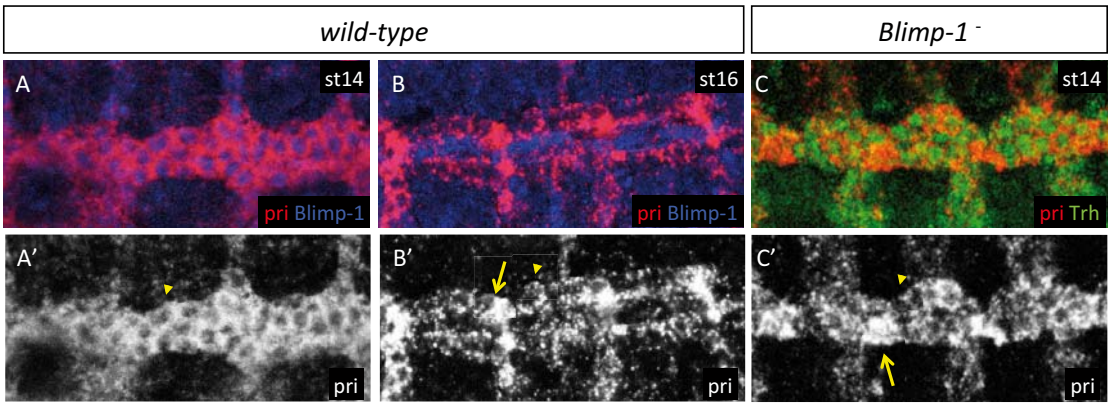

Figure 33: Expression of *pri* alters prematurely in the *Blimp-1* mutant embryo. Fluorescent *in-situ hybridization* of *pri* (red) co-stained with either anti-Blimp-1 (blue) to label *Blimp-1* expressing cells, or anti-Trh (green) to label tracheal cells, in *wild-type* stage 14 (A) and stage 16 (B), and *Blimp-1* mutant stage 16 (C) embryos. In *wild-type* embryos, at stage 14 *pri* is uniformly expressed throughout the tube (A', arrow head) later at stage 16 *pri* expression starts to gradually disappear (arrowhead) except at fusion points (B', arrow). In the *Blimp-1* mutant embryo this differential expression of *pri* starts already at stage 14. Note the gradually disappearing *pri* expression throughout the tube (arrowhead) except at fusion points (arrow) at stage 14 *Blimp-1* mutant embryo. (C). Both the *pri in-situ hybridization* and Blimp-1 antibody staining are shown in the merge images (A, B). Just the *pri in-situ hybridization* is shown (A', B'). Both the *pri in-situ hybridization* and anti-Trh antibody staining are shown in the merge image (C). Just the *pri in-situ hybridization* is shown (C'). All images are single stacks of confocal Z sections.

In order to verify whether those cells with higher pri expression are fusion cells, we performed a double labeling with the fusion cell marker *dysfusion* (*dys*) and showed that those cells are indeed fusion cells (**Figure 34**). These results suggest that *Blimp-1* is required for proper *pri* expression in non-fusion cells but dispensable in fusion cells.

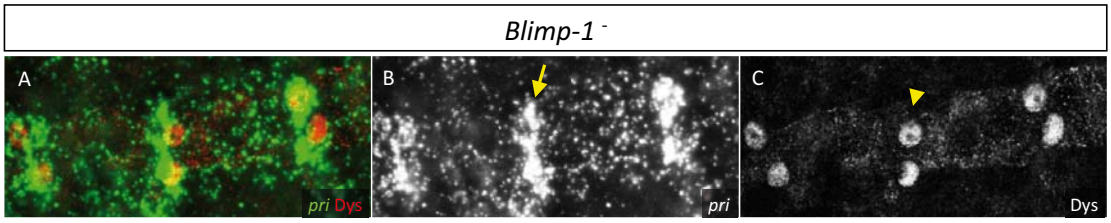

Figure 34: The *pri* expressing cells in the loss of function of *Blimp-1* correspond to the fusion cells. Fluorescent *in-situ hybridization* of pri (green) co-stained with anti-Dys (red) to label fusion cells, in a *Blimp-1* mutant embryo at stage 16. The *pri* expression (arrow) co-localizes with *dys* expression (arrow head) in the cells, indicating that those *pri* expressing cells are fusion cells. Both the *pri in-situ hybridization* and Dys antibody staining are shown in the merge image (A). Just the *pri in-situ hybridization* is shown (B). Just the anti-Dys staining is shown (C).

2.1.3.b Pri expression in Blimp-1 over/ectopic expression

As described in 2.1.1, *Blimp-1* expression fades away from the tracheal system starting from mid-stage 15 and there is no expression of *Blimp-1* in tracheal system at stage 16/17 of wild-type embryos. Our results in 2.1.3.a suggest that *Blimp-1* promotes *pri* expression in non-fusion cells, hence we hypothesized that sustained expression of *Blimp-1* could prevent *pri* expression fading away in non-fusion cells at stage 16 embryos. To test this hypothesis, we used the GAL4/UAS system to drive *UAS-Blimp-1* with *btl-GAL4* driver, which is active in all tracheal cells upon stage 11 (Brand and Perrimon, 1993). However we observed that expression of *pri* is still lower in non-fusion cells (when compared to the fusion cells) in *Blimp-1* over/ectopic expression condition **(Figure 35)**, indicating that the presence of *Blimp-1* is not able to prevent the decline in *pri* expression.

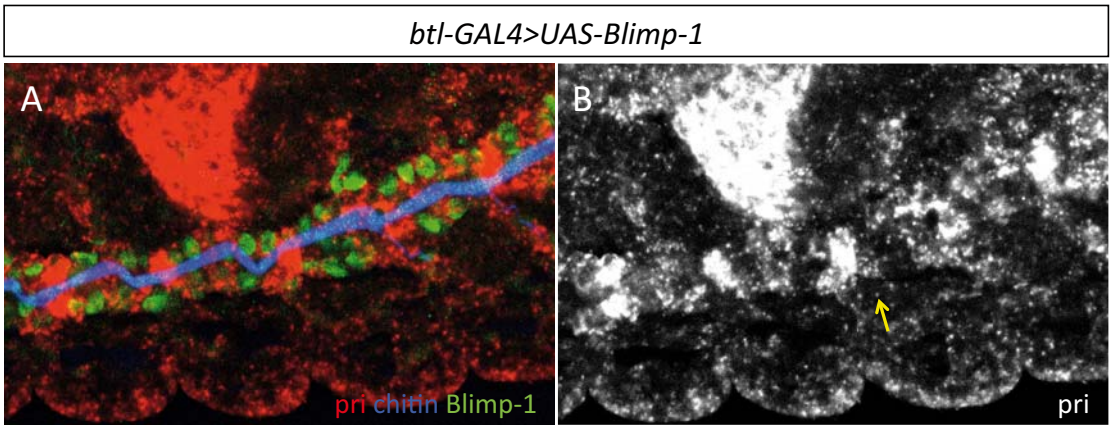

Figure 35: Expression pattern of *pri* in the loss of function of *Blimp-1*. Fluorescent *in-situ hybridization* of pri (red) co-stained with anti-Blimp-1 (green) to label *Blimp-1* expressing cells and fluostain to label chitin structures in an embryo expressing *Blimp-1* ectopically at stage 16. The *pri* expression is absent in non-fusion cells (arrow) as in *wild-type* stage 16 embryos. The *pri in-situ hybridization,* Blimp-1 antibody and fluostain staining are shown in the merge image (A). Just the *pri in-situ hybridization* is shown (B). The image is a single stack of confocal Z sections.

2.1.3.c. Blimp-1, pri double mutant

To understand whether *Blimp-1* and *pri* function together, we generated the double mutant via homologous recombination. The taenidial folds in the double mutants are misoriented yet formed, as in the case of both only *Blimp-1* and only *pri* mutant embryos. When we checked the F-actin in the double mutants, although there seems to be a disorganization in F-actin, we observed very faint F-actin bundles in places (**Figure 36)**. We concluded that the F-actin bundles phenotype of the double mutants resemble more of the *Blimp-1* mutant phenotype since we observed the

absence of F-actin bundling more frequently in *Blimp-1* mutant embryos rather than *pri* mutant embryos.

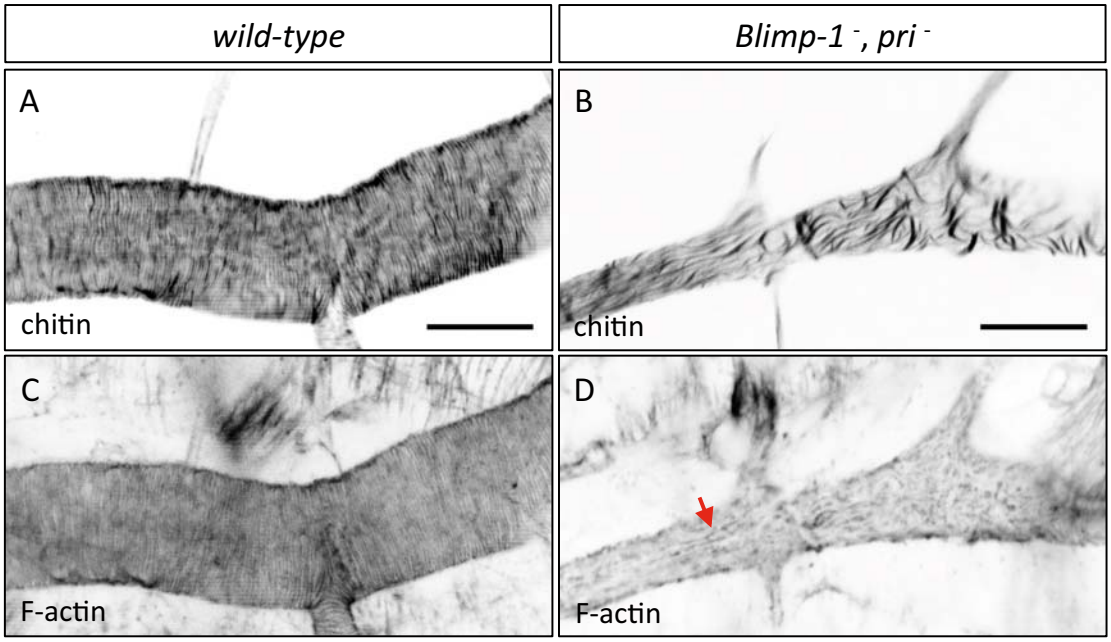

Figure 36: Taenidial folds and F-actin bundles in the *Blimp-1*, *pri* double mutant embryo. *Wild-type* (A, C) and *Blimp-1*, *pri double* mutant embryos (B, D) stained with fluostain to label the taenidial folds (A, B) and phalloidin to label F-actin bundles (C, D). Both the taenidial folds and F-actin bundles run perpendicular to the tube axis in the *wild-type* embryo (A, B) while in the *Blimp-1*, *pri* double mutant embryo F-actin bundles mostly fail to form, yet in places very faint F-actin bundles are formed (D, arrow). The double mutant images are single stacks of confocal Z sections (B, D). Scale bars =10μm.

We also measured the tube size in *Blimp-1*, *pri* double mutant in 3 positions fusion points (f.p.) of Tr7-Tr8 and Tr8-Tr9, and highest width (h.w) at Tr8. We observed that in all positions, the double mutant tube diameter is similar to *pri* mutant tubes while it is significantly lower than *wild-type* (p values for f.p. Tr7-Tr8 = 2.99E-07, f.p. Tr8-Tr9 = 5.27E-06, h.w. Tr8 = 0.015) and *Blimp-1* mutant (p values for f.p. Tr7-Tr8 = 2.76E-08, f.p. Tr8-Tr9 = 1.23E-06, h.w. Tr8 = 2.46E-07) tubes (**Figure 37**).

In summary, we checked 3 structures in double mutant embryos and observed that all are affected. The taenidial folds phenotype of the double mutant resembles both the only *Blimp-1* and only *pri* mutant phenotypes, while the F-actin bundles phenotype of the double mutant resembles more of the *Blimp-1* mutant phenotype, and the tube expansion phenotype of the double mutants resembles more of the *pri* mutant phenotype. These results indicate that there is not a proper hierarchy between

Blimp-1 and *pri*, and both of them seem to affect independently, with some variable degrees, the three aspects analyzed.

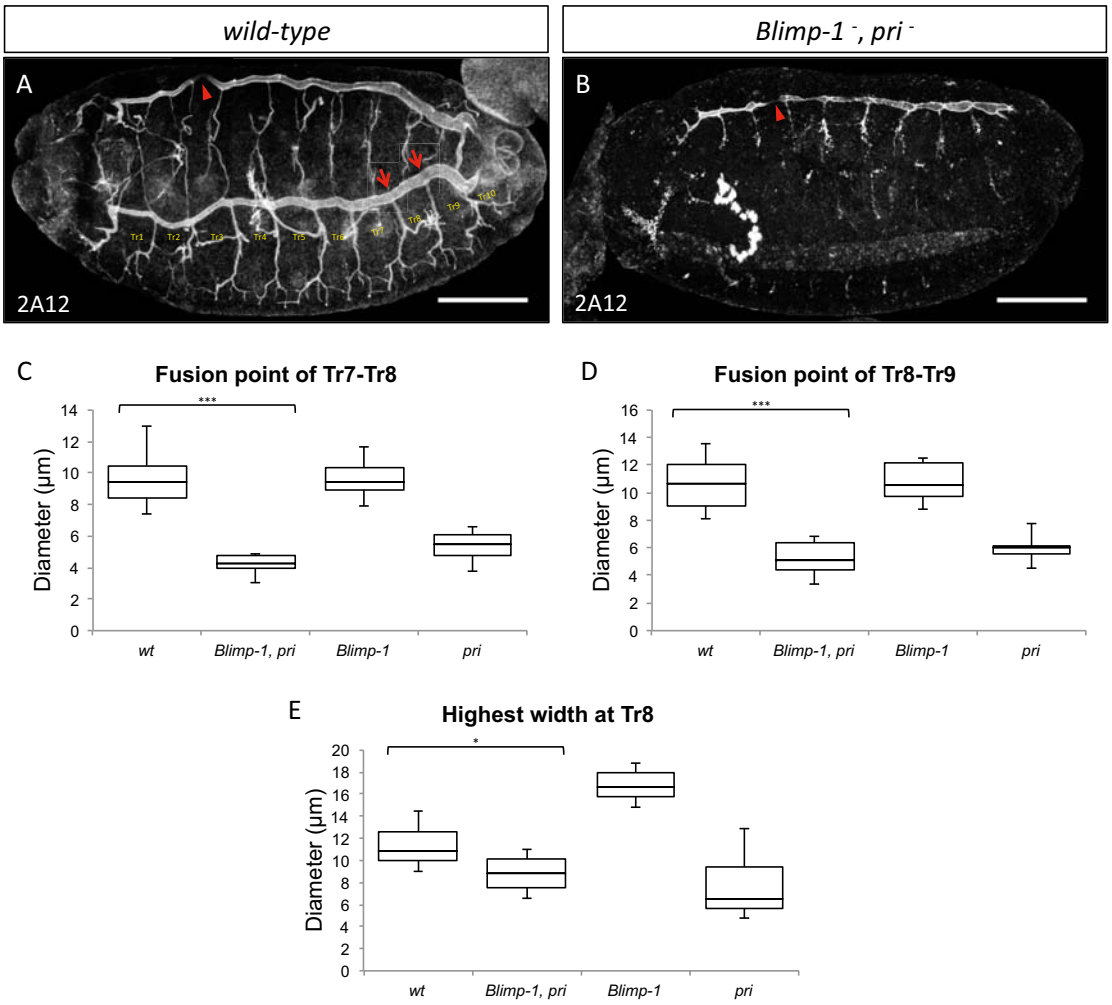

Figure 37: Tube expansion in *Blimp-1*, *pri* double mutant embryos. *Wild-type* (A) and *Blimp-1*, *pri* double mutant (B) embryos stained with luminal marker 2A12. The *wild-type* uniform tube expansion is disrupted in the double mutant embryo. Note the break in DT in *Blimp-1*, *pri* double mutant embryo (arrow head) that also occurs occasionally in the *wild-type* embryo (arrow head). The tube expansion phenotypes of *Blimp-1*, *pri* and *Blimp-1*, *pri* double mutant embryos represented in box plots (C-E). The diameter of *Blimp-1*, *pri* double mutant embryos at fusion points of Tr7-Tr8 and Tr8-Tr9, and along Tr8 is significantly lower than the *wild-types*. *Wild-type* n=15, *Blimp-1*, *pri* double mutant n=6, *Blimp-1* mutant n=10 and *pri* mutant n=10. The whiskers of the box plots represent the minimum and the maximum of the data values (Spear style); * represents the p value ≥ 0.015; *** represents p value < 0.001.

2.1.4 Downstream candidates of *Blimp-1* and *pri*

In order to characterize the role of *Blimp-1* and *pri* in tracheal development, we analyzed the mutant phenotypes using known markers for tracheal development, such as *knickkopf* (*knk*), *vermiform* (*verm*) and *piopio* (*pio*). *Knk* encodes an apical GPI-linked protein that acts at the plasma membrane and whose subcellular localization is important for chitinous matrix organization and tube expansion

(Moussian and collaborators 2005). *Verm* is involved in chitin modification process in the ECM after chitin secretion into the lumen (Luschnig and collaborators 2006). The last marker Pio is secreted into the lumen and suggested to function in the formation of ECM (Jaźwińska A and collaborators 2003). However, none of these protein patterns were modified either in *Blimp-1* or *pri* mutants (**Figures 38, 39 and 40**).

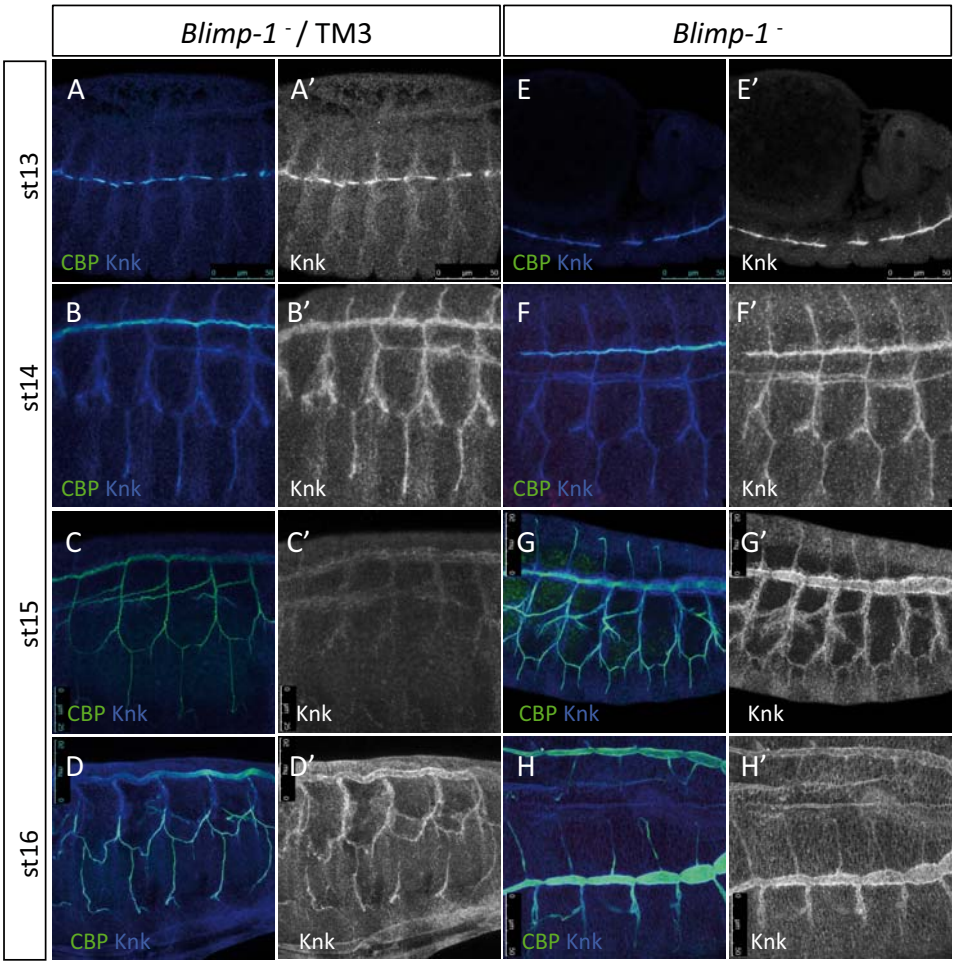

Figure 38: Expression pattern of Knk in *Blimp-1* mutant embryos. Stage 13 (A), 14 (B), 15 (C), and 16 (D) *Blimp-1* heterozygous (control) embryos and stage 13 (E), 14 (F), 15 (G), and 16 (G) *Blimp-1* homozygous embryos stained with CBP (green) to label chitin structures and anti-Knk (blue) to visualize localization of Knk. In *Blimp-1* homozygous embryos the luminal localization of Knk is not altered when compared to control embryos. The co-stainings are shown in the merge images (A-H). The anti-Knk staining is shown separately (A'-H').

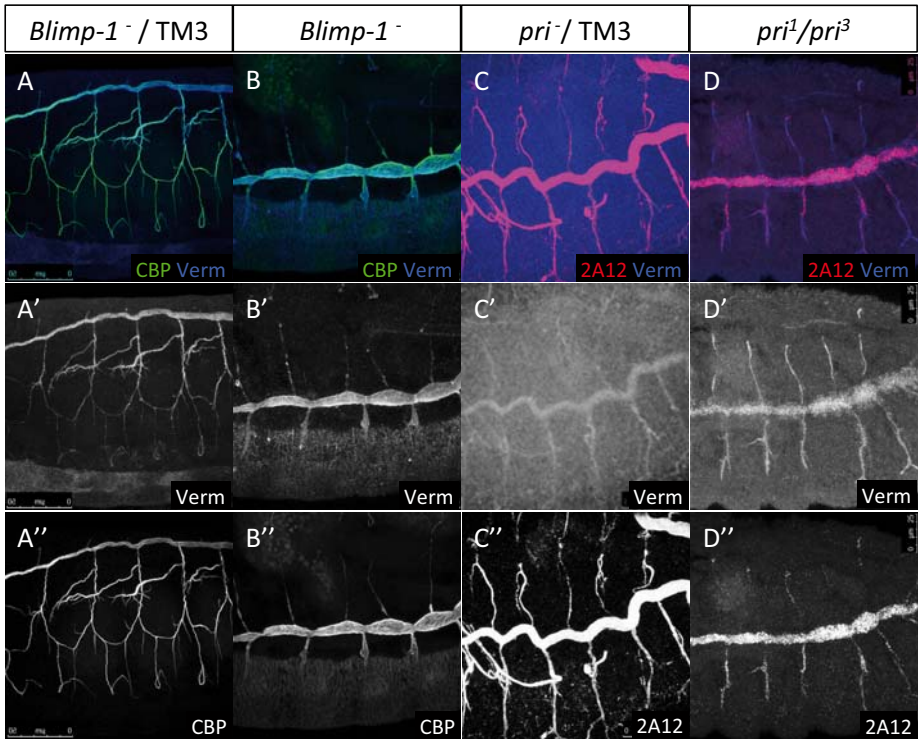

Figure 39: Expression pattern of Verm in *Blimp-1* and *pri* mutant embryos. Stage 16 *Blimp-1* heterozygous (A, control), *Blimp-1* homozygous (B), *pri* heterozygous (C, control) and *pri* homozygous (D) embryos co-stained with anti-Verm (blue) to visualize localization of Verm and either with CBP (green) to label chitin structures or luminal marker 2A12. In both *Blimp-1* and *pri* homozygous embryos, the luminal localization of Verm is not altered when compared to control embryos. Co-stainings are shown in the merge images (A-D). The anti-Verm (A'-D'), CBP (A'', B'') and 2A12 (C'', D'') stainings are shown separately.

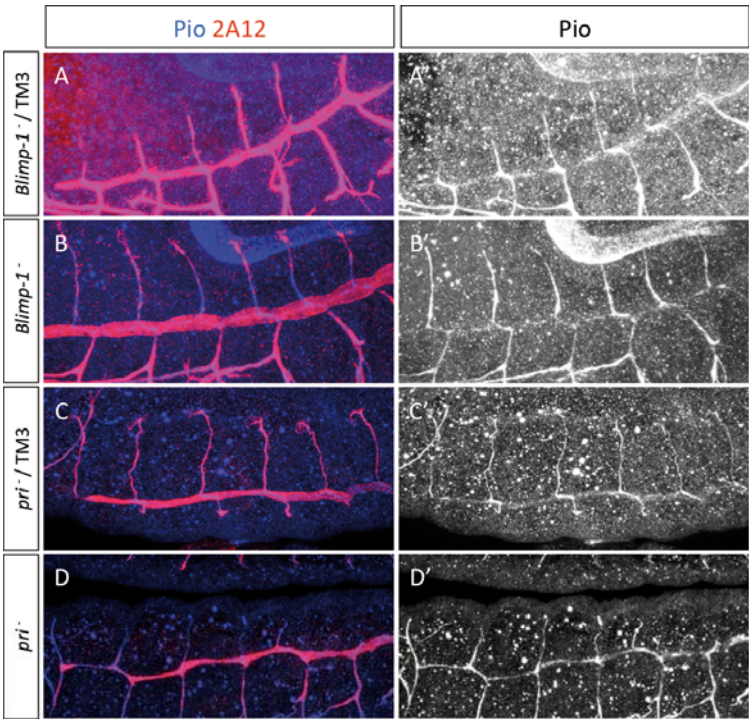

Figure 40: Expression pattern of Pio in *Blimp-1* and *pri* mutant embryos. Stage 16 *Blimp-1* heterozygous (A, control), *Blimp-1* homozygous (B), *pri* heterozygous (C, control) and *pri*

homozygous (D) embryos co-stained with anti-Pio (blue) to visualize localization of Pio and luminal marker 2A12. In both *Blimp-1* and *pri* homozygous embryos the luminal localization of Pio is not altered when compared to control embryos. Co-stainings are shown in the merge images (A-D). The anti-Pio stainings are shown separately (A'-D').

With the idea of revealing new genes functioning in the embryonic taenidial fold formation together with *Blimp-1* and *pri*, we checked the taenidial folds in mutant embryos of *shavenbaby* (*svb*) and *Ftz transcription factor 1*(*ftz-f1*).

Svb encodes a transcription factor and it is known to function downstream of *pri* during the denticle belt formation (Kondo and collaborators 2010). *Blimp-1* regulates expression of *ftz-f1* during embryogenesis and prepupal period (Agawa et al., 2007). To see whether *svb* and *ftz-f1* work as downstream factors of *pri* and *Blimp-1,* respectively, in the tracheal system we checked taenidial folds in *svb* and *ftz-f1* mutant embryos and observed that they are not affected.

2.1.5 Upstream candidates of *Blimp-1* and *pri*

Ecdysone has been already shown to regulate *Blimp-1* expression during embryonic development (Agawa et al., 2007; Chavoshi et al., 2010). To reveal some/other upstream factors of *Blimp-1* and *pri* we analyzed the expression pattern of *Blimp-1* and *pri* in the mutants of two important genes in tracheal development; *trachealess* (*trh*) and *ventral veinless* (*vvl*). And also to reveal whether ecdysone also regulates *pri* expression, we analyzed expression pattern of *pri* in the absence of ecdysone synthesis.

In the absence of *trh* the ectodermal cells are not specified into tracheal cells, and in the absence of *vvl* tracheal cells cannot migrate and stay at the placode stage (stage 11) during embryogenesis (Anderson et al., 1995b; de Celis et al., 1995b; Isaac and Andrew, 1996; Wilk et al., 1996). In *trh* mutant embryos the expression of *Blimp-1* and *pri* is observed in the epidermis, midgut (only for *Blimp-1*) and hindgut cells. Since at the early stages neither *Blimp-1* nor *pri* are expressed and in the later stages the unspecified "tracheal" cells transform into a tissue (ectoderm) that already has expression of *Blimp-1* and *pri,* these results does not allow us to distinguish whether there is a specific regulation of *Blimp-1* and *pri* in tracheal cells due to *trh*. In *vvl* mutant embryos the expression of *Blimp-1* and *pri* are observed in the epidermis,

midgut (only for *Blimp-1*), hindgut and tracheal cells **(Figure 41**). These results suggest that *vvl* is not required for the expression of *Blimp-1* and *pri* in neither tracheal cells nor epidermis.

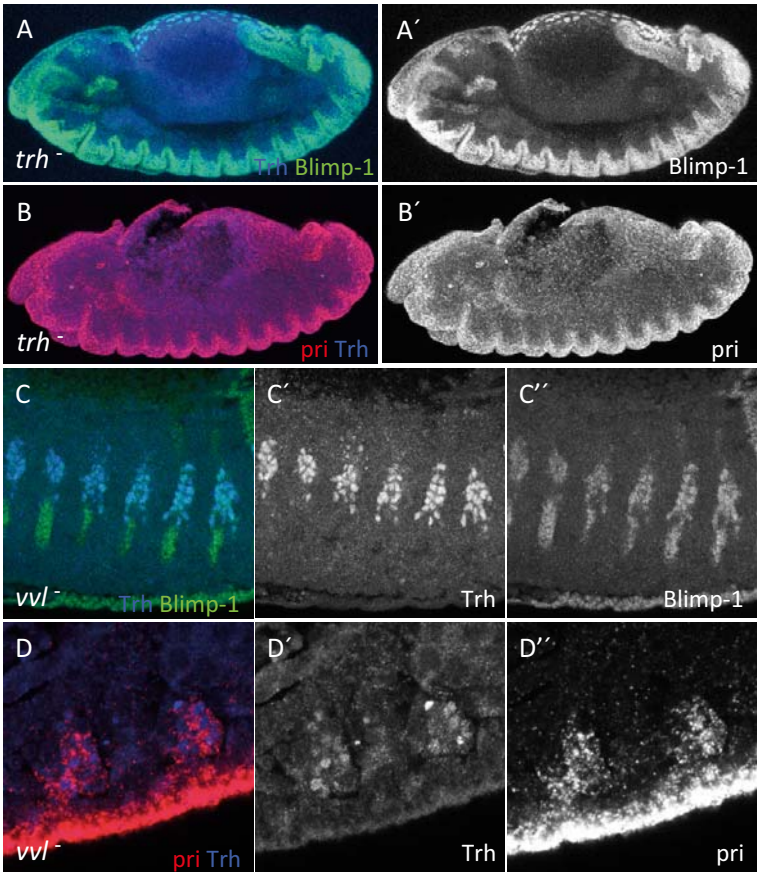

Figure 41: Expression pattern of *Blimp-1* and *pri* in *trh* and *vvl* mutant embryos. *Trh* mutant embryos co-stained either with anti-Blimp-1 (green) to label *Blimp-1* expressing cells and anti-Trh (blue) to label tracheal cells (A) or with fluorescent *in-situ hybridization* of *pri* (red) and anti-Trh (B, blue). *Vvl* mutant embryos co-stained either with anti-Blimp-1 (green) and anti-Trh (C, blue) or with fluorescent *in-situ hybridization* of *pri* (red) and anti-Trh (D, blue). In *trh* mutant embryos, the expression of *Blimp-1* and *pri* are observed in the epidermis, midgut (only for *Blimp-1*) and hindgut cells while in *vvl* mutant embryos the expression of *Blimp-1* and *pri* are observed in those cells and also in tracheal cells. Co-stainings are shown in the merge images (A-D). The fluorescent *in-situ hybridization* of *pri* (B'-D''), anti-Blimp-1 (A'-C'') and anti-Trh (C'-D') stainings are shown separately.

The synthesis of ecdysone relies on the function of the Halloween gene family members such as *shadow* (*sad*), *shade* (*shd*) and *disembodied* (*dib*) (Gilbert and Warren, 2005). In the absence of any of these members, the synthesis of ecdysone has been reported to be disrupted (Petryk et al., 2003; Warren et al., 2002). When we checked the expression of *pri* in *shade* (*shd*) mutant embryos we observed that *pri*

expression is down-regulated (**Figure 42**), suggesting that ecdysone regulates not only the expression of *Blimp-1* but also *pri* during embryogenesis.

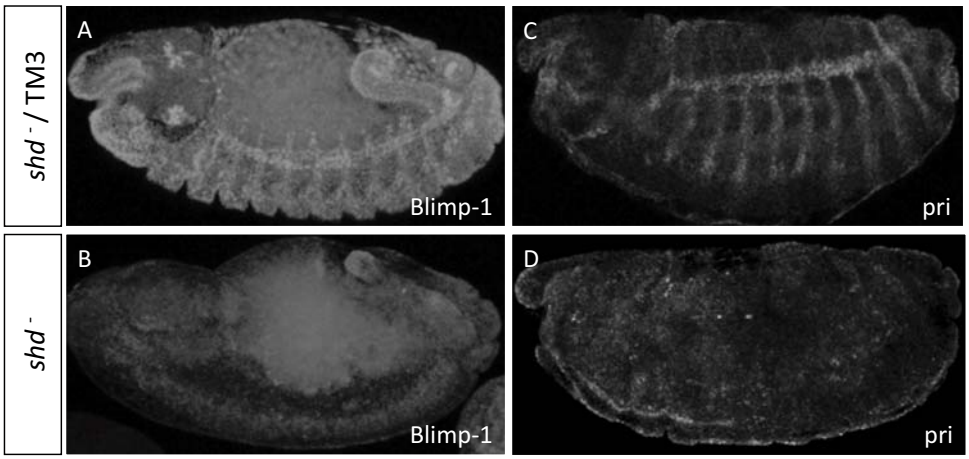

Figure 42: Expression pattern of *Blimp-1* and *pri* in the absence of ecdysone synthesis. *Shd* heterozygous (control, A, C) and *shd* homozygous mutant (B, D) embryos stained with either anti-Blimp-1 (A, B) to label *Blimp-1* expressing cells or fluorescent *in-situ* of *pri* (C, D) to label *pri* expressing cells. The expression of both *Blimp-1* and *pri* in the control embryos (A,C) are absent in *shd* mutant embryos (B, D).

2.1.6 Overexpression and ectopic expression phenotypes of *Blimp-1*

To check whether the amount of *Blimp-1* is important in trachea development, previously in the lab, Sofia Araújo generated the *UAS-Blimp-1* construct. Later, using that construct the transgenic *Drosophila* lines were generated.

2.1.6.a Taenidial folds phenotype

With the aim of visualizing the taenidial fold phenotype of *Blimp-1* over/ectopic expression and examine the effect of relative amounts of Blimp-1 via having an internal control, the anterior part of the embryo, we drove *UAS-Blimp-1* in the posterior part of the embryo using *AbdB-GAL4* as a driver. The expression domain of *AbdB-GAL4* driver at different stages of embryogenesis is shown in **Figure 43** by driving Green Fluorescent Protein (GFP).

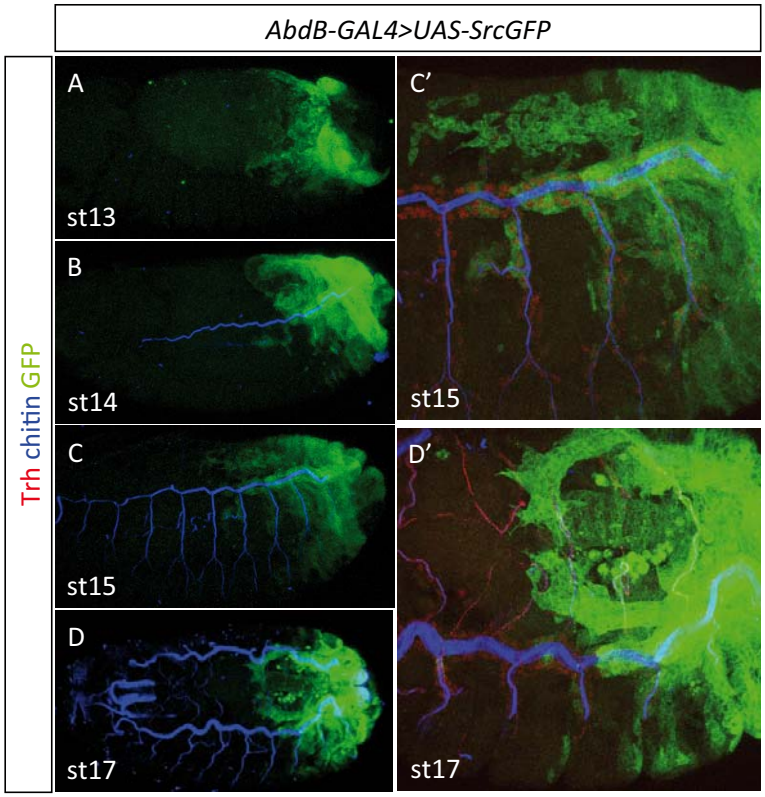

Figure 43: The expression domain of *AbdB-GAL4* driver at different stages of embryogenesis. *AbdB-GAL4* driven *UAS-SrcGFP* expression in *wild-type* embryos, at stage 13 (A), 14 (B), 15 (C, C') and 16 (D, D'), stained with anti-Trh (red) to label the tracheal cells, fluostain to label chitin structures and anti-GFP to detect expression of *UAS-SrcGFP* construct. Note the GFP expression at the posterior part of the embryo including the posterior tracheal metameres. The embryos visualized under confocal microscope with a 10x objective lens (A-D). The same embryos visualized under confocal microscope with a 63x objective lens (C' and D').

To image *AbdBGAL4>UAS-Blimp-1* embryos, we used fluostain to label chitin structures and Blimp-1 antibody to visualize cells which are ectopically expressing *Blimp-1* since at that late stage *Blimp-1* is not expressed in the wild-type cells in the wt/control region. As a result, we observed that the taenidial folds fail to form in the posterior part of the tube (**Figure 44A**). However when we imaged the same embryo with an increased laser power and gain, we observed that in the *AbdB-GAL4* domain there are taenidial folds but they seem to have lower chitin levels than the anterior part of the tube (**Figure 44B**). These results indicate that chitin levels are sensitive to the amount of Blimp-1, and both in the absence (described in 2.1.2.a) and abundance of Blimp-1 the levels of chitin are lower.

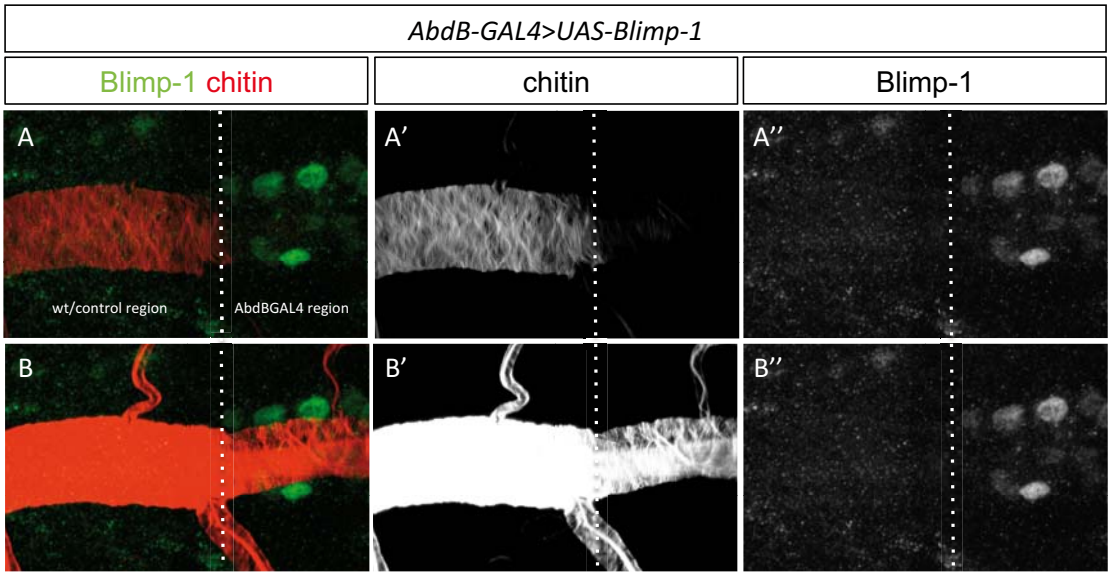

Figure 44: Taenidial folds in *Blimp-1* over/ectopic expression condition. *AbdB-GAL4* driven *UAS-Blimp-1* expression in a stage 17 *wild-type* embryo that is stained with fluostain (red) to label taenidial folds and anti-Blimp-1 (green) to label *Blimp-1* expressing cells that mark *AbdB* domain. When the embryo is imaged under the confocal microscope with "normal" laser power and gain, the taenidial folds are absent in the *AbdB* domain (A). However, when the same embryo is imaged with higher laser power and gain, the taenidial folds can be visualized in the *AbdB* domain. Co-stainings are shown in the merge images (A and B). The fluostain (A' and B') and anti-Blimp-1 (A'' and B'') stainings are shown separately.

2.1.6.b Tube expansion phenotype

Although the tube expansion phenotype of *btl-GAL4>UAS-Blimp-1* has been previously published by Ng and collaborators (Ng et al., 2006), we wondered whether we would obtain the same phenotype with the *UAS-Blimp-1* construct previously generated in our lab. By taking the advantage of GAL4/UAS system, we drove *UAS-Blimp-1* in tracheal cells using *btl-GAL4* as a driver. Then we labeled the tracheal tubes with luminal marker 2A12 in this over/ectopic expression condition of *Blimp-1* and we observed that the tube shape is bubbly as it was described by Ng and collaborators but contradicting with their results, we did not observe any interruptions of the DT (**Figure 45**). This can be explained by utilization of different constructs. Depending on the position of the construct, the *UAS-Blimp-1* might have been expressed in different levels and that might have caused the difference in the severity of the phenotype. Still, in both cases the tube is bubbly and seems not to expand uniformly as in the case of *Blimp-1* mutants. These results suggest that in both absence and abundance of Blimp-1 the tube expansion is affected.

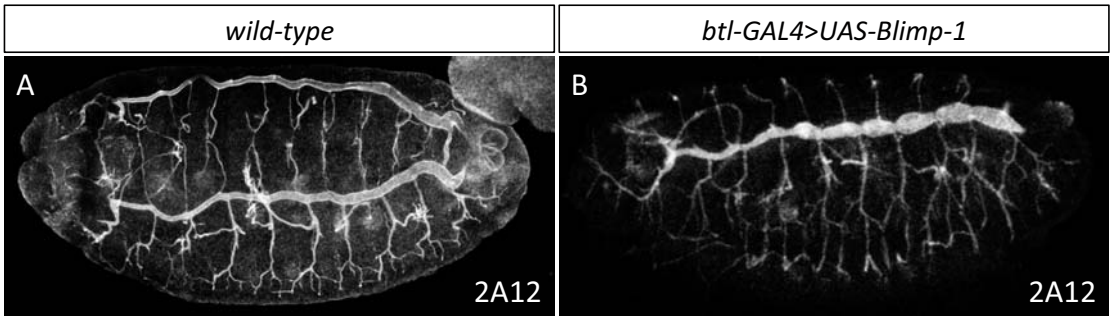

Figure 45: Tube expansion phenotype of *Blimp-1* over/ectopic expression condition. *Wild-type* (A) and *Blimp-1* over/ectopic expressing (B) embryos are stained with luminal marker 2A12. The uniform tube shape in the *wild-type* embryo is disturbed in the *Blimp-1* over/ectopic expression condition.

2.1.6.c Apical cell shape phenotype

By using the same driver (*AbdB-GAL4*) we checked the apical cell shape in *Blimp-1* over/ectopic expression condition. And we observed that the cells have smaller apical surface in *Blimp-1* over/ectopic expression condition when compared to the cells at anterior part of the embryo (**Figure 46**). Interestingly in one cell, labeled with asterisk, in the *AbdB-GAL4* domain, the apical cell surface is bigger than its neighboring cells (**Figure 46**). Moreover in this same cell the levels of chitin are similar to the ones in the anterior region. As a result of *AbdB-GAL4* not being active in all tracheal cells in the posterior region of the embryo, *UAS-Blimp-1* might not be over/ectopically expressed in that cell. The overall behavior of that single cell suggests that over/ectopically expressed *Blimp-1* functions cell autonomously.

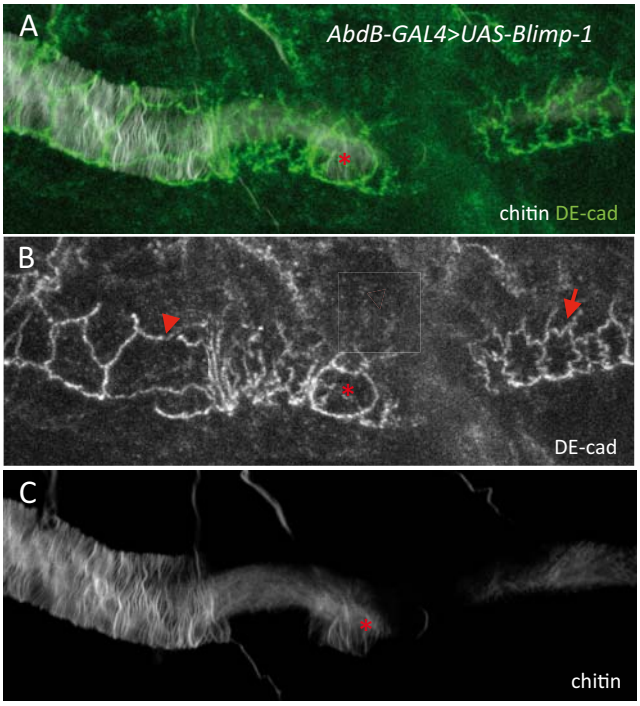

Figure 46: Apical cell shape and taenidial folds in *Blimp-1* over/ectopic expression condition. *AbdB-GAL4* driven *UAS-Blimp-1* expression in a stage 17 *wild-type* (*wt*) embryo that is stained with anti-DE-cad (green) to label apical surface of the cells and fluostain (gray) to label taenidial folds. In the anterior part of the embryo (left), the apical cell shape is similar to *wild-type* apical cell shape (arrowhead) whereas in the posterior part of the embryo (right) the apical surface of the cells are smaller (arrow) when compared to the cells in the anterior region (B). Note the cell labeled with an asterisk that has a "wt" apical cell surface and "wt" taenidial folds (A, B, C). Co-stainings are shown in the merge image (A). The anti-DE-cad (B) and fluostain (C) stainings are shown separately.

In conclusion all the processes we checked for the characterization of over/ectopic expression condition are disturbed, suggesting that all these processes require the correct amount of Blimp-1 protein.

3. Chitin is required for proper F-actin bundling

Our previous results and published data suggest that F-actin is required for proper chitin organization. Nonetheless the reduced amount of chitin and the improper F-actin organization in *Blimp-1* mutants suggest that either *Blimp-1* is effecting chitin and actin independently, or the effect of actin could be the consequence of the effect of *Blimp-1* on chitin. To address this question, we checked F-actin in *krotzkopf verkehrt* (*kkv*) mutant embryos. In *kkv* mutants, chitin synthesis is absent and this allowed us to check what happens to actin in the absence of chitin. In addition, we checked F-actin in *knk* mutant embryos. In *knk* mutants, chitin organization is disrupted and this allowed us to check what happens to actin in the

absence of proper chitin organization. Interestingly, we observed that apical F-actin is disorganized and does not form bundles when we impair either chitin synthesis or chitin organization (**Figure 47**). These results indicate that the existence of chitin and the proper chitin organization are required for the correct F-actin organization, as much as proper F-actin organization is required for proper formation of chitin structures. Thus, during tracheal system development there is a crosstalk between F-actin and chitin structures.

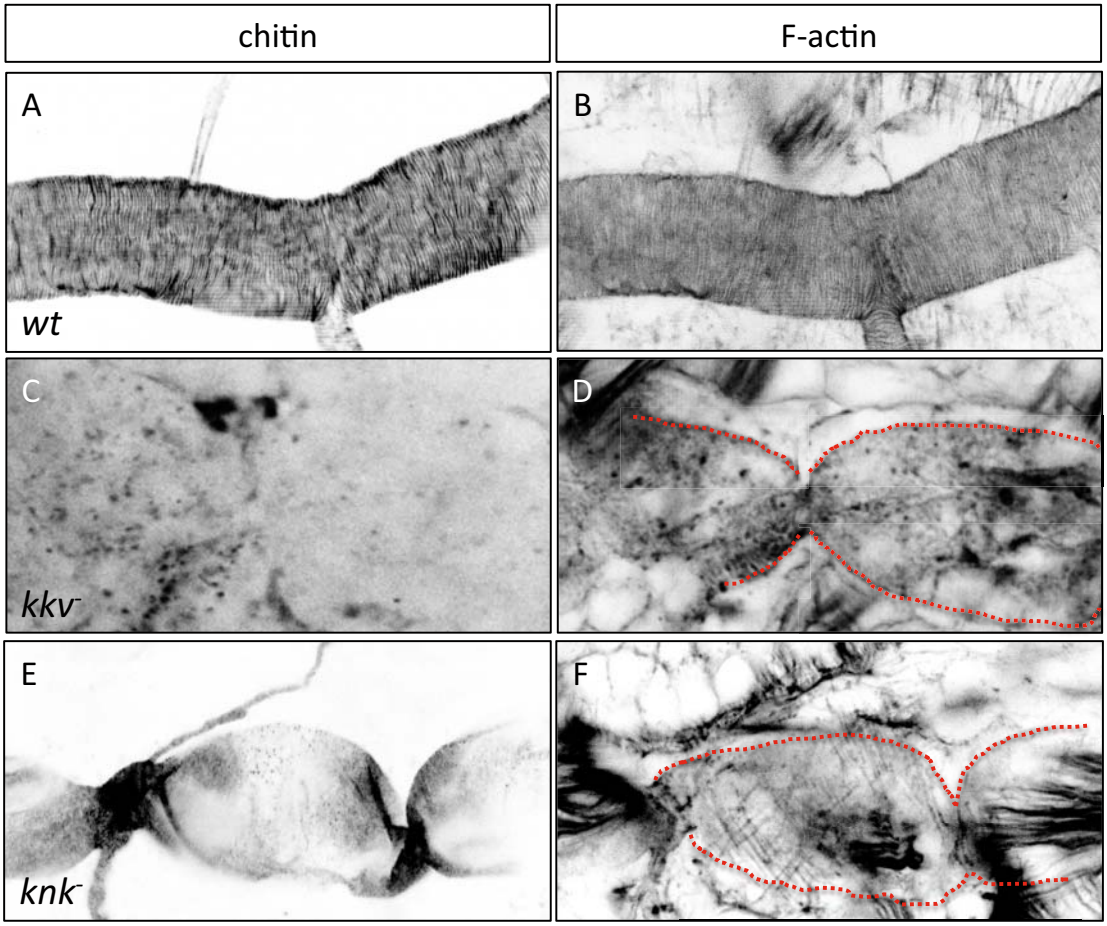

Figure 47: Taenidial folds and F-actin bundles in *kkv* and *knk* mutant embryos. *Wild-type* (A, B), *kkv* mutant (C, D) and *knk* (E, F) mutant embryos stained with fluostain to label the taenidial folds (A, C, E) and phalloidin to label F-actin bundles (B, D, F). The taenidial folds and F-actin bundles run perpendicular to the tube axis in the *wild-type* embryo (A, B) while in the both *kkv* and *knk* mutant embryos taenidial folds are absent and F-actin bundles fail to form (C-F). The red dotted lines label the apical surface of the cells in the *kkv* and *knk* mutant embryos (D, F). The images are single stacks of confocal Z sections (C-F).

4. The effect of "actin genes" on taenidial fold formation

The involvement of *DAAM* and *Tec29* in taenidial fold formation during larval development has been published in 2006 by Matusek *and collaborators*. The authors also showed that apical actin is disorganized in the absence of *DAAM* and *Tec29*. With the aim of understanding whether these genes also play a role in taenidial fold formation during embryonic development, we checked taenidial folds in their mutant embryos. We observed that taenidial folds are formed but misoriented in those embryos (**Figure 48**). When we checked F-actin organization in those embryos, we observed that and apical F-actin bundles are formed. Additionally, as in the case of *wild-type* and *pri* mutant embryos, the actin bundles have the same pattern of organization as the taenidial folds. If there is a delay in F-actin bundling in the absence of *DAAM* and *Tec29*, as in the case of *pri*, this could also be one of the reasons why the reported mutant F-actin phenotypes of *DAAM* and *Tec29* are different than ours. The other reason might be that the F-actin bundles formed in the absence of *DAAM* are very hard to observe since they are very thin when compared to the *wild-type* ones.

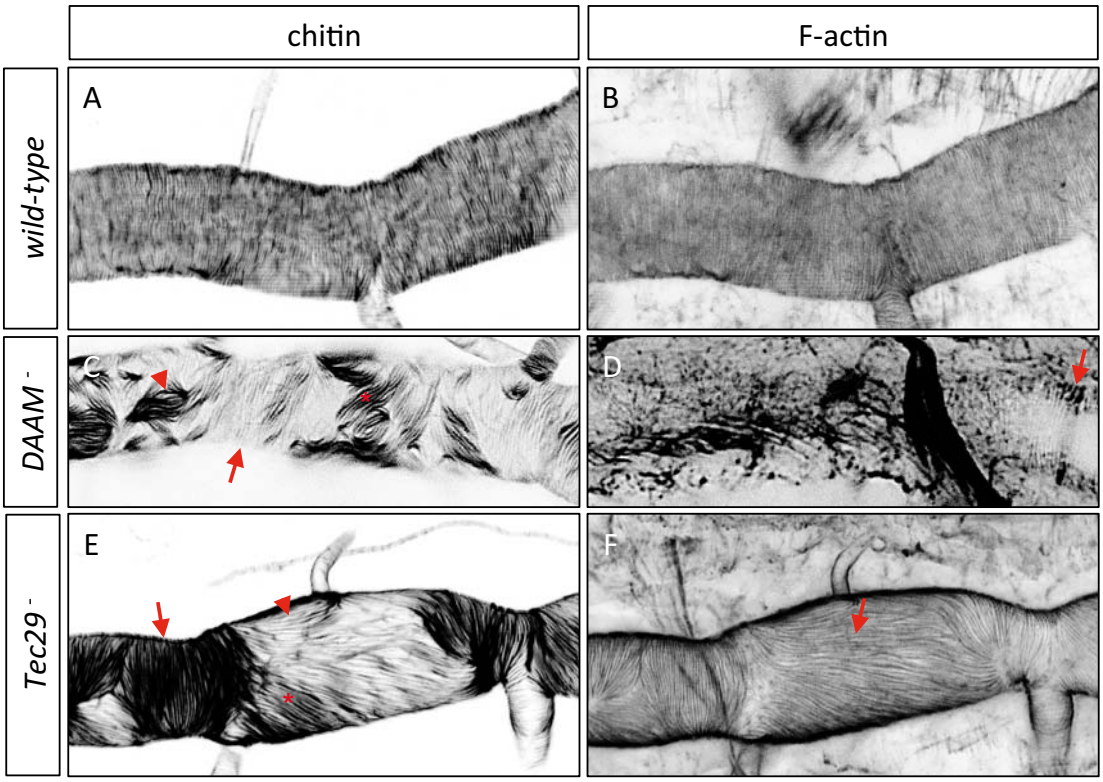

Figure 48: Taenidial folds and F-actin bundles in *DAAM* and *Tec29* mutant embryos. *Wild-type* (A, B), *DAAM* mutant (C, D) and *Tec29* (E, F) mutant embryos stained with fluostain to label the taenidial folds (A, C, E) and phalloidin to label F-actin bundles (B, D, F). The taenidial folds and F-

actin bundles run perpendicular to the tube axis in the *wild-type* embryo (A, B). In the both *DAAM* and *Tec29* mutant embryos taenidial folds are mis-oriented with chitin fibers that run sometimes perpendicular (arrow) or parallel (arrowhead) to the tube axis or with a 45° angle (asterisk). Although the F-actin bundles (arrow) in the *DAAM* mutant are thinner and harder to visualize than the ones in *Tec29* mutant (arrow), the F-actin bundles that underlie taenidial folds in both mutant embryos have a similar pattern as the taenidial folds (D , F).

Our previous results show that apical F-actin rings are formed prior to taenidial fold formation, suggesting that proper formation of actin bundles are required for the proper formation of taenidial folds, and this analysis in mutants for *DAAM* and *Tec29* confirms that hypothesis.

Singed (*sn*) is the *Drosophila* homolog of the actin bundling protein Fascin. And *forked* (*f*), another actin cross linker, function with *sn* in migration of tracheal cells during embryogenesis as well as formation of adult cuticle structures, bristles (Okenve-Ramos and Llimargas, 2014; Tilney et al., 1995). In order to investigate whether *sn* and/or *f* function/s in the formation of apical F-actin bundles and taenidial folds, we checked those structures in the absence of *sn, f* and both (via the double mutant of *sn* and *f*). Our analysis revealed that neither *sn* nor *f* functions in those processes since we did not observe any differences in apical F-actin rings and taenidial folds when compared to *wild-type*.

5. The effect of cell shape on taenidial fold orientation

The apical cell shape of *Blimp-1* mutants resembles the published apical cell shape of *Src42A* mutants, in which the longest axis of the apical surface of the cells is perpendicular to the tube axis (Matusek et al., 2006). The 90° angle change in both taenidial fold orientation and the longest axis of the apical cell surface in *Blimp-1* mutant embryos led us to think that the alteration of apical cell surface shape might be causing the taenidial fold orientation phenotype. Additionally, as in the case of *DAAM* and *Tec29, Src42A* was published to function in taenidial fold formation during larval development (Matusek et al., 2006). In order to reveal whether there is a correlation between apical cell shape and orientations of taenidial folds, and also reveal whether *Src42A* functions in formation of taenidial folds during embryonic development, we checked taenidial folds in *Src42A* mutants. However we did not observe any change in taenidial folds when compared to the *wild-types*, indicating that the apical cell shape does not have a direct effect on taenidial fold orientation (**Figure 49**).

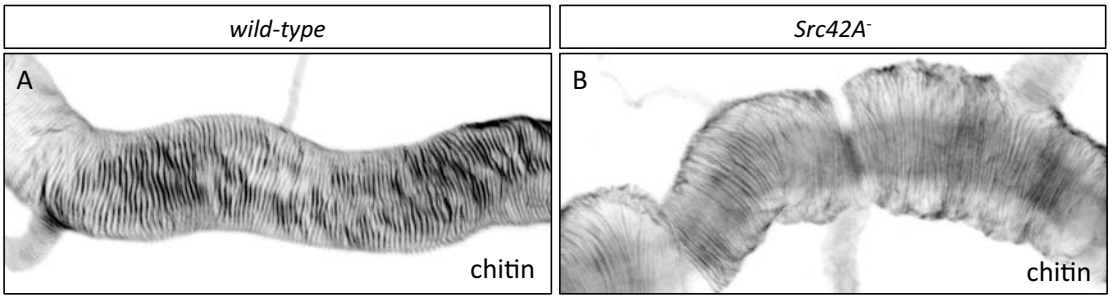

Figure 49: Taenidial folds in the *Src42A* mutant embryo. *Wild-type* (A) and *Src42A* mutant (B) embryos stained with fluostain to label the taenidial folds. The taenidial folds run perpendicular to the tube axis in the both *wild-type* (A) and *Src42A* mutant (B) embryos.

6. Single cells contribution to form a supra-cellular structure

Taking into consideration that taenidial folds are extracellular structures formed by multiple cells, we studied how individual cells contribute to generate this supra-cellular structure via three strategies: generating mutant/overexpression clones of *Blimp-1* and *pri,* rescuing the mutant phenotypes of *Blimp-1* and *pri*, and down-regulating cell-cell junctions.

6.1. Rescue of *Blimp-1* and *pri* mutant phenotypes

We started our analysis on how individual cells contribute to generate this supra-cellular structure, by performing the rescue experiments in which we tried to rescu the mutant phenotypes of *Blimp-1* and *pri* in the posterior part of the trachea, using *AbdB-GAL4* as a driver. We focused specifically on the taenidial folds at the border to see how they are oriented in relation to their neighbors. In both *Blimp-1* and *pri* rescues, we observed that the misoriented taenidial folds are restored to their *wild-type* orientations in the *AbdB* domain (**Figure 50**) indicating that both *UAS-Blimp-1* and *UAS-pri* are able to rescue their mutant phenotypes.

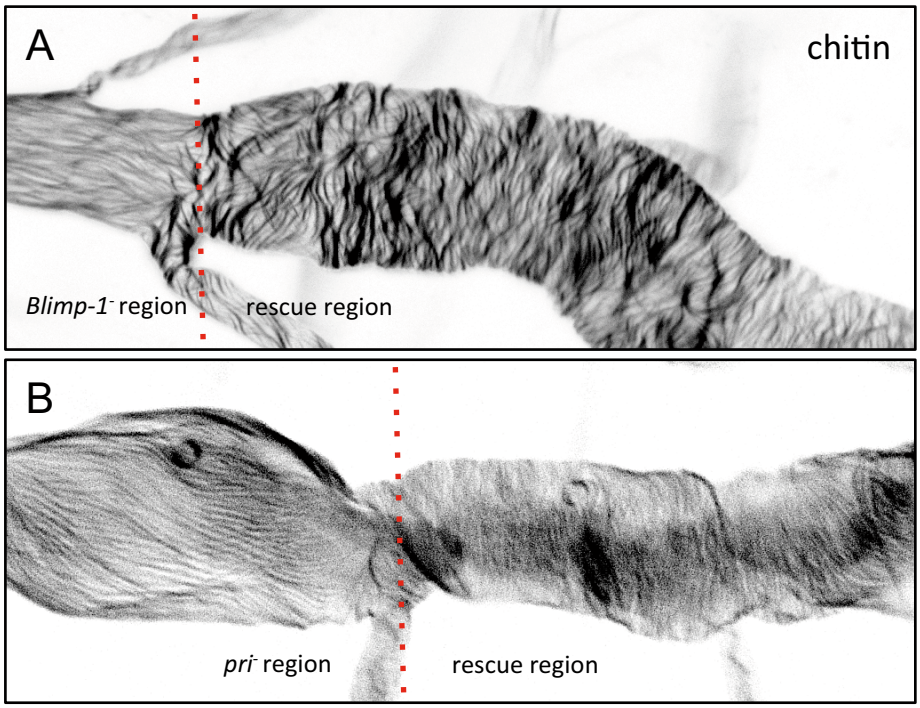

Figure 50: Taenidial folds orientation phenotype is rescued in the *Blimp-1* and *pri* mutant embryos. The *Blimp-1* mutant (A) and *pri* mutant (B) embryos, carrying *AbdB-GAL4>UAS-Blimp-1* (A) and *AbdB-GAL4>UAS-pri* (B) constructs, stained with fluostain to label taenidial folds (A, B). The orientation of taenidial folds that run parallel to the tube axis in *Blimp-1* and *pri* mutant regions are rescued at the posterior part of the embryos, the rescue regions (A, B).

To reach single-cell resolution, we used *Blimp-1* rescues by this way we were able to label the rescued cells with GFP, because of the *UAS-Blimp-1, UAS-SrcGFP* recombination. We observed that in some GFP positive cells, for example the cell marked with an asterisk in **Figure 51**, the orientation of taenidial folds is not completely rescued. While in some GFP negative cells, like the cell marked with two asterisks, the taenidial folds orientation is rescued (F**igure 51**). These results imply that for the orientation of taenidial folds, the genetic code of the cell is not as essential as the taenidial folds orientation in the neighboring cells, probably to sustain the continuity. Therefore, we concluded that orientation of taenidial folds is not cell-autonomously regulated and it depends highly on the taenidial folds in the neighboring cells.

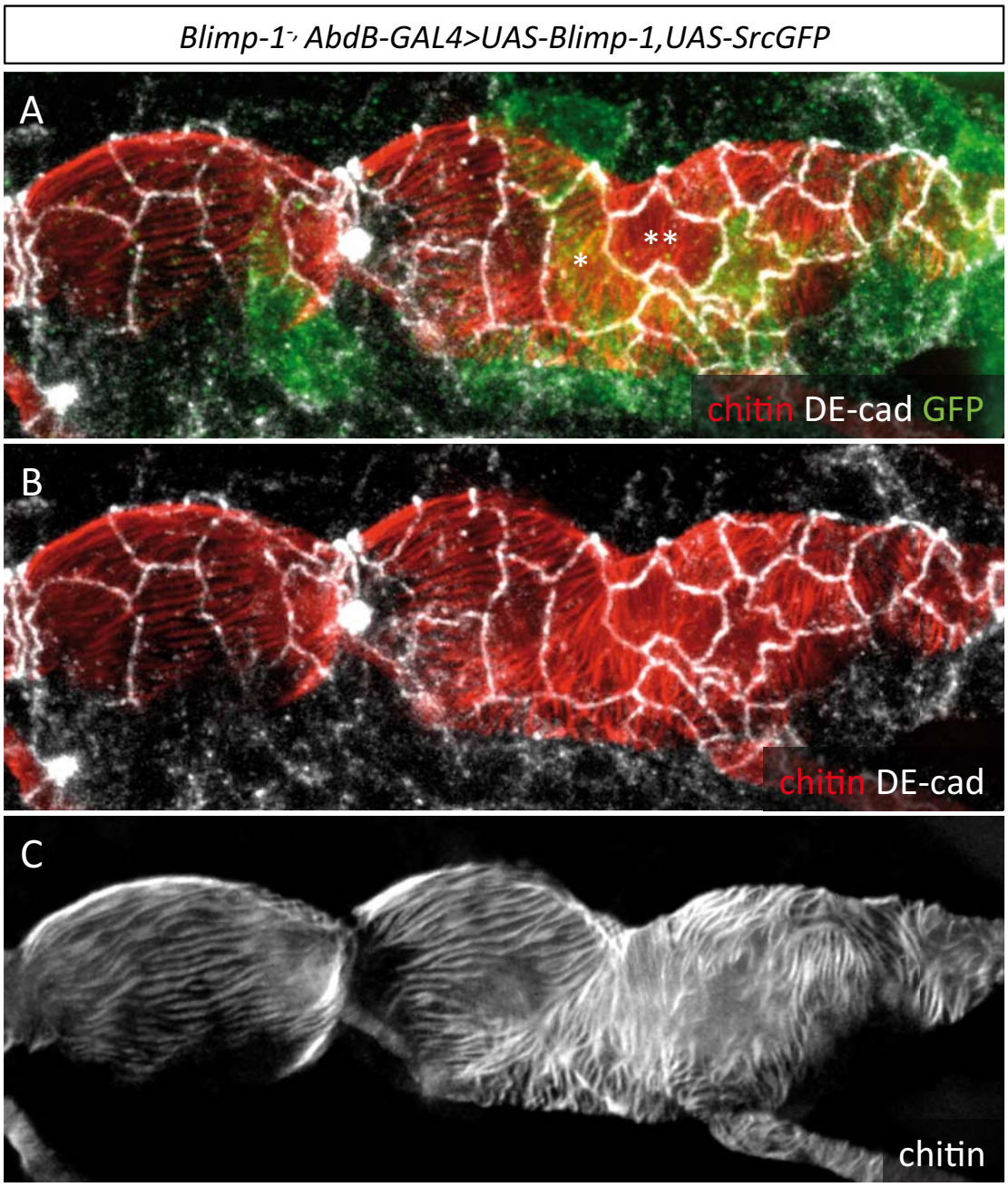

Figure 51: The orientation of taenidial folds is not regulated cell-autonomously. The *Blimp-1* mutant embryo, carrying *UAS-Blimp-1, UAS-SrcGFP* recombinant and *AbdB-GAL4* constructs, stained with fluostain (gray) to label taenidial folds, anti-DE-cad (red) to label apical surface of the cells and anti-GFP (green) to detect expression of *UAS-SrcGFP* (A, B, C). The taenidial folds in the cell marked with a single asterisk run parallel to the tube axis, although that cell carries *UAS-Blimp-1, UAS-SrcGFP* recombinant construct, thus it is "rescued". While the taenidial folds in the cell marked with double asterisk run perpendicular to the tube axis, although that cell does not carry the *UAS-Blimp-1, UAS-SrcGFP* recombinant construct, thus it is not "rescued". The tripple- and co-stainings are shown in the merge images (A, B). The fluostain staining is shown separately (C).

6.2. *Blimp-1* over/ectopic expression clones

With the idea of generating mutant clones, we used *RNA interference* (*RNAi*) method to down-regulate *Blimp-1* and *pri* but we did not observe any taenidial folds phenotype with the *RNAi* lines of *Blimp-1* and *pri*. Subsequently, we used *UAS-Blimp-1* and *UAS-pri* lines to generate overexpression clones of *Blimp-1* and *pri*. The *UAS-pri* line did not produce any taenidial folds phenotype indicating that increasing the amounts of Pri proteins does not have an effect. The *UAS-Blimp-1* line produced taenidial folds phenotype as described in part 2.1.6. So, we generated flip-out clones of over/ectopic expression of *Blimp-1* using *heat-shock-flippase* (*hs-FLP*) promoter to enable *btl-GAL4* activity at high temperatures. We used *UAS-Blimp-1, UAS-SrcGFP* recombinant flies to mark the clones with GFP. As a result, we observed that taenidial folds formed by the cells in the clones are thinner when compared to the taenidial folds formed in the *wild-type* cells, outside of the clones (**Figure 52**).

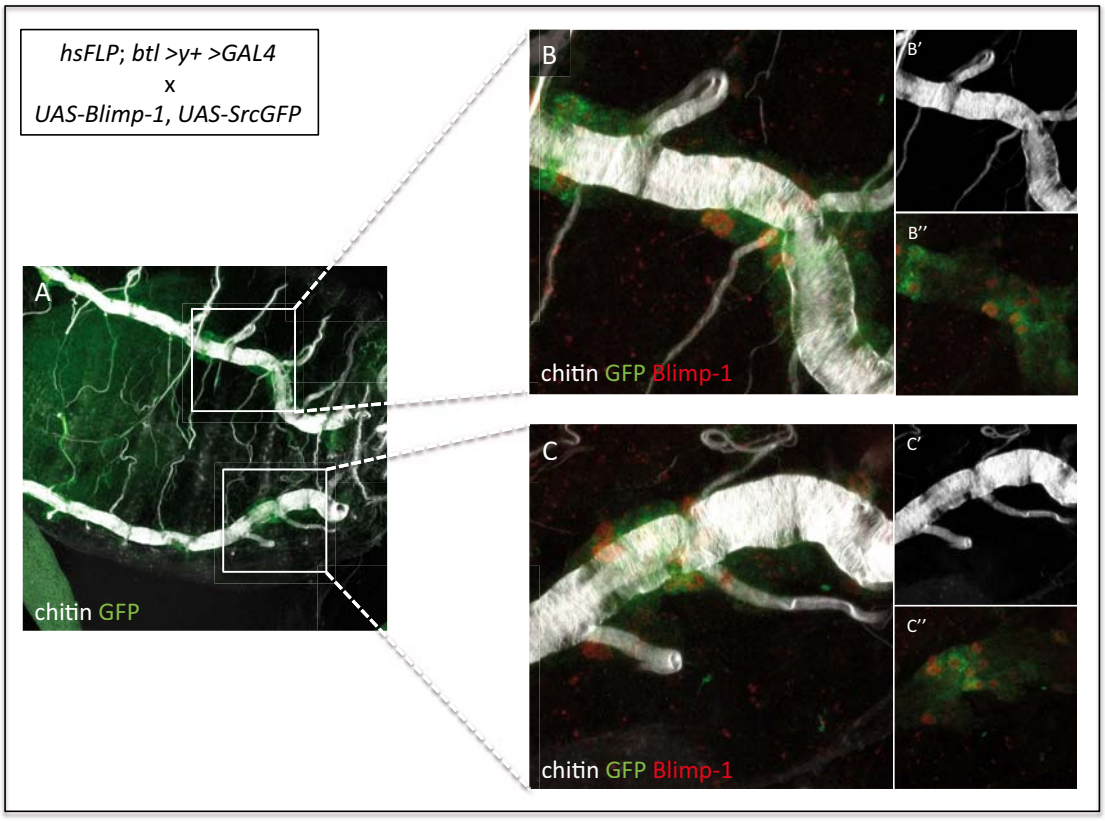

Figure 52: Taenidial folds in the *Blimp-1* over/ectopic expression clones. The embryo with flip-out clones of over/ectopic expression of *Blimp*-1 stained with anti-Blimp-1 (red) to label *Blimp-1* expressing cells, fluostain (gray) to label taenidial folds and anti-GFP (green) to detect expression of *UAS-SrcGFP* construct (hence the clones, A-C). Note that the taenidial folds that are formed in the clones are thinner than their neighboring taenidial folds formed by the cells outside of the clones. The co-/tripple-stainings are shown in the merge images (A-C). The anti-Blimp-1 and anti-GFP co-stainings and fluostain (B', C') staining are shown separately (B'', C''). The embryo visualized under

confocal microscope with a 40x objective lens (A). Different parts of the same embryo visualized under confocal microscope with a 63x objective lens (B, C).

Additionally we observed that the apical cell shape in clones is altered when compared to their neighboring *wild-type* cells (**Figure 53**). These results suggest that over/ectopically expressed *Blimp-1* functions cell-autonomously yet they do not answer whether taenidial folds are formed cell-autonomously or not.

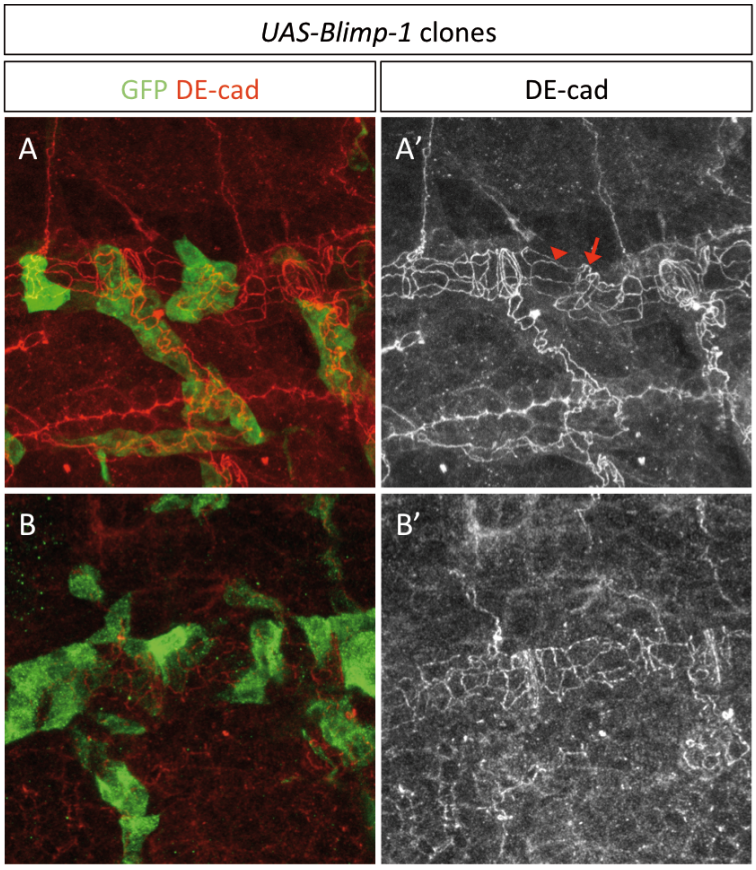

Figure 53: Apical cell shape in the *Blimp-1* over/ectopic expression clones. The embryos with flip-out clones of over/ectopic expression of *Blimp*-1 stained with anti-DE-cad (red) to label apical surface of the cells and anti-GFP (green) to detect expression of *UAS-SrcGFP* construct (hence the clones, A, B). Note that the apical surface of the cells in the clones (arrow) is altered in shape when compared to the cells outside of the clones (arrowhead). The co-stainings are shown in the merge images (A, B). The anti-DE-cad stainings are shown separately (A', B').

6.3. Effect of cellular junctions in taenidial fold formation

If the orientation of taenidial folds relies on the taenidial folds formed by the neighboring cells, we hypothesized that impairing cell-cell junctions (by the means of down-regulating cell-cell junctions) should interrupt the continuity of the taenidial folds. To test this hypothesis we used RNA interference method to down-regulate *alpha-catenin* (*α-cat*), which is an important component of adherens junctions. When

we checked the taenidial folds in *alpha-catenin* down-regulated embryos we did not observe any taenidial folds phenotype. However when we checked the 3rd instar larval tracheas, we observed that upon *alpha-catenin* down-regulation, the taenidial folds are formed but instead of being continuous and passing from one cell to another, they stop at specific points. Interestingly when we checked the actin rings structure in those tracheal tubes, we observed that the actin rings share the same pattern as the taenidial folds.

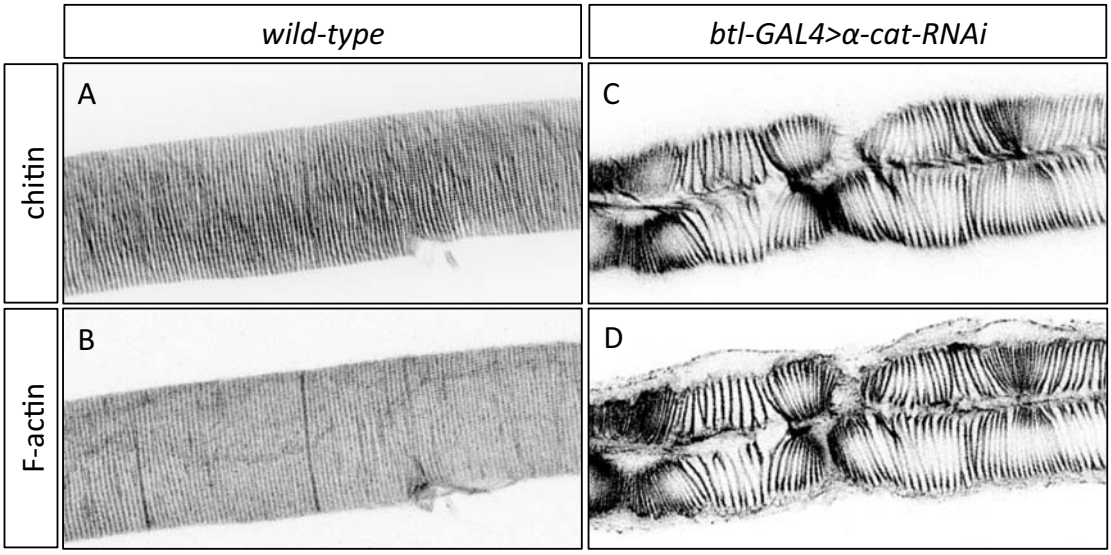

Figure 54: Taenidial folds and F-actin bundles in the absence of cellular junctions. *Wild-type* 3rd instar larval tracheas carrying either no constructs (A, B) or *btl-GAL4* and *α-cat-RNAi* constructs (C, D) are stained with fluostain (A, C) to label taenidial folds and phalloidin (B, D) to label F-actin bundles. The continuous taenidial folds and F-actin bundles in the *wild-type* larval trachea (A, B) are disrupted upon down regulation of cellular junctions (C, D). Single stacks of confocal Z sections of the same larval trachea (C, D).

Furthermore, by labeling the cell boundaries with Spectrin (Spec) antibody we observed that those specific points, where the taenidial folds become discontinuous, correspond to the cell boundaries.

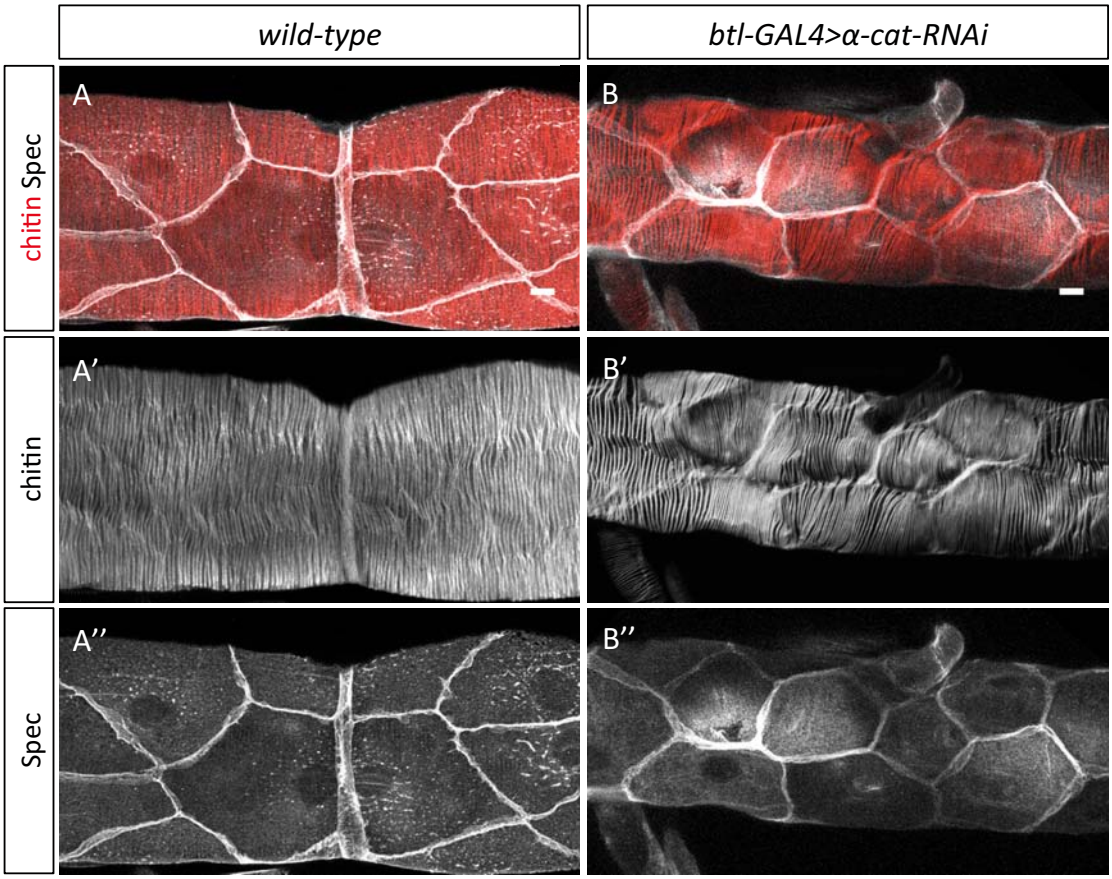

Figure 55: The taenidial folds in the absence of cellular junctions become discontinuous at the apical cell boundaries. *Wild-type* 3rd instar larval tracheas, carrying either no constructs (A) or *btl-GAL4* and *α-cat-RNAi* constructs (B) are stained with fluostain (red) to label taenidial folds and anti-Spec (gray) to label apical cell boundaries. The continuous taenidial folds in the *wild-type* larval trachea (A) become discontinuous at the apical cell boundaries upon down regulation of cellular junctions (B). The co-stainings are shown in the merge images (A, B). The fluostain (A', B') and anti-Spec (A'', B'') stainings are shown separately.

Altogether these results prove our hypothesis that orientation of taenidial folds relies on neighboring cells and impairing cell-cell communications results in the cells forming their taenidial folds independently of one another.

CONCLUSIONS

1. There is a strong spatial correlation between the formation of apical F-actin bundles and taenidial folds.

2. Both *Blimp-1* and *pri* are required for:
    a. proper orientation of taenidial folds
    b. proper apical F-actin organization
    c. proper apical cell surface
    d. proper tube expansion
    e. air-filling of the tracheal tubes

3. *Blimp-1* affectss the chitin levels in *Drosophila* embryos.

4. *Blimp-1* is specifically required for circumferential tube expansion in non-fusion cells of DT while *pri* is important for circumferential tube expansion throughout the DT.

5. The inability of tracheal tubes to fill with air in *Blimp-1* and *pri* mutants is not due to the lack of chitin clearance.

6. *Pri* does not regulate *Blimp-1* expression.

7. *Blimp-1* is required for proper *pri* expression in non-fusion cells but dispensable in fusion cells.

8. There is not a proper hierarchy between *Blimp-1* and *pri*, and both of them seem to affect independently, with some variable degrees, the taenidial fold formation, F-actin bundling and tube expansion.

9. Neither *knk* nor *verm* nor *pio* function as downstream factor of *Blimp-1* whilst neither *verm* nor *pio* function as downstream factor of *pri.*

10. *Vvl* is not required for the expression of *Blimp-1* and *pri* neither in the tracheal nor in the epidermis

11. Ecdysone regulates not only the expression of *Blimp-1* but also *pri* during embryogenesis.

12. The apical cell surface expansion and the levels of chitin, are affected in the both the absence and abundance of Blimp-1.

13. Chitin is required for proper F-actin bundling.

14. The apical cell shape does not have a direct effect on taenidial fold orientation.

15. Over/ectopically expressed *Blimp-1* functions cell-autonomously.

16. The orientation of taenidial folds is not cell-autonomously regulated and it depends highly on the taenidial folds formed by neighboring cells.

17. Impairing cell-cell junctions results in cells forming their taenidial folds independently of one another.

DISCUSSION

Formation of tubular organ systems like our lungs, kidneys and vascular system has been the focus of many scientists for several years. One of the fascinating properties of those systems is to generate tubes of efficient length and width that can resist both internal and external mechanical forces. In this study, we used *Drosophila melanogaster* as a model organism, and its tracheal network as a system to study the chitin structures, called taenidial folds, which are responsible for giving mechanical strength to the tubes.

1. The role of fusion cells in tube expansion as unveiled by *Blimp-1* and *pri* mutant phenotypes

Our analysis of *Blimp-1* and *pri* mutant embryos revealed that fusion cells are exempt of the effect of *Blimp-1* on tube expansion while in *pri* mutants the uniform diametric tube expansion is disrupted throughout the length of the tube. There may be two reasons behind this:

First, the absence of *pri* may be causing a general problem in tube expansion, and the phenotype becomes more obvious in the fusion cells because of the distinct genetic programming in those cells. However, if this was the case, then in the *Blimp-1* mutants, where *pri* expression is low in non-fusion cells, the tube diameter should be shorter too. Yet we observed that it is not, suggesting that *pri* does not have a general role in the tube expansion process.

Second, and more likely, is the possibility that the general problem of tube expansion in *pri* mutants is mediated by fusion cells that never expand as much as the rest. The small tube diameter at the fusion points might be the limiting factor for the diametric tube expansion in the other parts of the tube. This could be a mechanism that evolved to ensure that at these particular points the tube never expands more than in the rest of the DT, and hence preventing non-uniform tube expansion.

2. The effect of ecdysone on trachea maturation timing via *Blimp-1* and *pri*

The ecdysone peaks observed just before larval moltings and pupation indicate the importance of spatial regulation of ecdysone in these processes (Riddiford, 1993). A less studied ecdysone peak has also been observed during the embryonic stage 12 (Kozlova and Thummel, 2003). Agawa *and collaborators* showed that *Blimp-1* is one of the genes affected by this ecdysone peak (Agawa et al., 2007). We confirmed their data, and in addition showed that *pri* is another ecdysone-inducible gene, affected by the embryonic ecdysone peak. The involvement of ecdysone in the regulation of their expression indicates that the timing of *Blimp-1* and *pri* expression is crucial for the proper development of the embryo. Moreover, it suggests that ecdysone might be regulating the tracheal maturation through controlling the timing of *Blimp-1* and *pri* expression.

If the maturation of trachea can be measured by the ability of tracheal cells to execute late developmental processes like formation of F-actin bundles, the delay in F-actin bundling due to the absence of *pri* can be considered as a delay in tracheal maturation. Keeping in mind that ecdysone regulates the timing of *pri* expression, this result suggests that ecdysone might be regulating the tracheal maturation through controlling the timing of F-actin bundling.

In the mammalian immune system, *Blimp-1* is involved in maturation of the cells converting non-secreting cells into secreting cells. *Drosophila* tracheal cells are also capable of secreting materials into the ECM. It is possible that becoming secreting cells is a part of tracheal cell maturation. Based on our data, in *Blimp-1* mutant embryos, the tracheal cells are not capable of properly secreting chitin filaments into the lumen. Hence, *Blimp-1* might orchestrate the maturation of tracheal cells by inducing secretion, similar to its function in mammalian cells. However, it is highly unlikely that the loss of function of *Blimp-1* results in a general secretion problem because secretion of other molecules like, Verm and Pio, are not affected by the absence of Blimp-1.

Another result suggesting that ecdysone might be regulating the timing of trachea maturation through controlling *Blimp-1* and *pri* expression, originated from an hypothesis about whether *Blimp-1* and *pri* function together. To answer this question,

we checked the expression pattern of *pri* in *Blimp-1* mutant embryos and we observed that *pri* expression is altered in a subset of cells, non-fusion cells, in the DT upon loss of function of *Blimp-1*. The fact that the *pri* expression in *Blimp-1* mutant embryos resembles the *pri* expression in *wild-type* embryos at an earlier stage, suggests that the loss of function of *Blimp-1* might be affecting the developmental timing of the tracheal cells. Additionally, when we checked whether the decline in the expression of *pri* in non-fusion cells in *wild-type-stage-16* embryos can be prevented by the prolonged expression of *Blimp-1* at stage 16 embryos, we observed that the prolonged *Blimp-1* expression is not enough to prevent the decline. Possibly, the change in the *pri* expression pattern in *Blimp-1* mutants is merely a consequence of the change in developmental timing.

If we assume that loss of function of *Blimp-1* causes early maturation of the tracheal cells while the over/ectopic expression of *Blimp-1* causes a delay in the maturation of the tracheal cells, the overexpansion of the tracheal tubes in *Blimp-1* mutant embryos and the improper expansion of the tracheal tubes in the over/ectopic expression of *Blimp-1* can be explained by the premature and delayed development of tracheal cells, respectively. Besides, if there is a gradual increase in the chitin levels of taenidial folds and the diameter of the taenidia rings, then the taenidial fold phenotype we observed with the over/ectopic expression of *Blimp-1* might be another indication of *Blimp-1* controlling the timing of tracheal cells maturation. But if the chitin levels are gradually increasing during the development of taenidial folds, we should have observed high levels of chitin upon loss of function of *Blimp-1*, in which situation there is a premature development of the tracheal cells. Yet we observed low chitin levels in *Blimp-1* mutants. There can be two explanations for this:

1) The assumption that the chitin levels are gradually increasing during the development of taenidial folds is incorrect. Additionally, the presence of correct amount of Blimp-1 protein in the cells is crucial for the production of proper levels of chitin. Accordingly, in the absence/abundance of Blimp-1 the chitin levels are not as in the wt.

2) The assumption is correct. But apart from Blimp-1 dependency, there are other mechanisms, which do not depend on *Blimp-1* for their maturation, involved in establishing proper chitin levels, and without them proper chitin levels cannot be established, leading to low levels of chitin upon loss of function of *Blimp-1*.

3. Involvement of actin organization and adherens junctions in taenidial fold organization

Apical F-actin bundles with the same organization of taenidial folds have been identified in larval tracheas (Matusek et al., 2006). To check whether this is also the case in embryonic trachea, we labeled taenidial folds with fluostain and actin bundles with phalloidin in the same embryos. And we observed perpendicular lines of taenidial folds over the perpendicular lines of the actin bundles suggesting the strong correlation observed in larval trachea holds true also in embryonic trachea.

In the course of this study we checked apical F-actin bundles and taenidial folds in mutants of five "actin genes" *pri*/*tal*, *DAAM*, *Tec29*, *sn* and *f* that have previously published roles in actin cytoskeleton organization (Kondo et al., 2007; Matusek et al., 2006; Okenve-Ramos and Llimargas, 2014; Tilney et al., 1995). In mutants of all "actin genes" we observed that actin monomers are correctly localized in the apical domain. In mutants of *pri*/*tal*, *DAAM* and *Tec29* F-actin bundles are misoriented but still continuous from one cell to another (see below). Surprisingly we did not observe any change in apical F-actin bundles and taenidial folds in the absence of *sn* and *f* although they have published functions in adult cuticle structures, bristles, formation and also in filopodia formation in embryonic tracheal system (Okenve-Ramos and Llimargas, 2014; Tilney et al., 1995). The absence of any effect of *sn* and *f* on taenidial fold formation suggests that there are different types of actin organization in the cell, requiring different genes in different places and only those that affect apical F-actin bundles are required for taenidial fold formation. Perhaps in bristle and filopodia formation, longer F-actin bundles are required when compared to apical F-actin bundles formed during taenidial fold formation. Since the protrusions of the cells formed during taenidial fold formation are not as long as the ones formed during bristle and filopodia formation, the activity of actin cross linkers, Sn and F, might not be required during taenidial fold formation.

The degree of misorientation of F-actin bundles in the *pri*/*tal*, *DAAM* and *Tec29* mutant embryos is quite variable. In some cases we observed that most of the F-actin bundles are parallel to the tube axis whereas in others there is a mixture of misorientation ranging from an angle of 0° (representing the *wild-type* state, being

perpendicular to the tube axis) to 90° (being parallel to the tube axis). Since we could not see any pattern in these misorientations, it is possible that they are random. How this randomness occurs, in other words, how in one part the tube the F-actin bundle orientation differs than the other part of the tube is still an open question. But since the taenidial folds have the same pattern of orientation as the actin fibers, to preserve the continuity of the taenidial folds, the cells might be forming the F-actin bundles accordingly. Hence it is possible that in mutants of these three "actin" genes, the orientation of F-actin bundles and taenidial folds might not be so random, instead they depend on the taenidial folds of the neighboring cells. As a matter of fact, our results of rescue experiments of *Blimp-1* mutant phenotype in single cells indicate the importance of the neighboring taenidial folds in defining the taenidial fold orientation. Another hint that neighboring taenidial folds play a role in defining the position of taenidial folds in the cells came from our analysis of down-regulation of adherens junctions via α-catenin RNA interference. In this analysis we observed that when the adherens junctions are affected, the continuity of taenidial folds as well as F-actin bundles in the cells are disrupted. It is possible that neighboring cells are communicating through their adherens junctions to determine the position of F-actin cables and thus the position of taenidial folds.

4. Involvement of apical cell shape in taenidia formation

The apical cell shape of both *Blimp-1* and *pri* mutant embryos at stage 16 is different from the *wild-type*. In *Blimp-1* mutants the longest cell axis appears to be perpendicular to the tube axis, and the cells have a similar apical cell surface suggesting a uniform organization throughout the tube while in *pri* mutants the apical cell shape is severely affected and we could not define any repetitive pattern of similarities throughout the tube.

The 90° angle change in both taenidial fold orientation and the longest axis of the apical cell surface in *Blimp-1* mutant embryos led us to think that the alteration of apical cell surface shape might be causing the taenidial fold orientation phenotype. To test this idea we checked the taenidial folds in *Src42A* mutant embryos, in which the apical cell surface has a similar shape to *Blimp-1* mutant embryos. Our analysis revealed that the taenidial folds are formed properly in *Src42A* mutant embryos indicating that the longest axis of the apical cell surface and the orientation of taenidial folds are not directly related.

5. The effect of chitin on cellular processes

The effect of chitin on cellular processes has been previously reported. The uniform tube expansion has been attributed to the intraluminal chitin filament. In the absence of chitin synthesis due to the lack of *kkv*, or in the absence of proper chitin filament assembly due to the lack of *knk*, the tracheal tubes failed to expand uniformly. Moreover, the apical surface of the non-fusion cells show expanded apical profile as well as irregular apical accumulation of β-H spectrin in the absence of *kkv*, indicating that lack of chitin synthesis cause subapical cytoskeletal organization defects (Tonning et al., 2005). In this study, we observed that in the absence of proper chitin organization, via lack of chitin synthesis or lack of chitin modification or low levels of chitin, the F-actin bundles failed to form properly suggesting a two-way influence between F-actin and chitin structures.

How the absence of chitin synthesis or lack of chitin modification affects the formation of F-actin bundles in the cells, exactly how the tube expansion is affected by any problems in chitin metabolism, and how the lack of chitin synthesis causes subapical cytoskeletal organization defects are yet unanswered questions. Perhaps the problems of chitin at the aECM cause formation of an unstable aECM and this reflects on the cell shape by the absence of stiffness in the aECM. Another explanation might be that proper or improper chitin organization at the aECM signals to the cells and changes their behavior concomitantly. For example, during tube expansion, the presence of properly formed intraluminal chitin filaments might be signaling to cells to expand their apical cell surface and start the process of tube expansion. Finally, properly organized chitin in taenidial folds might be somehow signaling to the cells to stabilize the apical F-actin bundles. And in the absence of proper chitin organization, these processes are performed improperly.

11. Formation of taenidial folds

Taenidial folds extend beyond the limits of single cells, spanning through multiple cells creating a supra-cellular structure. The origin of this supra-cellular structure has been a curiosity for scientists almost over a century (reviewed in Uv and Moussian, 2010). Combining our observations and the previously published results, I would like to propose a model describing the events that occur during taenidial fold

formation in *wild-type* embryos and compare them to how these events probably occur in *Blimp-1*, *pri* and *kkv* mutant embryos.

In *wild-type* embryos taenidial folds are formed as follows. 1) In the beginning the actin monomers are randomly distributed in the apical surface of the tracheal cells. 2) As a result of an unknown signal, maybe upon completion of diametric tube expansion, the F-actin monomeres start to polymerize/depolymerize in specific repetitive positions in the apical cell membrane of each cell. 3) The adherens junctions ensure that orientation of F-actin bundles in each cell fits with the ones in the neighboring cells. 4) The newly formed F-actin bundles generate the mechanical forces to form the bulges on the apical cell membrane. They also trigger possible positioning of chitin synthase complex. 5) As the cell membrane flattens, the chitin secreted into aECM forms the rigid taenidial folds, which then contribute to the stability of the F-actin bundles.

In *Blimp-1* mutant embryos the taenidial folds are formed as follows: 1) As in the *wild-type* case,*in* the beginning the actin monomers are randomly distributed in the apical surface of the tracheal cells. 2) With a delay in relation to wild-type, the parallel F-actin bundles start to be formed in specific repetitive positions in the apical cell membrane of each cell. 3) The adherens junctions ensure that orientation of F-actin bundles in each cell fits with the ones in the neighbor cells. 4) The parallel F-actin bundles that sustain their stability generate the mechanical forces to form the bulges on the apical cell membrane. They also trigger possible positioning of chitin synthase complex. 5) As the cell membrane flattens, chitin secreted into aECM form the parallel taenidial folds. Because of the low levels of chitin in taenidial folds, F-actin bundles can not be stabilized and they depolymerize.

In the *pri* mutant embryos taenidial folds are formed as follows: 1) As in the case of the *wild-type*, in the beginning the actin monomers are randomly distributed in the apical surface of the tracheal cells. 2) With a delay in relation to wild-type, the parallel F-actin bundles start to be formed in specific repetitive positions in the apical cell membrane of each cell. 3) The adherens junctions ensure that orientation of F-actin bundles in each cell fits with the ones in the neighbor cells. 4) The newly formed F-actin bundles generate the mechanical forces to form the bulges on the apical cell

membrane. They also trigger possible positioning of chitin synthase complex. 5) As the cell membrane flattens, the chitin secreted into aECM forms the taenidial folds with the same orientation of F-actin bundles and then contribute to the stability of the same F-actin bundles.

In the *kkv* mutant embryos taenidial folds are formed as follows: 1) As in the case of the *wild-type*, in the beginning the actin monomers are randomly distributed in the apical surface of the tracheal cells. 2) Probably as in the case of *Blimp-1* and *pri,* with a little bit of delay the F-actin bundles start to be formed in specific repetitive positions in the apical cell membrane in each cell. 3) The adherens junctions ensure that orientation of F-actin bundles in each cell fits with the ones in the neighbor cells. 4) Only a few F-actin bundles can be formed that generate the mechanical forces to form the occasional bulges on the apical cell membrane. 5) The unstable F-actin cannot sustain the bundle form and dissociate into actin monomers. In the absence of chitin secretion into aECM, the cuticle detaches from the plasma membrane, which becomes flat at the end of the process.

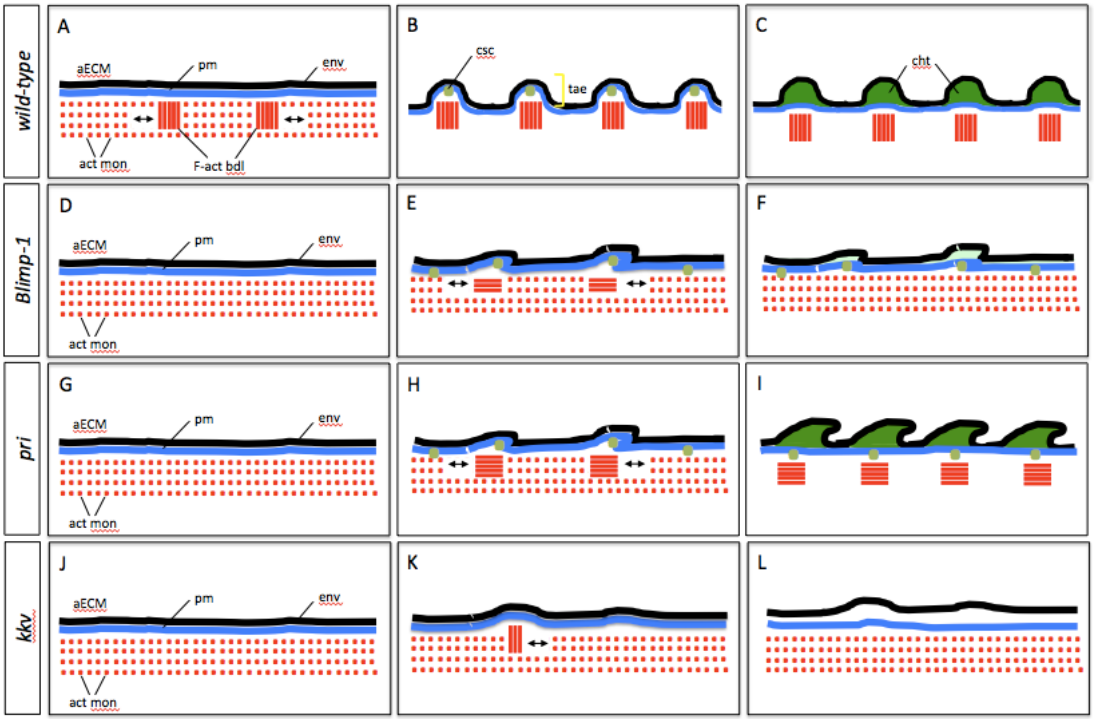

Figure 56: Formation of taenidial folds. The schematic representation of formation of taenidial folds in *wild-type* (A-C), *Blimp-1* mutant (D-F), *pri* mutant (G-I) and *kkv* mutant (J-L) embryos. aECM=apical extracellular matrix, act mon=actin monomers, pm=plasma membrane, F-act bdl=F-actin bundles, env=envelope, csc=chitin synthase complex, tae=taenidia, cht=chitin.

REFERENCES

Agawa, Y., Sarhan, M., Kageyama, Y., Akagi, K., Takai, M., Hashiyama, K., Wada, T., Handa, H., Iwamatsu, A., Hirose, S., et al. (2007). Drosophila Blimp-1 Is a Transient Transcriptional Repressor That Controls Timing of the Ecdysone-Induced Developmental Pathway. *Molecular and Cellular Biology* **27**, 8739–8747.

Ancelin, K., Lange, U. C., Hajkova, P., Schneider, R., Bannister, A. J., Kouzarides, T. and Surani, M. A. (2006). Blimp1 associates with Prmt5 and directs histone arginine methylation in mouse germ cells. *Nature Cell Biology* **8**, 623–630.

Anderson, M. G., Perkins, G. L., Chittick, P., Shrigley, R. J. and Johnson, W. A. (1995a). drifter, a Drosophila POU-domain transcription factor, is required for correct differentiation and migration of tracheal cells and midline glia. *Genes & Development* **9**, 123–137.

Anderson, M. G., Perkins, G. L., Chittick, P., Shrigley, R. J. and Johnson, W. A. (1995b). drifter, a Drosophila POU-domain transcription factor, is required for correct differentiation and migration of tracheal cells and midline glia. *Genes & Development* **9**, 123–137.

Andrew, D. J. and Ewald, A. J. (2010). Morphogenesis of epithelial tubes: Insights into tube formation, elongation, and elaboration. *Developmental Biology* **341**, 34–55.

Araújo, S. J., Aslam, H., Tear, G. and Casanova, J. (2005). mummy/cystic encodes an enzyme required for chitin and glycan synthesis, involved in trachea, embryonic cuticle and CNS development—Analysis of its role in Drosophila tracheal morphogenesis. *Developmental Biology* **288**, 179–193.

Araújo, S. J., Cela, C. and Llimargas, M. (2007). Tramtrack regulates different morphogenetic events during Drosophila tracheal development. *Development* **134**, 3665–3676.

Beitel, G. J. and Krasnow, M. A. (2000). Genetic control of epithelial tube size in the Drosophila tracheal system. *Development* **127**, 3271–3282.

Bikoff, E. K., Morgan, M. A. and Robertson, E. J. (2009). An expanding job description for Blimp-1/PRDM1. *Current Opinion in Genetics & Development* **19**, 379–385.

Brand, A. H. and Perrimon, N. (1993). Targeted gene expression as a means of altering cell fates and generating dominant phenotypes. *Development* **118**, 401–415.

Bryant, D. M. and Mostov, K. E. (2008). From cells to organs: building polarized tissue. *Nat Rev Mol Cell Biol* **9**, 887–901.

Brzezinski, J. A., Lamba, D. A. and Reh, T. A. (2010). Blimp1 controls photoreceptor versus bipolar cell fate choice during retinal development. *Development* **137**, 619–629.

Buyse, I. M., Shao, G. and Huang, S. (1995). The retinoblastoma protein binds to RIZ, a zinc-finger protein that shares an epitope with the adenovirus E1A protein. *Proc. Natl. Acad. Sci. U.S.A.* **92**, 4467–4471.

Campos-Ortega, J. A. and Hartenstein, V. (1997). Stages of *Drosophila* Embryogenesis. In *The Embryonic Development of Drosophila Melanogaster*, pp. 9–84. Berlin ; New York : Springer.

Chavoshi, T. M., Moussian, B. and Uv, A. (2010). Tissue-autonomous EcR functions are required for concurrent organ morphogenesis in the Drosophila embryo. *Mechanisms of Development* **127**, 308–319.

Chung, S., Vining, M. S., Bradley, P. L., Chan, C.-C., Wharton, K. A. and Andrew, D. J. (2009). Serrano (Sano) Functions with the Planar Cell Polarity Genes to Control Tracheal Tube Length. *PLoS Genet* **5**, e1000746.

David, R. and Wedlich, D. (2001). *PCR-based RNA probes: a quick and sensitive method to improve whole mount embryo in situ hybridizations.*

de Celis, J. F., Llimargas, M. and Casanova, J. (1995a). ventral veinless, the gene encoding the Cf1a transcription factor, links positional information and cell differentiation during embryonic and imaginal development in Drosophila melanogaster. 1–12.

de Celis, J. F., Llimargas, M. and Casanova, J. (1995b). Ventral veinless, the gene encoding the Cf1a transcription factor, links positional information and cell differentiation during embryonic and imaginal development in Drosophila melanogaster. *Development* **121**, 3405–3416.

Delon, I., Chanut-Delalande, H. and Payre, F. (2003). The Ovo/Shavenbaby transcription factor specifies actin remodelling during epidermal differentiation in Drosophila. *Mechanisms of Development* **120**, 747–758.

Devine, W. P., Lubarsky, B., Shaw, K., Luschnig, S., Messina, L. and Krasnow, M. A. (2005). Requirement for chitin biosynthesis in epithelial tube morphogenesis. *Proc. Natl. Acad. Sci. U.S.A.* **102**, 17014–17019.

Dutta, D., Bloor, J. W., Ruiz-Gomez, M., VijayRaghavan, K. and Kiehart, D. P. (2002). Real-time imaging of morphogenetic movements indrosophila using Gal4-UAS-driven expression of GFP fused to the actin-binding domain of moesin. *genesis* **34**, 146–151.

Edwards, K. A., Demsky, M., Montague, R. A., Weymouth, N. and Kiehart, D. P. (1997). GFP-moesin illuminates actin cytoskeleton dynamics in living tissue and demonstrates cell shape changes during morphogenesis in Drosophila. *Developmental Biology* **191**, 103–117.

Fisk, G. J. and Thummel, C. S. (1998). The DHR78 Nuclear Receptor Is Required

for Ecdysteroid Signaling during the Onset of Drosophila Metamorphosis. *Cell* **93**, 543–555.

Förster, D. and Luschnig, S. (2012). Src42A-dependent polarized cell shape changes mediate epithelial tube elongation in Drosophila. *Nature Cell Biology* **14**, 526–534.

Förster, D., Armbruster, K. and Luschnig, S. (2010). Sec24-Dependent Secretion Drives Cell-Autonomous Expansion of Tracheal Tubes in Drosophila. *Current Biology* **20**, 62–68.

Fumasoni, I., Meani, N., Rambaldi, D., Scafetta, G., Alcalay, M. and Ciccarelli, F. D. (2007). Family expansion and gene rearrangements contributed to the functional specialization of PRDM genes in vertebrates. *BMC Evol Biol* **7**, 187.

Gilbert, L. I. and Warren, J. T. (2005). A molecular genetic approach to the biosynthesis of the insect steroid molting hormone. *Vitamins & Hormones* **73**, 31–57.

Glasheen, B. M., Robbins, R. M., Piette, C., Beitel, G. J. and Page-McCaw, A. (2010). A matrix metalloproteinase mediates airway remodeling in Drosophila. *Developmental Biology* **344**, 772–783.

Győry, I., Wu, J., Fejér, G., Seto, E. and Wright, K. L. (2004). PRDI-BF1 recruits the histone H3 methyltransferase G9a in transcriptional silencing. *Nat Immunol* **5**, 299–308.

Hashimoto, Y., Kondo, T. and Kageyama, Y. (2008). Lilliputians get into the limelight: Novel class of small peptide genes in morphogenesis. *Development, Growth & Differentiation* **50**, S269–S276.

Hemphälä, J., Uv, A., Cantera, R., Bray, S. and Samakovlis, C. (2003). Grainy head controls apical membrane growth and tube elongation in response to Branchless/FGF signalling. *Development* **130**, 249–258.

Hohenauer, T. and Moore, A. W. (2012). The Prdm family: expanding roles in stem cells and development. *Development* **139**, 2267–2282.

Huang, S. (1994). Blimp-1 is the murine homolog of the human transcriptional repressor PRDI-BF1. *Cell* **78**, 9 EP –.

Huang, S., Shao, G. and Liu, L. (1998). The PR Domain of the Rb-binding Zinc Finger Protein RIZ1 Is a Protein Binding Interface and Is Related to the SET Domain Functioning in Chromatin-mediated Gene Expression. *Journal of Biological Chemistry* **273**, 15933–15939.

Isaac, D. D. and Andrew, D. J. (1996). Tubulogenesis in Drosophila: a requirement for the trachealess gene product. *Genes & Development* **10**, 103–117.

Jayaram, S. A., Senti, K.-A., Tiklová, K., Tsarouhas, V., Hemphälä, J. and Samakovlis, C. (2008). COPI Vesicle Transport Is a Common Requirement for Tube Expansion in Drosophila. *PLoS ONE* **3**, e1964.

Jaźwińska, A., Ribeiro, C. and Affolter, M. (2003). Epithelial tube morphogenesis during Drosophila tracheal development requires Piopio, a luminal ZP protein. *Nature Cell Biology* **5**, 895–901.

Jiang, L. and Crews, S. T. (2003). The Drosophila dysfusion Basic Helix-Loop-Helix (bHLH)-PAS Gene Controls Tracheal Fusion and Levels of the Trachealess bHLH-PAS Protein. *Molecular and Cellular Biology* **23**, 5625–5637.

Katoh, K., Omori, Y., Onishi, A., Sato, S., Kondo, M. and Furukawa, T. (2010). Blimp1 Suppresses Chx10 Expression in Differentiating Retinal Photoreceptor Precursors to Ensure Proper Photoreceptor Development. *Journal of Neuroscience* **30**, 6515–6526.

Keller, A. D. and Maniatis, T. (1991). Identification and characterization of a novel repressor of beta-interferon gene expression. *Genes & Development* **5**, 868–879.

Kinameri, E., Inoue, T., Aruga, J., Imayoshi, I., Kageyama, R., Shimogori, T. and Moore, A. W. (2008). Prdm Proto-Oncogene Transcription Factor Family Expression and Interaction with the Notch-Hes Pathway in Mouse Neurogenesis. *PLoS ONE* **3**, e3859.

Klambt, C., Glazer, L. and Shilo, B. Z. (1992). breathless, a Drosophila FGF receptor homolog, is essential for migration of tracheal and specific midline glial cells. *Genes & Development* **6**, 1668–1678.

Knust, E. and Bossinger, O. (2002). Composition and formation of intercellular junctions in epithelial cells. *Science* **298**, 1955–1959.

Kondo, T., Hashimoto, Y., Kato, K., Inagaki, S., Hayashi, S. and Kageyama, Y. (2007). Small peptide regulators of actin-based cell morphogenesis encoded by a polycistronic mRNA. *Nature Cell Biology* **9**, 660–665.

Kondo, T., Plaza, S., Zanet, J., Benrabah, E., Valenti, P., Hashimoto, Y., Kobayashi, S., Payre, F. and Kageyama, Y. (2010). Small Peptides Switch the Transcriptional Activity of Shavenbaby During Drosophila Embryogenesis. *Science* **329**, 336–339.

Kozlova, T. and Thummel, C. S. (2003). Essential roles for ecdysone signaling during Drosophila mid-embryonic development. *Science* **301**, 1911–1914.

Luschnig, S., Bätz, T., Armbruster, K. and Krasnow, M. A. (2006). serpentine and vermiform Encode Matrix Proteins with Chitin Binding and Deacetylation Domains that Limit Tracheal Tube Length in Drosophila. *Current Biology* **16**, 186–194.

Manning, G. and Krasnow, M. A. (1993). Development of the *Drosophila* Tracheal System. In *The Development of Drosophila Melanogaster* (eds. Bate, M. and Martínez-Arias, A., pp. 609–685. Cold Spring Harbor Laboratory Press, Cold Spring Harbor, NY.

Massarwa, R. A., Schejter, E. D. and Shilo, B.-Z. (2009). Apical Secretion in Epithelial Tubes of the Drosophila Embryo Is Directed by the Formin-Family

Protein Diaphanous. *Developmental Cell* **16**, 877–888.

Matusek, T., Djiane, A., Jankovics, F., Brunner, D., Mlodzik, M. and Mihály, J. (2006). The Drosophila formin DAAM regulates the tracheal cuticle pattern through organizing the actin cytoskeleton. *Development* **133**, 957–966.

Mercader, N., Fischer, S. and Neumann, C. J. (2006). Prdm1 acts downstream of a sequential RA, Wnt and Fgf signaling cascade during zebrafish forelimb induction. *Development* **133**, 2805–2815.

Merzendorfer, H. and Zimoch, L. (2003). Chitin metabolism in insects: structure, function and regulation of chitin synthases and chitinases. *J. Exp. Biol.* **206**, 4393–4412.

Moussian, B. (2010). Recent advances in understanding mechanisms of insect cuticle differentiation. *Insect Biochemistry and Molecular Biology* **40**, 363–375.

Moussian, B., Schwarz, H., Bartoszewski, S. and N sslein-Volhard, C. (2005). Involvement of chitin in exoskeleton morphogenesis inDrosophila melanogaster. *J. Morphol.* **264**, 117–130.

Moussian, B., Seifarth, C., Müller, U., Berger, J. and Schwarz, H. (2006a). Cuticle differentiation during Drosophila embryogenesis. *Arthropod Structure & Development* **35**, 137–152.

Moussian, B., Tång, E., Tonning, A., Helms, S., Schwarz, H., Nüsslein-Volhard, C. and Uv, A. E. (2006b). Drosophila Knickkopf and Retroactive are needed for epithelial tube growth and cuticle differentiation through their specific requirement for chitin filament organization. *Development* **133**, 163–171.

Nellen, D., Burke, R., Struhl, G. and Basler, K. (1996). Direct and long-range action of a DPP morphogen gradient. *Cell* **85**, 357–368.

Ng, T., Yu, F. and Roy, S. (2006). A homologue of the vertebrate SET domain and zinc finger protein Blimp-1 regulates terminal differentiation of the tracheal system in the Drosophila embryo. *Dev Genes Evol* **216**, 243–252.

Norum, M., Tång, E., Chavoshi, T., Schwarz, H., Linke, D., Uv, A. and Moussian, B. (2010). Trafficking through COPII Stabilises Cell Polarity and Drives Secretion during Drosophila Epidermal Differentiation. *PLoS ONE* **5**, e10802.

Ohinata, Y., Payer, B., O'Carroll, D., Ancelin, K., Ono, Y., Sano, M., Barton, S. C., Obukhanych, T., Nussenzweig, M., Tarakhovsky, A., et al. (2005). Blimp1 is a critical determinant of the germ cell lineage in mice. *Nature Cell Biology* **436**, 207–213.

Okenve-Ramos, P. and Llimargas, M. (2014). Fascin links Btl/FGFR signalling to the actin cytoskeleton during Drosophila tracheal morphogenesis. *Development* **141**, 929–939.

Petryk, A., Warren, J. T., Marqués, G., Jarcho, M. P., Gilbert, L. I., Kahler, J.,

Parvy, J.-P., Li, Y., Dauphin-Villemant, C. and O'Connor, M. B. (2003). Shade is the Drosophila P450 enzyme that mediates the hydroxylation of ecdysone to the steroid insect molting hormone 20-hydroxyecdysone. *Proc. Natl. Acad. Sci. U.S.A.* **100**, 13773–13778.

Pi, H., Huang, Y.-C., Chen, I.-C., Lin, C.-D., Yeh, H.-F. and Pai, L.-M. (2011). Identification of 11-amino acid peptides that disrupt Notch-mediated processes in Drosophila. *Journal of Biomedical Science* **18**, 42.

Price, M. H., Roberts, D. M., McCartney, B. M., Jezuit, E. and Peifer, M. (2006). Cytoskeletal dynamics and cell signaling during planar polarity establishment in the Drosophila embryonic denticle. *Journal of Cell Science* **119**, 403–415.

Pueyo, J. I. and Couso, J. P. (2011). Tarsal-less peptides control Notch signalling through the Shavenbaby transcription factor. *Developmental Biology* **355**, 183–193.

Pueyo, J. I. and Couso, J. P. (2008). The 11-aminoacid long Tarsal-less peptides trigger a cell signal in Drosophila leg development. *Developmental Biology* **324**, 192–201.

Ren, B., Chee, K. J., Kim, T. H. and Maniatis, T. (1999). PRDI-BF1/Blimp-1 repression is mediated by corepressors of the Groucho family of proteins. *Genes & Development* **13**, 125–137.

Riddiford, L. M. (1993). Hormones and *Drosophila* Development. In *The Development of Drosophila Melanogaster* (eds. Bate, M. and Martínez-Arias, A., pp. 899–940. Cold Spring Harbor Laboratory Press, Cold Spring Harbor, NY.

Robertson, E. J., Charatsi, I., Joyner, C. J., Koonce, C. H., Morgan, M., Islam, A., Paterson, C., Lejsek, E., Arnold, S. J., Kallies, A., et al. (2007). Blimp1 regulates development of the posterior forelimb, caudal pharyngeal arches, heart and sensory vibrissae in mice. *Development* **134**, 4335–4345.

Samakovlis, C., Hacohen, N., Manning, G., Sutherland, D. C., Guillemin, K. and Krasnow, M. A. (1996a). Development of the Drosophila tracheal system occurs by a series of morphologically distinct but genetically coupled branching events. *Development* **122**, 1395–1407.

Samakovlis, C., Manning, G., Steneberg, P., Hacohen, N., Cantera, R. and Krasnow, M. A. (1996b). Genetic control of epithelial tube fusion during Drosophila tracheal development. 1–6.

Schindelin, J., Arganda-Carreras, I., Frise, E., Kaynig, V., Longair, M., Pietzsch, T., Preibisch, S., Rueden, C., Saalfeld, S., Schmid, B., et al. (2012). Fiji: an open-source platform for biological-image analysis. *Nat. Methods* **9**, 676–682.

Shaye, D. D., Casanova, J. and Llimargas, M. (2008). Modulation of intracellular trafficking regulates cell intercalation in the Drosophila trachea. *Nature Cell Biology* **10**, 964–970.

Strigini, M., Cantera, R., Morin, X., Bastiani, M. J., Bate, M. and Karagogeos, D.

(2006). The IgLON protein Lachesin is required for the blood–brain barrier in Drosophila. *Molecular and Cellular Neuroscience* **32**, 91–101.

Struhl, G. and Basler, K. (1993). Organizing activity of wingless protein in Drosophila. *Cell* **72**, 527–540.

Su, S. T., Ying, H. Y., Chiu, Y. K., Lin, F. R., Chen, M. Y. and Lin, K. I. (2009). Involvement of Histone Demethylase LSD1 in Blimp-1-Mediated Gene Repression during Plasma Cell Differentiation. *Molecular and Cellular Biology* **29**, 1421–1431.

Sun, X.-J., Xu, P.-F., Zhou, T., Hu, M., Fu, C.-T., Zhang, Y., Jin, Y., Chen, Y., Chen, S.-J., Huang, Q.-H., et al. (2008). Genome-Wide Survey and Developmental Expression Mapping of Zebrafish SET Domain-Containing Genes. *PLoS ONE* **3**, e1499.

Sutherland, D., Samakovlis, C. and Krasnow, M. A. (1996). branchless Encodes a Drosophila FGF Homolog That Controls Tracheal Cell Migration and the Pattern of Branching. *Cell* **87**, 1091–1101.

Swanson, L. E., Yu, M., Nelson, K. S., Laprise, P., Tepass, U. and Beitel, G. J. (2009). Drosophila convoluted/dALS Is an Essential Gene Required for Tracheal Tube Morphogenesis and Apical Matrix Organization. *Genetics* **181**, 1281–1290.

Tanaka-Matakatsu, M., Uemura, T., Oda, H., Takeichi, M. and Hayashi, S. (1996). Cadherin-mediated cell adhesion and cell motility in Drosophila trachea regulated by the transcription factor Escargot. 1–9.

Tiklová, K., Tsarouhas, V. and Samakovlis, C. (2013). Control of Airway Tube Diameter and Integrity by Secreted Chitin-Binding Proteins in Drosophila. *PLoS ONE* **8**, e67415.

Tilney, L. G., Tilney, M. S. and Guild, G. M. (1995). F actin bundles in Drosophila bristles. I. Two filament cross-links are involved in bundling. *The Journal of Cell Biology* **130**, 629–638.

Tonning, A., Hemphälä, J., Tång, E., Nannmark, U., Samakovlis, C. and Uv, A. (2005). A Transient Luminal Chitinous Matrix Is Required to Model Epithelial Tube Diameter in the Drosophila Trachea. *Developmental Cell* **9**, 423–430.

Tsarouhas, V., Senti, K.-A., Jayaram, S. A., Tiklová, K., Hemphälä, J., Adler, J. and Samakovlis, C. (2007). Sequential Pulses of Apical Epithelial Secretion and Endocytosis Drive Airway Maturation in Drosophila. *Developmental Cell* **13**, 214–225.

Tunyaplin, C., Shapiro, M. A. and Calame, K. L. (2000). Characterization of the B lymphocyte-induced maturation protein-1 (Blimp-1) gene, mRNA isoforms and basal promoter. *Nucleic Acids Res.* **28**, 4846–4855.

Turner, C. A., Jr, Mack, D. H. and Davis, M. M. (1994). Blimp-1, a novel zinc finger-containing protein that can drive the maturation of B lymphocytes into immunoglobulin-secreting cells. *Cell* **77**, 297–306.

Ueda, H. and Hirose, S. (1990). Identification and purification of a Bombyx mori homologue of FTZ-F1. *Nucleic Acids Res.* **18**, 7229–7234.

Uv, A. and Moussian, B. (2010). The apical plasma membrane of Drosophila embryonic epithelia. *European Journal of Cell Biology* **89**, 208–211.

Uv, A., Cantera, R. and Samakovlis, C. (2003). Drosophila tracheal morphogenesis: intricate cellular solutions to basic plumbing problems. *Trends Cell Biol.* **13**, 301–309.

Walters, J. W., Dilks, S. A. and DiNardo, S. (2006). Planar polarization of the denticle field in the Drosophila embryo: Roles for Myosin II (Zipper) and Fringe. *Developmental Biology* **297**, 323–339.

Wang, S., Jayaram, S. A., Hemphälä, J., Senti, K.-A., Tsarouhas, V., Jin, H. and Samakovlis, C. (2006). Septate-Junction-Dependent Luminal Deposition of Chitin Deacetylases Restricts Tube Elongation in the Drosophila Trachea. *Current Biology* **16**, 180–185.

Wang, S., Meyer, H., Ochoa-Espinosa, A., Buchwald, U., Onel, S., Altenhein, B., Heinisch, J. J., Affolter, M. and Paululat, A. (2012). GBF1 (Gartenzwerg)-dependent secretion is required for Drosophila tubulogenesis. *Journal of Cell Science* **125**, 461–472.

Warren, J. T., Petryk, A., Marqués, G., Jarcho, M., Parvy, J.-P., Dauphin-Villemant, C., O'Connor, M. B. and Gilbert, L. I. (2002). Molecular and biochemical characterization of two P450 enzymes in the ecdysteroidogenic pathway of Drosophila melanogaster. *Proc. Natl. Acad. Sci. U.S.A.* **99**, 11043–11048.

Wilk, R., Reed, B. H., Tepass, U. and Lipshitz, H. D. (2000). The hindsight Gene Is Required for Epithelial Maintenance and Differentiation of the Tracheal System in Drosophila. *Developmental Biology* **219**, 183–196.

Wilk, R., Weizman, I. and Shilo, B. Z. (1996). trachealess encodes a bHLH-PAS protein that is an inducer of tracheal cell fates in Drosophila. *Genes & Development* **10**, 93–102.

Wilkin, M. B., Becker, M. N., Mulvey, D., Phan, I., Chao, A., Cooper, K., Chung, H. J., Campbell, I. D., Baron, M. and MacIntyre, R. (2000). Drosophila dumpy is a gigantic extracellular protein required to maintain tension at epidermal-cuticle attachment sites. *Curr. Biol.* **10**, 559–567.

Wu, V. M., Schulte, J., Hirschi, A., Tepass, U. and Beitel, G. J. (2004). Sinuous is a Drosophila claudin required for septate junction organization and epithelial tube size control. *The Journal of Cell Biology* **164**, 313–323.

Wulf, E., Deboben, A., Bautz, F. A., Faulstich, H. and Wieland, T. (1979). Fluorescent phallotoxin, a tool for the visualization of cellular actin. *Proc. Natl. Acad. Sci. U.S.A.* **76**, 4498–4502.

Yu, J., Angelin-Duclos, C., Greenwood, J., Liao, J. and Calame, K. (2000).

Transcriptional Repression by Blimp-1 (PRDI-BF1) Involves Recruitment of Histone Deacetylase. *Molecular and Cellular Biology* **20**, 2592–2603.

Zecca, M., Basler, K. and Struhl, G. (1996). Direct and long-range action of a wingless morphogen gradient. *Cell* **87**, 833–844.

RESUMEN EN CASTELLANO

En el reino animal hay numerosos ejemplos de sistemas de órganos tubulares, como los pulmones y el sistema vascular de los mamíferos. En este estudio hemos usado el sistema traqueal de *Drosophila melanogaster* para estudiar el desarrollo de este tipo de órganos. En particular, nos centramos en los pliegues taenidiales, estructuras de quitina que rodean el lumen tubular y dan resistencia mecánica a los tubos traqueales. Formados por la secreción de quitina en la matriz extracelular apical, estos pliegues se extienden más allá de los límites de una sola célula, abarcando múltiples células. Esto implica un alto nivel de coordinación intra e intercelular. Hay una serie de genes cuya ausencia produce perturbaciones en los pliegues taenidiales. De éstos, nuestro estudio se centra en *Blimp-1* y *pri*.

En ausencia de cada uno de estos genes, los pliegues taenidiales no se desarrollan correctamente mientras que otros aspectos del desarrollo traqueal no se ven demasiado afectados. Hemos analizado el patrón de expresión de *Blimp-1* y *pri*, y hemos encontrado que ambos genes se expresan en las células traqueales de *Drosophila* durante el desarrollo embrionario. Los pliegues taenidiales todavía se forman en ausencia de *Blimp-1* o *pri*, pero no están organizados correctamente, lo que indica que *Blimp-1* y *pri* contribuyen a su adecuada formación.

Existen varios sistemas en *Drosophila* en que estructuras de actina contribuyen a la organización de la quitina, como los dentículos de la epidermis y el lumen el sistema traqueal. En los mutantes *Blimp-1*, no se forman los anillos de actina apical, que si que lo hacen en los mutantes *pri* pero con una mala orientacion, lo que indica que la función de *Blimp-1* y *pri* se requiere para el ensamblaje de la F-actina. Por otra parte, nuestros resultados indican que perturbar la síntesis de quitina o su organización, desorganiza la F-actina apical que no forma haces. Por lo tanto, durante el desarrollo del sistema traqueal se establece una interacción mútua entre la organización de la F-actina y de las estructuras de quitina.

Mediante la expresión de la forma silvestre del gen en una sola célula en un fondo mutante, hemos estudiado cómo las células individuales contribuyen a generar

una estructura supra-celular. Los resultados de nuestro análisis revelan que la orientación de los pliegues taenidiales no es regulada de manera autónoma y que depende en gran medida de los pliegues taenidiales formados por las células vecinas. Por último, mostramos que perturbar las uniones entre células, a través de la reducción de los niveles de α-catenina, da lugar a que las células traqueales formen su pliegues taenidiales de forma independiente a sus vecinas.

APPENDICIES

Appendix A. List of Abbreviations

aECM	apical Extracellular Matrix
BSA	Bowine Serum Albumin
CA	Constitutively Active
CBP	Chitin Binding Probe
cd8	cluster of differentiation 8
Cy3	Cyanine Dye 3
DB	Dorsal Branch
DIG	Digoxigenin
DN	Dominant Negative
DNA	Deoxyribonucleic Acid
DNasin	DNAse inhibitor
dNTP	deoxynucleotide triphosphate
DT	Dorsal Trunk
ECM	Extracellular Matrix
EDTA	Ethylenediaminetetraacetic acid
EE	Early endosomes
EM	Electron Microscopy
EtOH	Ethanol
F-actin	Filamentous actin
FGF	Fibroblast Growth Factor
FLP	Flippase
FRT	Flippase Recognition Target
GB	Ganglionic Branch
GFP	Green Fluorescent Protein
GlcNAc	1,4-N-Acetlyglucosamine
HRP	Horseradish peroxide
hs-FLP	heat-schock-flippase
LE	Late endosomes
LT	Lateral Trunk
MeOH	Methanol
NaOAc	Sodium Acetate
ncRNAs	non-protein-coding RNAs
PBS	Phosphate Buffered Saline
PCR	Polmerase Chain Reaction
PR domain	Positive Regulatory domain
pSrc	phospho Src
RNA	Ribonucleic Acid
RNAi	Ribonucleic Acid interference
RNasin	RNAse inhibitor
SAR	Subapical Region

SB	Spiracular Branch
SJ	Septate Junctions
sORFs	short Open Reading Frames
TEM	Transmission Electron Microscope
TSA	Tyramide Signal Amplification
UAS	Upstream Activating Sequence
UDP-GlcNAc	uridine diphosphate-N-aceytlglucosamine
VB	Visceral Branch
wt	wild-type
ZA	Zonula Adherens
βGAL	β-galactosidase

Appendix B. Movie Legends

Movie 1: F-actin dynamics in the *wild-type* embryo. Wild-type embryo carrying *btl-MoeGFP* construct visualized from a lateral view. Time-lapse images were taken every 5 minutes. Note the actin monomers polymerize and generate the F-actin bundles in the form of rings at the end of the movie.

Movie 1: F-actin dynamics in the *Blimp-1* mutant embryo. *Blimp-1* mutant embryo carrying *btl-MoeGFP* construct visualized from a lateral view. Time-lapse images were taken every 5 minutes. Note the actin monomers fail to polymerize and generate F-actin bundles except in the fusion point.